



Universidade do Estado do Rio de Janeiro

Centro de Tecnologia e Ciências

Instituto de Física Armando Dias Tavares

Matheus Curado Ferreira

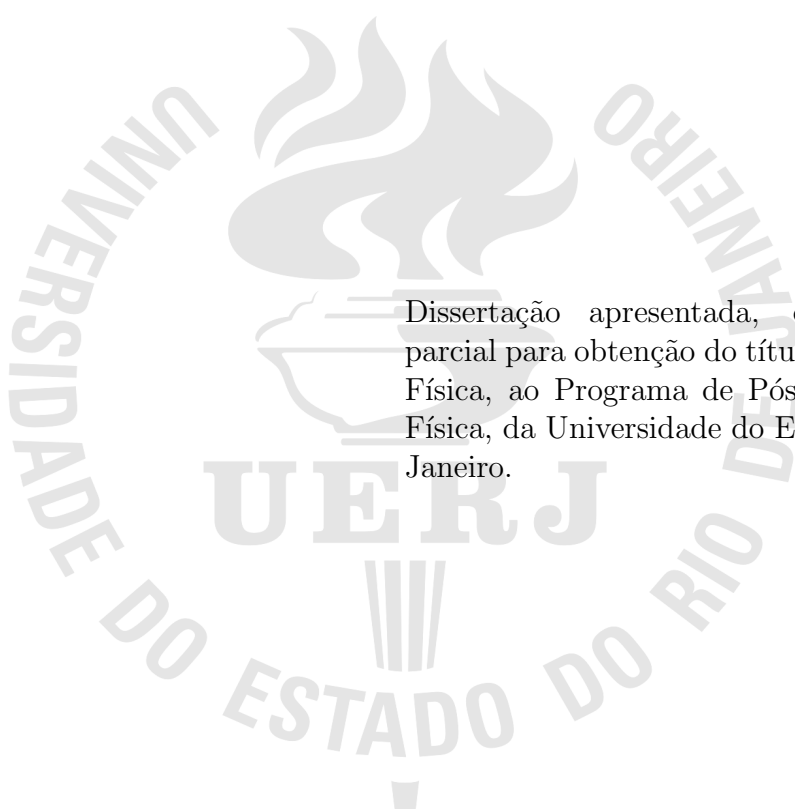
Nonperturbative free energy and phase transition for a complex
scalar field theory

Rio de Janeiro

2022

Matheus Curado Ferreira

**Nonperturbative free energy and phase transition for a complex scalar field
theory**



Dissertação apresentada, como requisito parcial para obtenção do título de Mestre em Física, ao Programa de Pós-Graduação em Física, da Universidade do Estado do Rio de Janeiro.

Orientador: Prof. Dr. Rudnei de Oliveira Ramos

Rio de Janeiro

2022

CATALOGAÇÃO NA FONTE
UERJ/ REDE SIRIUS / BIBLIOTECA CTC/D

F383n Ferreira, Matheus Curado.
Nonperturbative free energy and phase transition for a complex scalar
field theory / Matheus Curado Ferreira. - 2022.
140 f. : il.

Orientador: Rudnei de Oliveira Ramos.
Dissertação (mestrado) - Universidade do Estado do Rio de Janeiro,
Instituto de Física Armando Dias Tavares.

1. Teoria de campos (Física) – Teses. 2. Transformações de fase (Física
estatística) – Teses. 3. Simetria quebrada (Física) – Teses. I. Ramos, Rudnei
de Oliveira. II. Universidade do Estado do Rio de Janeiro. Instituto de Física
Armando Dias Tavares. III. Título.

CDU 530.145

Bibliotecária: Teresa da Silva CRB7/5209

Autorizo, apenas para fins acadêmicos e científicos, a reprodução total ou
parcial desta dissertação, desde que citada a fonte.

Assinatura

Data

Matheus Curado Ferreira

**Nonperturbative free energy and phase transition for a complex scalar field
theory**

Dissertação apresentada, como requisito parcial para obtenção do título de Mestre em Física, ao Programa de Pós-Graduação em Física, da Universidade do Estado do Rio de Janeiro.

Aprovada em: 22 de Agosto de 2022

Banca Examinadora:

Prof. Dr. Rudnei de Oliveira Ramos (Orientador)
Instituto de Física Armando Dias Tavares - UERJ

Profa. Dra. Letícia Faria Domingues Palhares
Instituto de Física Armando Dias Tavares - UERJ

Prof. Dr. Marcus Emmanuel Benghi Pinto
Universidade Federal de Santa Catarina - UFSC

Prof. Dr. Ricardo Luciano Sonogo Farias
Universidade Federal de Santa Maria - UFSM

Profa. Dra. Dyana Cristine Duarte
Universidade Federal de Santa Maria - UFSM

Prof. Dr. Marcelo Santos Guimarães
Instituto de Física Armando Dias Tavares - UERJ

Rio de Janeiro

2022

DEDICATION

I dedicate this work to the true King Artur, my father. And my mother, Rosa, who despite any storm, is always on her feet, bringing color and hope to difficult times.

ACKNOWLEDGMENTS

I would like to thank all my friends who, in the midst of social isolation, always kept in touch and managed to make me feel welcomed. Especially Manuela Correa, my research friend. The only person I could share the ideas and progress of the work with in a technical way. Which was a big help.

I also want to thank my family for their support and especially Larissa Zucatelli, my partner in life. In addition to putting up with me most of the time, she helped me a lot and helps me whenever she can to improve my fluency, whether in writing or speaking the English language.

Finally, I would like to thank my advisor, Professor Rudnei. That in addition to accepting me as a student, he supported me and believed in me for the construction of this work.

This work was carried out with the support of the Coordination for the Improvement of Higher Education Personnel - Brazil (CAPES) - Financing Code 001.

ABSTRACT

FERREIRA, M. C. *Nonperturbative free energy and phase transition for a complex scalar field theory*. 2022. 140 f. Dissertação (Mestrado em Física) - Instituto de Física Armando Dias Tavares, Universidade do Estado do Rio de Janeiro, Rio de Janeiro, 2022.

In this work we study thermal and chemical potential contributions to the mass at two loops and to the free energy at three loops for a charged scalar field. We also make use of the optimized perturbation theory to obtain nonperturbative results and for the phase transition analysis of the model at finite temperature and chemical potential, in the high temperature approximation.

Keywords: Chemical potential. Complex field. Symmetry breaking restoration. Thermal field theory. Quantum field theory at finite temperature.

RESUMO

FERREIRA, M. C. *Energia livre e transição de fase não perturbativa para uma teoria escalar complexa*. 2022. 140 f. Dissertação (Mestrado em Física) - Instituto de Física Armando Dias Tavares, Universidade do Estado do Rio de Janeiro, Rio de Janeiro, 2022.

Neste trabalho estudamos contribuições térmicas e de potencial químico finito para a massa a dois laços, e para a energia livre a três laços, de um campo escalar carregado. Também fazemos uso da teoria de perturbação otimizada para obter resultados não perturbativos e para a análise de transição de fase do modelo à temperatura e potencial químico finitos, na aproximação de altas temperaturas.

Palavras-chave: Potencial químico. Transição de fase. Campo complexo. Quebra de simetria. Teoria de campos a temperatura e potencial químico finitos.

LIST OF FIGURES

Figure 1 - Diagrammatic description of the propagators in a QFT	26
Figure 2 - Tadpole Feynman diagram	27
Figure 3 - Possible combinations of the interaction three level	27
Figure 4 - Wick theorem for Feynman diagram involving the leading order correction for the propagator of the ϕ_1 field	28
Figure 5 - The Keldysh Contour	29
Figure 6 - Two loop self-energy diagram	30
Figure 7 - Real-time path formalism, the consistent description of the Feynman diagrams in the real-time formulation	31
Figure 8 - Pictorial diagrammatic representation of the effective potential, up to two-loop order	36
Figure 9 - Diagrammatically representation of the effective potential, up to one-loop order with the finite temperature contributions, where the n^\pm stands for the Bose-Einstein distribution factor	39
Figure 10 - Free energy of a scalar theory at order λ^2	40
Figure 11 - The setting sun diagram, a Feynman diagram with two loops and two external legs	47
Figure 12 - Pictorial representation of the setting sun diagram at finite temperature and chemical potential	58
Figure 13 - The basketball diagram	72
Figure 14 - Pictorial representation of the basketball contributions	75
Figure 15 - Self-energy contributions to the scalar field at $T=0$	84
Figure 16 - One-loop pressure P varying with T	88
Figure 17 - One-Loop Pressure P varying with T	89
Figure 18 - One-loop entropy S varying with the temperature T	90
Figure 19 - Bose-Einstein integrals h' 's varying with μ	91
Figure 20 - Thermal Free energy normalized by the one-loop free energy, for $\alpha = 0.1$ and $\alpha = 0.4$	92

Figure 21 - Thermal pressure ($P \equiv P_{T \neq 0} - P_{T=0}$) as a function of the temperature T , at $\mu/M = 0.5$, for $\alpha = 0.4$, normalized by the ideal gas pressure P_{ideal} ..	93
Figure 22 - Thermal pressure ($P \equiv P_{T \neq 0} - P_{T=0}$) as a function of the chemical potential μ , at $T/M = 4$, for $\alpha = 0.4$, normalized by the ideal gas pressure P_{ideal}	94
Figure 23 - The normalized thermal pressure at $\mu/M = 0.5$, $T/M = 20$ and $m^2 = M^2$ varying with the coupling λ	95
Figure 24 - The normalized thermal pressure at $\mu/M = 0.6$ and $\mu/M = 0$. $T/M = 20$ and $m^2 = M^2$ varying with the coupling $\sqrt{\lambda/24}$	96
Figure 25 - The normalized thermal pressure at $\mu/M = 0.5$, $T/M = 20$ and $m^2 = M^2$ varying with the coupling $\sqrt{\lambda/24}$	97
Figure 26 - Perturbative critical point	102
Figure 27 - The scalar field expectation value ξ against T in the minima energy configuration of the theory	106
Figure 28 - Perturbative critical point, without neglecting the mas term (blue curve) and neglecting the mass term (black dashed curve)	106
Figure 29 - V_{eff} against ϕ showing the vacuum degeneracy, the broken phase	107
Figure 30 - The physical masses against T	108
Figure 31 - V_{eff} against ϕ showing the symmetry restoration	109
Figure 32 - OPT effective potential up to order δ , where the green dot is the η insertion	113
Figure 33 - Critical point of the theory, via OPT and perturbation theory, considering $\lambda = 10$	115
Figure 34 - Comparison between the OPT condensate with the perturbative one, where $m^2 = -M^2$ and $\lambda = 1$	116
Figure 35 - Comparison between the OPT condensed for $\lambda = 1$, $m^2 = -M^2$	116
Figure 36 - Comparison between the OPT effective mass and the perturbative one, for $\lambda = 1$ and $m^2 = -M^2$	117
Figure 37 - Effective OPT mass with $\lambda = 1$ and $m^2 = -M^2$	117
Figure 38 - Degenerate vacua, an OPT effective potential with three minimum	118
Figure 39 - OPT effective potential diagrams until order δ^2 , the green dot is the an η^2 insertion	119
Figure 40 - Critical point from OPT δ^2 and δ and considering $\lambda = 1$	121

Figure 41 - Broken phase OPT effective potential to δ^2 order	122
Figure 42 - Chemical potential of coexistence and the critical temperature extracted from the effective mass	123
Figure 43 - Pressure against the coupling, via OPT and perturbation theory. We used $\mu/M = 0.5$, $m^2 = M^2$ and $M = T$	124
Figure 44 - Pressure against the coupling, via OPT. We used $m^2 = M^2$ and $M = T$.	125
Figure 45 - Pressure against Temperature for all orders, via OPT and perturbation theory. We used $\mu/M = 0.5$, $m^2 = M^2$, $\alpha = 0.2 \rightarrow \lambda \approx 31$ and $M = T$	125
Figure 46 - Different variational parameters, with and without chemical potential. For all of them $\lambda = 31$ and $m^2 = M^2$	126
Figure 47 - Mass counterterms that cancel all the divergences associated to the two point function of a U(1) $\lambda\phi^4$ theory up to two-loop	136
Figure 48 - Vertex counterterm	136
Figure 49 - Zero point energy corrections, the vacuum counterterms of a U(1) $\lambda\phi^4$ theory	137
Figure 50 - Bubble corrections	138
Figure 51 - OPT Bubble corrections, the OPT mass counterterms	139

CONTENTS

	INTRODUCTION	14
1	THERMAL FIELD THEORY	17
1.1	Statistical Mechanics	17
1.2	Path Integrals	18
1.2.1	<u>U(1) Scalar Field Theory</u>	21
1.2.2	<u>Dimensional Regularization</u>	24
1.2.3	<u>Interacting Fields and Feynman Diagrams</u>	26
1.3	Effective Potential	32
1.3.1	<u>U(1) One-loop effective potential</u>	36
1.4	Free Energy	39
1.4.1	<u>Vacuum Contributions</u>	40
1.4.1.1	One-loop	41
1.4.1.2	Two-Loops	42
1.4.1.3	Three Loops	43
1.5	Setting Sun	46
1.5.1	<u>Non-thermal Contribution</u>	47
1.6	Thermal Setting Sun	57
1.6.1	<u>Off-Shell Contributions</u>	59
1.6.1.1	One Bose-Einstein Contribution	59
1.6.1.2	Two Bose-Einstein Contribution	60
1.6.1.3	Off-Shell High-T Expansion	61
1.6.2	<u>On-Shell Setting sun Diagram</u>	65
1.6.2.1	One Bose-Einstein	65
1.6.2.2	Two Bose-Einstein	66
1.6.2.3	On-Shell High-T Expansion	67
1.7	Basketball Diagram	72
1.7.1	<u>I_0 Term</u>	72
1.8	Thermal Basketball	73
1.8.1	<u>One Bose-Einstein factor</u>	76

1.8.2	<u>Two Bose-Einstein factors</u>	77
1.8.3	<u>Three Bose-Einstein factors</u>	79
1.9	Physical Parameters	83
1.9.1	<u>Physical Mass</u>	84
1.9.1.1	One-Loop Contribution	84
1.9.1.2	Two-Loop Contributions	85
1.9.2	<u>Physical Coupling</u>	86
2	PERTURBATIVE ANALYSES	88
2.1	Two and Three loops Free energy	91
2.2	The Thermal Mass	98
2.3	Phase Transition	103
2.3.1	<u>The One-Loop Thermodynamic Potential</u>	103
3	OPTIMIZED PERTURBATION THEORY	110
3.1	OPT Effective Potential at order δ	112
3.1.1	<u>Critical Point in the OPT Approach</u>	114
3.1.2	<u>OPT Phase Transition</u>	115
3.1.2.1	OPT Effective Potential at order δ^2	119
3.2	OPT Thermal Mass	122
3.3	Symmetric Phase	124
3.4	Changing the prescription for the OPT optimization	126
3.4.1	<u>PMS</u>	126
	CONCLUSIONS	128
	REFERENCES	129
	APPENDIX A - REGULARIZATION FORMULAS	133
	APPENDIX B - THERMAL FUNCTIONS	135
	APPENDIX C - COUNTERTERMS AND CORRECTIONS	136

INTRODUCTION

Many systems in nature are subject to thermal effects, where the ambient temperature is different from zero (KAPUSTA, 2006; LE BELLAC, 1996; KLEINERT, 1990). Likewise, in the presence of conserved charges, chemical potentials can play an important role. These effects may be present in the early Universe, and also in dense astrophysical objects such as compact stars, or even materials subjected to high pressures.

Of key interest, when we examine the history of the Universe, the ideas of phase transition emerge. Phase transitions, in the early Universe, have received much attention (GUTH; WEINBERG, 1981b; STEINHARDT, 1981; LINDE, 2008) in conjunction with a desire to unify the laws of particle physics. The idea is that nature has a high degree of symmetry, which relates the various observed particles to one primordial state. The Universe once existed in this unified state but, through a series of phase transitions, the symmetry (or symmetries) was spontaneously broken. This phenomena (known as spontaneous broken symmetry) is well observed today and it is a part of the Higgs mechanism, which is related to the electro-weak unification (PICH, 2007; SALAM, 1968; WEINBERG, 1967). The consequences of phase transitions reach beyond particle physics and can be used to solve various cosmological questions. It is possible that a phase transition may have driven a period of accelerated expansion of the Universe, also known as inflation (LINDE, 2008; GUTH, 1981a).

Besides the Higgs particle, which is described by a scalar field, effective scalar field theories can describe elements of quantum chromodynamics (QCD), for example in the description of pions as approximate Goldstone bosons (WEINBERG, 2013). Also, in terrestrial systems, such as atomic fluids, the atoms and their interactions can be effectively described by a model with an interacting scalar field (YUKALOV, 2011).

As cosmologists and condensed matter theorists have learnt to exchange their ideas, we may also examine the laboratory phenomenon of phase transition in a cosmological setting. We may investigate how finite scalar charges may affect phase transition in general.

Perturbation theory is one of the most important tools in physics, especially in high energy physics. In the last topic, when temperature effects can emerge from high energy scattering, the perturbation is not always applicable (WEINBERG, 1974; FARIAS;

RAMOS; KREIN, 2008). In high orders of perturbation theory, the thermal corrections can start to deviate from low order terms. This is a well known problem of thermal field theory. All attempts to study particle physics in extreme conditions have this problem. There are many of ways to handle this problem related to thermal fields. In this dissertation, we will work with the Optimized Perturbation Theory (OPT) (STEVENSON, 1981; KNEUR; PINTO, 2015; FARIAS; RAMOS; KREIN, 2008; KNEUR, 2002; PINTO, 2004; FARIAS, 2013; FERNANDEZ; KNEUR, 2021; DUARTE, 2011; MILTON, 1987; JONES; PARKIN, 2001), as a nonperturbative method in our calculations. The OPT has shown to produce results that are in very good agreement with the lattice computations (BENGHI, 2021) and gives us convergent results in terms of Feynman integrals (SEZNEC; ZINN-JUSTIN, 1979; STEVENSON, 1981; FARIAS; RAMOS; KREIN, 2008; KNEUR; PINTO, 2015).

Applying this technique, in this dissertation, for the thermal mass and the free energy of a relativistic superfluid model, with spontaneous symmetry breaking, we derive essential thermodynamic quantities. We derive the mass spectrum of the theory up to second order using the aforementioned nonperturbative scheme (which, as we are going to show, includes up to three loop terms explicitly). We also developed the same construction for the effective thermodynamic potential of the model, which is derived by including one, two and three loop terms, the calculation of the potential including the effects of chemical potential is new in the literature. In the phase transition for this model, there is an issue that appears frequently in literature. This type of theory corresponds to a well known universality class, which has a second order phase transition (YUKALOV; YUKALOVA, 2014). However, since we are summing different terms, this type of system can undergo a first-order transition. We are studying proposals to solve this problem, using the Optimized Perturbation Theory (OPT) with the Renormalization Group Equations (RGE).

This work is organized as follows. In chapter 1, we begin with the presentation of the relevant field theory framework, which is necessary to tackle our problems, at the same time we introduce the model for our applications. We also elucidate some concepts about the theory of thermal fields and compute all the desired terms needed for the discussions carried out throughout this work.

Chapter 2 presents the advantages and disadvantages of applying perturbative

calculations to thermodynamic quantities and for the phase transition analysis. Along this, we begin to show some motivations that imply that nonperturbative techniques are required.

Chapter 3 proposes the Optimized Perturbation Theory as an alternative to deal with most of problems discussed in previous chapters. In chapter 4, we finish the work with a discussion about the applications of the concepts and results developed here, with views for possible future works.

1 THERMAL FIELD THEORY

In this chapter we present the formalism of a thermal field theory and all the required computations for the further discussions. Throughout this work we consider the metric signature $(+ - - -)$ and the natural units, where $c = \hbar = k_B = 1$.

1.1 Statistical Mechanics

We shall consider a system characterization by a Hamiltonian H , and a set of conserved charge operators Q_i which satisfy $[H, Q_i] = 0$. Equilibrium in a large volume V is described by the grand-canonical density operator,

$$\rho = e^{-\beta(H - \mu_i Q_i)}. \quad (1)$$

The β is related to the temperature by $\beta = T^{-1}$ and μ_i are the chemical potentials. After defining the partition function as

$$Z = \text{Tr}\{\rho\}, \quad (2)$$

we can relate it to various thermodynamic quantities,

$$N_i = T \frac{\partial}{\partial \mu_i} \ln Z, \quad (3)$$

$$S = \frac{\partial}{\partial \mu_i} T \ln Z, \quad (4)$$

$$P = T \frac{\partial}{\partial V} \ln Z, \quad (5)$$

$$E = TS - T \ln Z + \mu_i N_i, \quad (6)$$

which corresponds to the particles number, entropy, pressure and energy respectively. By performing the differentiation in these expressions, we have:

$$N_i = \frac{1}{Z} \text{Tr}\{\rho Q_i\} , \quad (7)$$

$$S = \ln Z - \frac{1}{Z} \text{Tr}\{\rho \ln \rho\} , \quad (8)$$

$$E = \frac{1}{Z} \text{Tr}\{\rho H\} . \quad (9)$$

The above quantities are constructed as weighted averages over a complete set of quantum field states. In the next few sections we shall demonstrate how the grand partition function Z is typically calculated, through a path integral formalism.

1.2 Path Integrals

The path integral quantization (KLEINERT, 1990) follows a different methodology than the canonical quantization, in a sense that, instead of promoting the fields to operators, we will think in terms of a functional that can give us the probability amplitude of a particle. The probability amplitude can be a superposition, for example, of the two possible amplitudes if you have a double slit experiment. Now, if you have more slits in this "experiment", you could have more and more ways or paths that the amplitude could assume. In this way, we can build a functional that considers all paths, from a point A to B. It is possible from the amplitude transition representation of two quantum states to obtain

$$\langle \phi_a | e^{-iHt} | \phi_a \rangle = \int [d\pi] \int_{\phi(\vec{x},0)=\phi_a(\vec{x})}^{\phi(\vec{x},t)=\phi_a(\vec{x})} [d\phi] e^{i \int_0^t dt' \int d^3x \left(\pi(\vec{x},t) \frac{\partial \phi(\vec{x},t)}{\partial t} - \mathcal{H}(\pi(\vec{x},t), \phi(\vec{x},t)) \right)} , \quad (10)$$

where the symbols $[d\pi]$ and $[d\phi]$ denote functional integration. The integration over $\pi(\vec{x}, t)$ is unrestricted, but the integration over $\phi(\vec{x}, t)$ is such that the field starts at $\phi_a(\vec{x})$ at

$t' = 0$ and ends at $\phi_a(\vec{x})$ at $t' = t$. Note that,

$$Z = \text{Tr} e^{-\beta(H - \mu_i N_i)} = \sum_a \int d\phi_a \langle \phi_a | e^{-\beta(H - \mu_i N_i)} | \phi_a \rangle, \quad (11)$$

where the sum runs over all states and we have used a completeness relation built with the field ket state $|\phi_a\rangle$ to write the trace operation. This expression is very similar to that for the transition amplitude defined in the previous section. In fact we can express Z as an integral over fields and their conjugate momenta by making use of (10). In order to make that connection, we switch to an imaginary time variable $t \rightarrow i\tau$. The trace operator in (11) simply means that we must integrate over all ϕ_a . Finally, if the system admits a conserved charge then we must make the replacement

$$\mathcal{H} \rightarrow \mathcal{H} - \mu\mathcal{N} \quad (12)$$

where \mathcal{H} and \mathcal{N} are the Hamiltonian and conserved charge density. We arrive at,

$$Z = \int [d\pi] \int_{\text{periodic}} [d\phi] e^{\int_0^\beta d\tau' \int d^3x \left(i\pi \frac{\partial\phi}{\partial\tau} - \mathcal{H}(\pi, \phi) + \mu\mathcal{N} \right)}, \quad (13)$$

where ‘‘periodic’’ means that the integration over the field is constrained in such a way that $\phi(\vec{x}, 0) = \phi(\vec{x}, \beta)$. This follows from the trace operation, setting $\phi_a(\vec{x}) = \phi(\vec{x}, 0) = \phi(\vec{x}, \beta)$, (LE BELLAC, 1996).

The periodic conditions discussed above, gives also origin to the so called Kubo-Martin-Schwinger (KMS) relation (KAPUSTA, 2006; LE BELLAC, 1996). Given some two-point correlation functions, we have

$$\langle \phi(\vec{x}, -i\beta) \phi(\vec{y}, -i\tau) \rangle = \langle \phi(\vec{x}, 0) \phi(\vec{y}, -i\tau) \rangle, \quad \text{where } \beta \equiv 1/T. \quad (14)$$

The relation above is called the KMS condition. It is a fundamental result that follows from the fact that for a system in a thermal equilibrium, any measure of some observable \mathcal{O} is written in terms of the ensemble,

$$\langle \mathcal{O}(t) \rangle = \frac{1}{Z} \text{Tr}(e^{-\beta H} \mathcal{O}(t)). \quad (15)$$

But since $O(t) = e^{tHi}O(0)e^{-tHi}$ and using the trace cyclicity,

$$\langle \mathcal{O}(t) \rangle = \frac{1}{Z} \text{Tr}(e^{-\beta H} \mathcal{O}(t)) = (e^{-\beta H} e^{iH(t-i\beta)} O(0) e^{-iH(t-i\beta)}) = \langle \mathcal{O}(t - i\beta) \rangle, \quad (16)$$

we extract once more the thermal condition $\phi(\vec{x}, 0) = \phi(\vec{x}, \beta)$ for the fields. The observables of the theory are described in terms of these two-point correlation functions (14) called propagators and they obey the same periodicity (for simplicity, we will omit the space labeling),

$$\Delta(\tau) = \Delta(\tau - \beta). \quad (17)$$

In order to capture physical answers, the propagators and the fields need to be single-valued functions and, because of that, the time component of the field has to be discrete. Because of the periodic conditions the fields are delimited to the interval like $[0, \beta]$ and our correlation functions appear in terms of Bose-Einstein factors (LE BELLAC, 1996), which will give us a precise description about some observable quantities, like temperature (T), chemical potential (μ), in the case of charged fields, entropy (S) and others thermodynamic variables. Now, we need to show how to compute these propagators. The functional (13) has the same general structure of an integral over all possible configurations of an exponential statistical weight. Observable properties of a system can be extracted from the correlation functions, or the Green's functions. This applies to extensive thermodynamical quantities such as the energy and charge density. The n -leg scalar Green's function is defined as

$$\begin{aligned} G(x_1 \dots x_n) &= \langle 0 | T \phi(x_1) \phi(x_2) \dots \phi(x_n) | 0 \rangle \\ &= Z[0]^{-1} \left(-i \frac{\delta}{\delta J(x_1)} \right) \left(-i \frac{\delta}{\delta J(x_2)} \right) \dots \left(-i \frac{\delta}{\delta J(x_n)} \right) Z[J] |_{J=0}, \end{aligned} \quad (18)$$

where T is the time-ordering operator¹ (DYSON, 1949),

$$T(O_1(t_2), O_2(t_1)) = \begin{cases} O_1(t_1)O_2(t_2) & t_1 > t_2 \\ O_1(t_2)O_2(t_1) & t_2 > t_1 \end{cases}, \quad (19)$$

and $Z[J]$ is

$$Z[J] = Z[0]^{-1} \int d[\phi][d\pi] e^{\int_0^\beta d\tau \int d^3x (i\pi\dot{\phi} - \mathcal{H} + \mu\mathcal{N} + J\phi)}, \quad (20)$$

where the source $J(x)$ plays the role of an external field. In fact, our method of computing correlation functions by differentiating them with respect to $J(x)$, give us the correlation functions of our model. The $Z[0]$ is just the thermodynamic partition function without external sources.

1.2.1 U(1) Scalar Field Theory

In this work we shall investigate a model consisting of one complex scalar field $\phi = (\phi_1 + i\phi_2)/\sqrt{2}$, with $U(1)$ -invariant Hamiltonian and conserved charge Q :

$$\mathcal{H} = \frac{1}{2} [\dot{\phi}_1^2 + \dot{\phi}_2^2 + (\nabla\phi_1)^2 + (\nabla\phi_2)^2 + m\phi_1^2 + m\phi_2^2] + \frac{1}{24} \lambda(\phi_1^2 + \phi_2^2)^2, \quad (21)$$

$$Q = \int d^3x \mathcal{N} = \int d^3x (\phi_2\dot{\phi}_1 - \phi_1\dot{\phi}_2), \quad (22)$$

where $\dot{\phi} \equiv \pi$. The complex field ϕ describes bosons of positive and negative electric charge, where they represents the particle and the anti-particle of the model. Note that, if $\phi_2 = 0$ we can get a \mathcal{Z}_2 theory there will be no charge associated with this theory, because $Q = 0$. The Lagrangian density, that follows from Eq. (21) is,

$$\mathcal{L} = \partial_\mu\phi^*\partial^\mu\phi - m^2\phi^*\phi - \frac{\lambda}{3!}(\phi^*\phi)^2. \quad (23)$$

¹Introduced by Freeman Dyson (DYSON, 1949), in order to deal with situations like $[H(t_1), H(t_2)] \neq 0$ as well.

Now, let us turn our attention to the partition function (13). Using (21) and (22) in (13), we obtain

$$Z[J] = N' \int_{\text{periodic}} d[\phi_1]d[\phi_2] \exp \left\{ \int_0^\beta d\tau \int d^3x \left[-\frac{1}{2}(\dot{\phi}_1 - i\mu\phi_2)^2 - \frac{1}{2}(\dot{\phi}_2 + i\mu\phi_1)^2 \right. \right. \\ \left. \left. - \frac{1}{2}(\nabla\phi_1)^2 - \frac{1}{2}(\nabla\phi_2)^2 - \frac{1}{2}m^2\phi_1^2 - \frac{1}{2}m^2\phi_2^2 - \frac{\lambda}{24}(\phi_1^2 + \phi_2^2)^2 + J_1\phi_1 + J_2\phi_2 \right] \right\}, \quad (24)$$

where we have integrated out the conjugate momenta π_1 and π_2 and N' is just a normalization factor. Let us use the notation ϕ_a , ($a = 1, 2$) and split the Lagrangian density into free and interaction components, in the Minkowski space we have

$$\mathcal{L}_0 = \frac{1}{2}(\partial_t\phi_1 + \mu\phi_2)^2 + \frac{1}{2}(\partial_t\phi_2 + \mu\phi_1)^2 - \frac{1}{2}(\nabla\phi_a)^2 - \frac{1}{2}m^2\phi_a^2, \quad (25)$$

$$\mathcal{L}_I = -\frac{\lambda}{24}(\phi_a\phi_a)^2. \quad (26)$$

In the same way that functional differentiation can be used to generate Green functions from the generating functional, we may account for the interaction Lagrangian density as follows,

$$Z[J] = N \exp \left\{ \int_0^\beta d\tau \int d^3x \mathcal{L}_I \left[\frac{\delta}{i\delta J(z)} \right] \right\} Z_0[J]. \quad (27)$$

Here, $Z_0[J]$ is the generating functional for the free theory,

$$Z_0[J] = N \int [d\phi_{1,2}] e^{i \int d^4x [\mathcal{L}_0 + J_a\phi_a]}. \quad (28)$$

It becomes convenient to write the free Lagrangian density in the form,

$$\mathcal{L}_0 = \frac{1}{2}\phi_a K_{ab}\phi_b, \quad (29)$$

where K is a differential operator given by,

$$K_{ab} = \begin{pmatrix} -\partial_t^2 + \nabla^2 - m^2 + \mu^2 & -2\mu\partial_t \\ 2\mu\partial_t & -\partial_t^2 + \nabla^2 - m^2 + \mu^2 \end{pmatrix}, \quad (30)$$

which allow us to define the propagator matrix of the theory,

$$G_{ab}(\vec{k}) = \frac{1}{\det K_{ab}} \begin{pmatrix} k_4^2 + \vec{k}^2 + m^2 - \mu^2 & -2\mu k_4 \\ 2\mu k_4 & k_4^2 + \vec{k}^2 + m^2 - \mu^2 \end{pmatrix} = \begin{pmatrix} G_{11} & G_{12} \\ G_{21} & G_{22} \end{pmatrix} \quad (31)$$

where, in passing from Eq. (30) to (31), we have gone to momentum space and considered the transformation to Euclidean space, where $k_0 = ik_4$ and

$$\det K_{ab} = [(k_4 + i\mu)^2 + \vec{k}^2 + m^2][(k_4 - i\mu)^2 + \vec{k}^2 + m^2]. \quad (32)$$

To show how we can handle with these propagators, let us take $\ln Z_0[0]$,

$$\begin{aligned} \ln Z_0[0] &= V \ln\{G_{ab}(\vec{k})^{-1/2}\} \\ &= -\frac{1}{2} \sum_n \sum_p \ln\{\beta^2[\omega_n^2 + (\omega_p - \mu)^2]\} - \frac{1}{2} \sum_n \sum_p \ln\{\beta^2[\omega_n^2 + (\omega_p + \mu)^2]\} \end{aligned} \quad (33)$$

where $\omega_n = 2\pi nT$ (with $n \in \mathbf{Z}$) are the Matsubara frequencies and $\omega_p = \sqrt{\vec{p}^2 + m^2}$.

Using the following identities,

$$\ln[(\beta^2\omega_n^2 + \beta^2\omega_p^2)] = \int_1^{\beta^2\omega_p^2} \frac{d\theta^2}{\theta^2 + \omega_n^2} + \ln[1 + \omega_n^2], \quad (34)$$

$$\sum_{n=-\infty}^{\infty} \frac{1}{\omega_n^2 + \omega_p^2} = \frac{1}{2\omega_p} \left[1 + \frac{2}{e^{\beta(\omega_p)} - 1} \right], \quad (35)$$

and dropping a temperature-independent term, we can write

$$\ln Z = - \sum_{\vec{p}} \int_1^{\beta\omega_p} d\theta \left(\frac{1}{2} + \frac{1}{e^\theta - 1} \right). \quad (36)$$

Carrying out the integral and dropping terms that are independent of temperature and volume, we finally get,

$$\ln Z_0 = -V \int \frac{d^3p}{(2\pi)^3} [\beta\omega_p + \ln(1 - e^{-\beta(\omega_p - \mu)}) + \ln(1 - e^{-\beta(\omega_p + \mu)})].$$

The $\mathcal{F}_0 = -(\ln Z_0)/\beta$ is the free energy of the system. For that we have,

$$\mathcal{F}_0 = V \int \frac{d^3p}{(2\pi)^3} \left[\omega_p + \frac{1}{\beta} \ln(1 - e^{-\beta(\omega_p - \mu)}) + \frac{1}{\beta} \ln(1 - e^{-\beta(\omega_p + \mu)}) \right], \quad (37)$$

where the first term represents the zero point energy and the second the thermal contribution to the vacuum of the theory. For the first term we need to define the regularization method that we will use here and along the work. We will use the dimension regularization with the modified minimal subtraction scheme (\overline{MS}) (T'HOOFT; VELTMAN, 1972), which means,

$$\int \frac{d^4p}{(2\pi)^4} \rightarrow \left(\frac{e^{\gamma_E} M}{4\pi} \right)^{2-d/2} \int \frac{d^d p}{(2\pi)^d} \quad (38)$$

where M is a regularization scale which has dimension of mass, $d = 4 - 2\epsilon$ and γ_E is the Euler-Mascheroni constant ($\gamma_E = 0.5772156649$). Here is a good moment to make some important observations about dimensional regularization:

1.2.2 Dimensional Regularization

This regularization scheme was introduced by t'Hoof and Veltman (T'HOOFT; VELTMAN, 1972). It consists of treating loop integrals over arbitrary d-dimensional momenta and then, taking the limit $d \rightarrow 4$. The divergences of the integrals arise in the form of singularities with poles in $(d - 4)^{-1}$ and have to be subtracted out. By choice, we will work with the modified minimal subtraction renormalization scheme (\overline{MS}) (T'HOOFT; VELTMAN, 1972). In dimensional regularization we replace the four-momenta integrals

by a d -dimensional integral of the form

$$\int \frac{d^4 k}{(2\pi)^4} \rightarrow (M'^2)^{2-d/2} \int \frac{d^d k}{(2\pi)^d} \quad (39)$$

where the (\overline{MS}) means $M'^2 \rightarrow M^2 e^{\gamma_E}/(4\pi)$. The parameter M is called the regularization scale, all the parameters of the theory will depend on him, defining naturally a "validation scale" of our model. For example, the behavior of the coupling constant λ as a function of M determines the strength of the interaction and the conditions under which perturbation theory is valid. Now, before we start applying the method, it is useful to discuss the power counting². We can count the degree of the divergence by an algebraic analysis of the momenta dependency in the propagators or simply apply that:

$$d(\gamma) = dL - 2I \quad (40)$$

where $d(\gamma)$ is the superficial degree of divergence of a certain diagram, where d is the dimension of the theory, L the loops and I the internal legs of the desired topology. In case of a tadpole, we have $d(\gamma) = 2$, which means a quadratic divergence. If $d(\gamma) = 0$ we have a logarithm divergence. Applying the dimensional regularization to the first term of (37),

$$\left(\frac{e^{\gamma_E} M}{4\pi}\right)^{2-d/2} \int \frac{d^{d-1} p}{(2\pi)^{d-1}} \frac{1}{(\vec{p}^2 + m^2)^{-1/2}} = \frac{m^4}{(4\pi)^2} \left(\frac{M}{m}\right)^{2\epsilon} e^{\gamma_E \cdot \epsilon} \frac{\Gamma[\epsilon - 1]}{(1 - \epsilon)} \quad (41)$$

where we use the formula in the Appendix A and set $d = 4 - 2\epsilon$. The second term is finite and can be written in terms of the thermal functions of the Appendix B,

$$\mathcal{F}_0 = \frac{m^4}{(4\pi)^2} \left(\frac{M}{m}\right)^{2\epsilon} e^{\gamma_E \cdot \epsilon} \frac{\Gamma[\epsilon - 1]}{(1 - \epsilon)} - \frac{8T^4}{\pi^2} h_5^\epsilon(y, r), \quad (42)$$

where $y = m\beta$, $r = \mu/m$ and h_5^ϵ is the integral in Eq. (37), also defined in Appendix B. We will understand the meaning of this result in the next sections, but basically the first term of the equation above (42) will give us the counterterms required to subtract the divergence associated with this contribution. The second term of (42) gives us all the information about the temperature and the chemical potential of this interaction.

²For details about the power counting or anything on renormalization theory, see (PIGUET; SORELLA, 1995)

1.2.3 Interacting Fields and Feynman Diagrams

Considering the interaction, the J_a -independent path integral of (27) is the free partition function $Z_0[0]$ and we have,

$$Z[J] = Z_0[0]^{-1} \exp \left\{ i \int d^4x \mathcal{L}_I \left[\frac{\delta}{i\delta J(z)} \right] \right\} \\ \times \exp \left\{ -i \int d^4x d^4y \left[\frac{1}{2} J_a(x) G_{ab}(x-y) J_b(y) \right] \right\}. \quad (43)$$

It is not trivial to do the identification $\phi \rightarrow \delta/\delta J(x)$; for this and other details, see (RYDER, 1996). The functional above can give us all possible interactions that the theory can assume, but doing all those functional derivatives can be a little exhausting for high order interactions. For that, Feynman has created a beautiful way to write down any desired interaction that came from this functional.

Basically, we will separate them in two types: Figure 1. Any other topology can be built by the combination of those two.

Figure 1. - Diagrammatic description of the propagators in a QFT

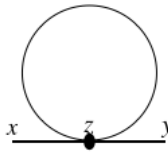
$$G(x-y) \equiv \overset{x}{\text{---}} \text{---} \overset{y}{\text{---}} \quad G(0) \equiv \bigcirc$$

Source: The author, 2022.

All diagrams come with a symmetry factor, that can be determined explicitly doing the functional derivatives, or via Wick theorem (PESKIN; SCHROEDER, 1995). It basically states that a string of creation and annihilation operators can be rewritten as the normal-ordered product of the string plus the normal-ordered product, after all single contractions among operator pairs. But there is a simple way to understand this theorem, in terms of diagrams. Take the interaction term in terms of the real fields

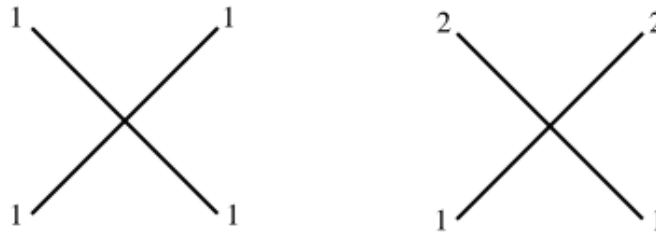
$$\frac{\lambda}{24} (\phi\phi^*)^2 = \frac{\lambda}{24} (\phi_1^2 + \phi_2^2)^2. \quad (44)$$

Now, write down the desired diagram. Let us take, for example, the tadpole diagram. Once we have two fields ϕ_1 and ϕ_2 , we will have two tadpole diagrams like the one at Figure 2. - Tadpole Feynman diagram

$$(-\lambda)G(0) \int d^4z G(x-z)G(z-y) \equiv \text{Diagram}$$


Source: The author, 2022.

Figure 2. The black dot is the vertex of the diagram, meaning a $(-i\lambda)$ insertion. We already know how many diagrams there are, but we don't know the symmetry factor. For that, we need to re-write these two tadpole diagrams in terms of the interaction, counting Figure 3. - Possible combinations of the interaction three level



Source: The author, 2022.

all the possible ways to connect two legs and form the tadpoles. By doing that, and multiplying by $\lambda/24$ we get the symmetry factors identifying the diagrams of Figure 3 as the following figure, in other words connecting the legs of Figure 3 in all possibilities to form Figure 4.

The result in terms of the propagators are, what stands for one possible contributions of the chemical potential $\pm\mu$, for both possible signs:

$$G^{(2)}(0) = \frac{1}{2} \frac{2\lambda}{3} \int \frac{d^4k_E}{(2\pi)^4} \frac{(-1)}{(k_4 + i\mu)^2 + \vec{k}^2 + m^2} + \frac{1}{2} \frac{2\lambda}{3} \int \frac{d^4k_E}{(2\pi)^4} \frac{(-1)}{(k_4 - i\mu)^2 + \vec{k}^2 + m^2}, \quad (45)$$

where the superscript in $G^{(2)}(0)$ means a two point correlation function (in the limit

Figure 4. - Wick theorem for Feynman diagram involving the leading order correction for the propagator of the ϕ_1 field

Source: The author, 2022.

$x \rightarrow y$). In the above equations we have also expressed the momentum integrals in Euclidean space, with $d^4k_E = dk_4 d^3\vec{k}$. These propagators are Green's function. Using the translation property

$$\int d^d p \Delta_F(p+q) = \int d^d p \Delta_F(p) \quad (46)$$

satisfied by the propagators, we can re-write them as

$$G^{(2)}(0) = \frac{-2\lambda}{3} \int \frac{d^4k_E}{(2\pi)^4} \frac{1}{k_4^2 + \vec{k}^2 + m^2} . \quad (47)$$

Note that, it is not always possible to get rid of the chemical potential! Actually, we can do it for the vacuum contributions of the theory, since in the vacuum $\mu = 0$ and $T = 0$. For any other diagram that has external legs, we need to look carefully. In case of two external legs diagrams, even with the translation property (46), the chemical potential does not vanish in the propagators. Instead of using the imaginary time formalism, we can also apply the real-time formulation, elucidated by Dolan and Jackiw in the 70's (DOLAN; JACKIW, 1974), meaning (in the Minkowski space):

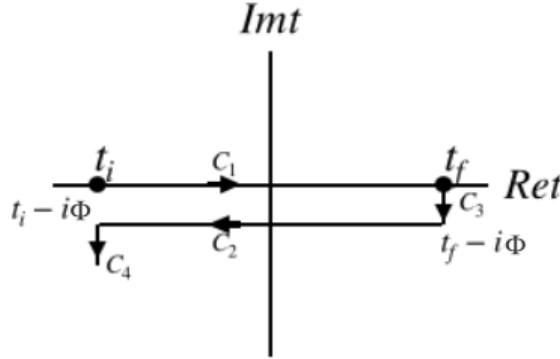
$$\frac{i}{(p_0 + \mu)^2 - \omega_p^2 + i\sigma} \rightarrow i \left[\frac{i}{(p_0 + \mu)^2 - \omega_p^2 + i\sigma} + n^{(\mu)}(p_0 \text{sgn}(p_0 + \mu)) \right. \\ \left. \times 2\pi \delta((p_0 + \mu)^2 - \omega_p^2) \right] , \quad (48)$$

where $\omega_p = \sqrt{p^2 + m^2}$. The $n^{(\mu)}$ is defined as

$$n^{(\mu)}(p_0 \text{sgn}(p_0 + \mu)) = \begin{cases} n(p_0), & \text{for } p_0 + \mu > 0 \\ n(-p_0), & \text{for } p_0 + \mu < 0 \end{cases}, \quad (49)$$

and the $n(p_0)$ is the Bose-Einstein distribution. The time variable of those fields goes from some initial time $t = t_i$ to $t = t_i - i\beta$. We can then express the fields in terms of a contour in the complex time plane. In the imaginary time formalism this contour involves only the imaginary axis, a straight line from $t = t_i$ down to $t = t_i - i\beta$. We can always make an appropriate choice of contour in order to include the real time axis. One possible choice of contour that satisfies the above requirements is the one shown in Figure 5, called the Keldysh contour (KAPUSTA, 2006; LE BELLAC, 1996). For the complex scalar field with a chemical potential, the components of the propagator in the closed time (or Keldysh contour) path formalism become complicated:

Figure 5. - The Keldysh Contour



Source: The author, 2022.

The initial and final times are then set to infinity: $t_i \rightarrow -\infty$ and $t_f \rightarrow +\infty$.

$$G_{\text{Keldysh}}(x - x') = i \int \frac{d^4 k}{(2\pi)^4} e^{ik(x-x')} \begin{pmatrix} G_{++}^{(T,\mu)} & G_{+-}^{(T,\mu)} \\ G_{-+}^{(T,\mu)} & G_{--}^{(T,\mu)} \end{pmatrix}, \quad (50)$$

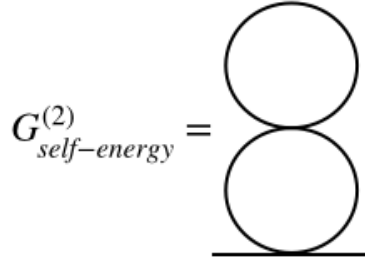
where,

$$G_{++}^{(T,\mu)} = \frac{i}{(p_0 + \mu)^2 - \omega_p^2 - i\sigma} + n^{(\mu)}(p_0 \text{sgn}(p_0 + \mu)) 2\pi \delta((p_0 + \mu)^2 - \omega_p^2)$$

$$\begin{aligned}
G_{+-}^{(T,\mu)} &= 2\pi \left[\theta(-p_0 - \mu) + n^{(\mu)}(p_0 \operatorname{sgn}(p_0 + \mu)) \right] \delta\left((p_0 + \mu)^2 - \omega_p^2\right) \\
G_{-+}^{(T,\mu)} &= 2\pi \left[\theta(p_0 + \mu) + n^{(\mu)}(p_0 \operatorname{sgn}(p_0 + \mu)) \right] \delta\left((p_0 + \mu)^2 - \omega_p^2\right) \\
G_{--}^{(T,\mu)} &= \frac{-i}{(p_0 + \mu)^2 - \omega_p^2 + i\sigma} + n^{(\mu)}(p_0 \operatorname{sgn}(p_0 + \mu)) 2\pi \delta\left((p_0 + \mu)^2 - \omega_p^2\right). \quad (51)
\end{aligned}$$

The consequence of this choice gives us a right prescription of the theory, eliminating all the pinch singularities (DADIĆ, 1999). Those singularities came from all diagrams that have two or more loops, because of the product of the delta functions in the propagators. This is well understood in literature (LE BELLAC, 1996; KAPUSTA, 2006) and you can see explicitly in the work of Ramos and Gleiser (GLEISER; RAMOS, 1994). Let us show an explicitly example: the two loop self-energy diagram (Figure 6). Using the wick theorem as discussed above, is quite easy determinate the symmetry factor and the propagator,

Figure 6. - Two loop self-energy diagram



Source: The author, 2022.

$$G_{Keldysh}^{(2)} = -\frac{4\lambda}{9} \int \frac{d^4p}{(2\pi)^4} \frac{1}{(p_4^2 - \omega_p^2 + i\sigma)^2} \int \frac{d^4k}{(2\pi)^4} \frac{1}{k_4^2 - \omega_k^2 + i\sigma}. \quad (52)$$

Now, if we apply Eq. (48), making the change of variable $p_0 \rightarrow p_0 - \mu$ and $k_0 \rightarrow k_0 - \mu$, we obtain

$$G_{Keldysh}^{(2)} = \frac{4\lambda}{9} \left[\int \frac{d^4p}{(2\pi)^4} \frac{-1}{(p_0^2 - \omega_p^2 + i\sigma)} + in((p_0 - \mu) \operatorname{sgn}(p_0)) 2\pi \delta(p_0^2 - \omega_p^2) \right]^2$$

$$\begin{aligned}
& \times \left[\int \frac{d^4k}{(2\pi)^4} \frac{-1}{(k_0^2 - \omega_k^2 + i\sigma)} + in((k_0 - \mu)sgn(k_0))2\pi\delta(k_0^2 - \omega_k^2) \right] \\
& = \frac{4\lambda}{9} \int_p \int_k \left\{ \frac{1}{(p_0^2 - \omega_p^2 + i\sigma)^2} \times \frac{-1}{(k_0^2 - \omega_k^2 + i\sigma)} + \frac{i}{(p_0^2 - \omega_p^2 + i\sigma)^2} \right. \\
& \times n((k_0 - \mu)sgn(k_0))2\pi\delta(k_0^2 - \omega_k^2) + 2n((p_0 - \mu)sgn(p_0))2\pi\delta(p_0^2 - \omega_p^2) \\
& \times \frac{i}{(k_0^2 - \omega_k^2 + i\sigma)} \frac{1}{(p_0^2 - \omega_p^2 + i\sigma)} + \frac{8\pi^2}{p_0^2 - \omega_p^2 + i\sigma} n((p_0 - \mu)sgn(p_0))\delta(p_0^2 - \omega_p^2) \\
& \times n((k_0 - \mu)sgn(k_0))\delta(k_0^2 - \omega_k^2) + \left. \frac{4\pi^2}{(k_0^2 - \omega_k^2 + i\sigma)} \left[n((p_0 - \mu)sgn(p_0))\delta(p_0^2 - \omega_p^2) \right]^2 \right. \\
& \left. - i8\pi^3 n((k_0 - \mu)sgn(k_0))\delta(k_0^2 - \omega_k^2) \left[n((p_0 - \mu)sgn(p_0))\delta(p_0^2 - \omega_p^2) \right]^2 \right\}, \quad (53)
\end{aligned}$$

where $\int_p = \int d^4p/(2\pi)^4$. Note that the last two lines of (53) are problematic, these terms generate what we called before as the pinch singularities. These singularities are not physical, they are related to prescription of the real-time formulation, this is the main reason why we need a good prescription, in other words the reason why we used the Keldysh contour Figure 5. There is a simple way to apply the Keldysh contour (or the closed real-time path formalism): writing the Feynman diagrams for this formalism (Figure 7). Now the desired interaction become:

Figure 7. - Real-time path formalism, the consistent description of the Feynman diagrams in the real-time formulation

$$G_{Keldysh}^{(2)} = \begin{array}{c} \text{+} \\ \text{+} \\ \text{+} \\ \text{+} \end{array} + \begin{array}{c} \text{-} \\ \text{-} \\ \text{+} \\ \text{+} \end{array}$$

Source: The author, 2022.

$$G_{Keldysh}^{(2)} = -\frac{4\lambda}{9} \int_p \int_k \left[G_{++}^{(T,\mu)}(p)G_{++}^{(T,\mu)}(p)G_{++}^{(T,\mu)}(k) - G_{+-}^{(T,\mu)}(p)G_{+-}^{(T,\mu)}(p)G_{--}^{(T,\mu)}(k) \right], \quad (54)$$

where fields from above and below the real time axis (Figure 5) are not mixed at a vertex and the vertex of these fields has an additional minus sign coming from the anti-time ordering of the fields below the real time axis. For the term $G_{+-}^{(T,\mu)}(p)G_{+-}^{(T,\mu)}(p)G_{--}^{(T,\mu)}(k)$ in Eq. (54) what remains if integrated in p_0 will be the delta product, which is a divergent term and the exact delta product we have in $G_{++}^{(T,\mu)}(p)G_{++}^{(T,\mu)}(p)G_{++}^{(T,\mu)}(k)$, then these non-physical divergences cancel out. The Eq. (54) can be rewritten as follows,

$$G_{Keldysh}^{(2)} = -\frac{4\lambda}{9} I_1 \int_p \left[G_{++}^{(T,\mu)}(p)G_{++}^{(T,\mu)}(k) - G_{+-}^{(T,\mu)}(p)G_{+-}^{(T,\mu)}(p) \right], \quad (55)$$

and using that,

$$\delta(p^2 - m^2) = -\frac{1}{\pi} \lim_{\sigma \rightarrow 0} \left(\text{Im} \frac{1}{p^2 - m^2 + i\sigma} \right), \quad (56)$$

we have

$$\begin{aligned} \int_p G_{++}^{(T,\mu)}(p)G_{++}^{(T,\mu)}(k) - G_{+-}^{(T,\mu)}(p)G_{+-}^{(T,\mu)}(p) &= \int \frac{d^4p}{(2\pi)^4} \left(\frac{1}{p^2 - m^2 + i\sigma} \right)^2 \\ -n((p_0 - \mu)\text{sgn}(p_0)) \left[\left(\frac{1}{p^2 - m^2 + i\sigma} \right)^2 - \left(\frac{1}{p^2 - m^2 - i\sigma} \right)^2 \right] &= I_2 \end{aligned} \quad (57)$$

The solution of these integrals are represented explicitly in the Appendix A as,

$$G_{Keldysh}^{(2)} = -\frac{4\lambda}{9} I_1 I_2. \quad (58)$$

All other pinch singularities are handle in the same manner, if the reader still have doubts or do not understand the procedure, these concepts are well understood in many textbooks (LE BELLAC, 1996; KAPUSTA, 2006; DAS, 1997) and it is well known in literature (GLEISER; RAMOS, 1994; BRANDT, 2006), the reader should consult them.

1.3 Effective Potential

To have a complete description of our theory it is convenient to define the effective potential, which is very useful to study the phase transition and spontaneous symmetry

breaking.

The generating functional is related to the connected diagrams by,

$$W[J] = -i \ln Z[J] . \quad (59)$$

The effective action is related to $W[J]$ by a Legendre transform

$$\Gamma[\bar{\phi}] = W[J] - \int d^d x \bar{\phi}(x) J(x) , \quad (60)$$

where $\bar{\phi}$ is the background field, a classical field that is related to an external source $J(x)$. We take $\bar{\phi}$ to be the expectation value of the field in the limit that $J \rightarrow 0$,

$$\bar{\phi}[J = 0] = \left. \frac{\delta W}{\delta J} \right|_{J=0} = \left. \frac{\delta Z}{\delta J} \right|_{J=0} = \langle \phi \rangle . \quad (61)$$

Extending the definition of $\bar{\phi}$ to all J values,

$$\frac{\delta W}{\delta J} = \bar{\phi}[J] , \quad (62)$$

which implicates that,

$$\frac{\delta \Gamma}{\delta \bar{\phi}} = J . \quad (63)$$

The effective action $\Gamma[\bar{\phi}]$ (not be confused with the Γ functions) can be treated in the same way as the action S . We find its extrema with respect to the fields by computing $\delta\Gamma/\delta\bar{\phi}$ at $J = 0$. The solution $\bar{\phi}[0]$, corresponds to the quantum expectation value of the field. Summarizing, by Eq. (59) we have the effective action in terms of the classical action,

$$\Gamma[\bar{\phi}] = S[\bar{\phi}] - \int d^d x \bar{\phi}(x) J(x) , \quad (64)$$

In order to show the association of Γ with the effective action, let us start by evaluating $W[J]$ by the method of saddle-points for path integrals. Let us restore the Planck constant

to $Z[J]$ for a moment. We have that

$$Z[J] = e^{\frac{i}{\hbar}W[J]} = \int [d\phi_{1,2}] e^{\frac{i}{\hbar} \int d^4x [\mathcal{L}_0 + J_a \phi_a]}, \quad (65)$$

where $S[\phi, J] = \int d^4x [\mathcal{L}_0 + \hbar J_a \phi_a]$. If S is stationary for some ϕ_0 :

$$\left. \frac{\delta S[\phi, J]}{\delta \phi} \right|_{\phi_0} = 0. \quad (66)$$

Now, by expanding the action around ϕ_0 ,

$$\begin{aligned} S[\phi, J] &= S[\phi_0, J] + \phi_a(x) \left. \frac{\delta S[\phi, J]}{\delta \phi_a} \right|_{\phi_0} + \phi_a(x) \phi_a(y) \left. \frac{\delta^2 S}{\delta \phi_a(x) \delta \phi_a(y)} \right|_{\phi_0} + \\ &+ \phi_a(x) \phi_b(y) \left. \frac{\delta^2 S}{\delta \phi_a(x) \delta \phi_b(y)} \right|_{\phi_0} + \dots \end{aligned} \quad (67)$$

Applying (66), we have

$$S[\phi, J] = S[\phi_0, J] + \phi_a(x) \phi_a(y) \left. \frac{\delta^2 S}{\delta \phi_a(x) \delta \phi_a(y)} \right|_{\phi_0} + \phi_a(x) \phi_b(y) \left. \frac{\delta^2 S}{\delta \phi_a(x) \delta \phi_b(y)} \right|_{\phi_0} + \dots \quad (68)$$

In this construction we retain only even powers of these derivatives, as a pedagogical example we will show explicit for these quadratic terms (68). For are model they are,

$$\begin{aligned} S[\phi_0, J] &= - \int d^4x \left(\frac{1}{2} \phi_0(x) \square \phi_0(x) + V(\phi_0) - \hbar J \phi_0(x) \right), \\ \phi_a(x) \phi_a(y) \left. \frac{\delta^2 S}{\delta \phi_a(x) \delta \phi_a(y)} \right|_{\phi_0} &= - \frac{1}{2} \int d^4x \phi_a(x) \left(\square + m^2 + \frac{\lambda}{6} \phi_0^2 \right) \phi_a(x), \\ \phi_a(x) \phi_b(y) \left. \frac{\delta^2 S}{\delta \phi_a(x) \delta \phi_b(y)} \right|_{\phi_0} &= - \frac{1}{2} \int d^4x \phi_a(x) \left(\square + m^2 + \frac{\lambda}{2} \phi_0^2 \right) \phi_b(x), \end{aligned} \quad (69)$$

where $\square = \partial_0^2 - \nabla^2$. Replacing (69) in (68) and applying the Legendre transformation

(64), we have

$$\Gamma[\phi_0] = S[\phi_0] + \frac{i\hbar}{2} \text{tr} \ln [\det(-\square + m^2 + \frac{\lambda}{6}\phi_0^2)] + \frac{i\hbar}{2} \text{tr} \ln [\det(-\square + m^2 + \frac{\lambda}{2}\phi_0^2)] \quad (70)$$

where we used,

$$Z[J] = e^{\frac{i}{\hbar}W[J]} = e^{\frac{i}{\hbar}S[\phi_0, J]} [\det(-\square + V''(\phi_0))]^{-1/2}. \quad (71)$$

If $\phi_0(x) = \phi_c = \text{constant}$, then

$$\begin{aligned} \Gamma[\phi_c] &= S[\phi_c] + \frac{i\hbar}{2} \text{tr} \ln [\det(-\square + m^2 + \frac{\lambda}{6}\phi_c^2)] + \frac{i\hbar}{2} \text{tr} \ln [\det(-\square + m^2 + \frac{\lambda}{2}\phi_c^2)] \\ &= \int d^4x V(\phi_c) + \frac{i\hbar}{2} \text{tr} \ln [\det(-\square + m^2 + \frac{\lambda}{6}\phi_c^2)] + \frac{i\hbar}{2} \text{tr} \ln [\det(-\square + m^2 + \frac{\lambda}{2}\phi_c^2)], \end{aligned} \quad (72)$$

what can be understood as,

$$V_{eff}(\phi_c) = V(\phi_c) + \frac{1}{\beta V} \left(\text{Quantum Corrections} \right), \quad (73)$$

or

$$\begin{aligned} V_{eff}(\phi_c) &= V(\phi_c) + \frac{\hbar}{2\beta} \sum_n \int \frac{d^3\vec{k}}{(2\pi)^3} \ln [\det(\omega_n^2 + \vec{k}^2 + m^2 + \frac{\lambda}{6}\phi_c^2)] \\ &+ \frac{\hbar}{2\beta} \sum_n \int \frac{d^3\vec{k}}{(2\pi)^3} \ln [\det(\omega_n^2 + \vec{k}^2 + m^2 + \frac{\lambda}{2}\phi_c^2)], \end{aligned} \quad (74)$$

where the first term of (73) is the classical action written in terms of these constant background fields ϕ_c and the "quantum corrections" are the corrections that came from the Taylor series of the action S of the theory, Eq. (68), that depends on the physical fields and the external source J . There are many ways to establish an effective potential

or a effective action, we can build the effective action/potential in terms of the loop corrections, like we shown above, or we could construct the above quantities in terms of the background fields, that is, expanding the effective action Γ in terms of ϕ_c . This choice give us the 1PI diagrams as corrections of the classical action. There are another possible choices, like expand the effective action to λ , that can lead us to catch 2PI diagrams if we go to high orders like $O(\lambda^2)$ and so on. There are many ways, but a important comment is needed: the effective action described here (which is, using Eq. (68)) is already a perturbative quantity, expand with respect other variable would be a perturbative approach inside another perturbative approach, what lead us to think: Are we losing physical information, using so many approximations? This question will be answered in the next chapters. Among others constructions for the effective potential, this one that is shown here, is the most standard one. We could construct an effective potential with only 2PI diagrams, a interesting can be find in (GERGELY, 2014). These choices establish different models for the same theory, where a theory here means the same Lagrangian (83). Diagrammatically, the effective potential stands for We will see,

Figure 8. - Pictorial diagrammatic representation of the effective potential, up to two-loop order

$$V_{eff}(\phi_c) = V_{tree} + \text{[one-loop bubble]} + \text{[one-loop tadpole]} + \text{[two-loop sunset]} + \dots$$

Source: The author, 2022.

for a complex scalar theory, the number of diagrams are increased, since we have more than one field (e.g., ϕ_1 and ϕ_2 for the real components of the complex scalar field ϕ).

1.3.1 U(1) One-loop effective potential

Applying (73) to the complex scalar theory, we have

$$V_{eff}(\phi_c) = \frac{1}{2}m^2\phi_c^2 - \frac{1}{2}\mu^2\phi_c^2 + \frac{\lambda}{4!}\phi_c^4 + \frac{1}{2\beta} \sum_n \int \frac{d^3\vec{k}}{(2\pi)^3} \ln [\omega_n^2 + \vec{k}^2 + m^2 + \frac{\lambda}{2}\phi_c^2] +$$

$$+\frac{1}{2\beta} \sum_n \int \frac{d^3\vec{k}}{(2\pi)^3} \ln [\omega_n^2 + \vec{k}^2 + m^2 + \frac{\lambda}{6}\phi_c^2], \quad (75)$$

where the presence of the chemical potential is only at the tree level, since the one-loop here is a vacuum contribution. We can define two different masses,

$$m_H^2(\phi_0^2) = m^2 + \frac{\lambda}{2}\phi_c^2 ,$$

$$m_G^2(\phi_0^2) = m^2 + \frac{\lambda}{6}\phi_c^2 . \quad (76)$$

By doing that, it becomes clear the contribution of two different fields. We call them the Higgs (corresponding to m_H^2) and the Goldstone fields (corresponding to m_G^2), they follow the fact that the system has a spontaneous symmetry breaking. The vacuum of the theory or the configuration of minimal energy, do not share the same symmetry of the original Lagrangian (23), the symmetry is broken. As a consequence of that we have in this broken phase two different contributions, the Higgs particle and the Goldstone particle. We will see in the next chapters that, when we consider temperature effects, this broken phase can occur for a specific value of T or for a critical temperature T_c . By using the following trick,

$$\int \frac{d^d k}{(2\pi)^d} \ln(k^2 + m^2) = \frac{\partial}{\partial \alpha} \int \frac{d^d k}{(2\pi)^d} \frac{1}{(k^2 + m^2)^\alpha} \Big|_{\alpha=0} \quad (77)$$

we can regularize the effective potential applying the the integral equation from Appendix A,

$$V_{eff}(\phi_c) = \frac{1}{2}m^2\phi_c^2 - \frac{1}{2}\mu^2\phi_c^2 + \frac{\lambda}{4!}\phi_c^4 - \frac{m_H^2(\phi_c^2)}{2(4\pi)^2} \left(\frac{M^2 e^{\gamma_E}}{m_H^2(\phi_c^2)} \right)^\epsilon \Gamma(\epsilon - 2) +$$

$$-\frac{4}{\pi^2} h_5^\epsilon(m_H(\phi_c)/T, \mu/m_H(\phi_c)) - \frac{m_G^2(\phi_c^2)}{2(4\pi)^2} \left(\frac{M^2 e^{\gamma_E}}{m_G^2(\phi_c^2)} \right)^\epsilon \Gamma(\epsilon - 2) .$$

$$-\frac{4}{\pi^2}h_5^e(m_G(\phi_c)/T, \mu/m_G(\phi_c)) , \quad (78)$$

Expanding in ϵ we will have divergences and for that we need a coupling correction, a mass correction and a vacuum counterterm. Applying the following,

$$\delta m^2 = -\left. \frac{d^2 V_{eff}}{d\phi_c^2} \right|_{\phi_c=0, \mu=0} \rightarrow \delta m^2 = \frac{\lambda m^2}{24\pi^2\epsilon}$$

$$\delta \lambda = -\left. \frac{d^4 V_{eff}}{d\phi_c^4} \right|_{\phi_c=0, \mu=0} \rightarrow \delta \lambda = \frac{5\lambda^2}{48\pi^2\epsilon} \quad (79)$$

summing the vacuum counterterm,

$$\Delta \mathcal{E}_0^{(1)} = \frac{m^4}{(4\pi)^2 2\epsilon} , \quad (80)$$

and re-writing the tree level $m^2 \rightarrow m^2 + \delta m^2$, $\lambda \rightarrow \lambda + \delta \lambda$, we have

$$V_{R-eff}(\phi_c) = \frac{1}{2}m^2\phi_c^2 - \frac{1}{2}\mu^2\phi_c^2 + \frac{\lambda}{4!}\phi_c^4 + \frac{M_H^4(\phi_c^2)}{64\pi^2} \left[\ln \left(\frac{M_H^2(\phi_c^2)}{M^2} \right) - \frac{3}{2} \right]$$

$$-\frac{4}{\pi^2}h_5^e(m_H(\phi_c)/T, \mu/m_H(\phi_c)) + \frac{M_G^4(\phi_c^2)}{64\pi^2} \left[\ln \left(\frac{M_G^2(\phi_c^2)}{M^2} \right) - \frac{3}{2} \right]$$

$$-\frac{4}{\pi^2}h_5^e(m_G(\phi_c)/T, \mu/m_G(\phi_c)) , \quad (81)$$

This is the renormalized one-loop effective potential for the U(1) theory and it can be understood diagrammatically as Figure 9.

Figure 9. - Diagrammatic representation of the effective potential, up to one-loop order with the finite temperature contributions, where the n^\pm stands for the Bose-Einstein distribution factor

$$V_{eff}(\phi_c) = V_{tree} + \text{[solid circle]} + \text{[dashed circle]} + \text{[solid circle with } n^\pm \text{]} + \text{[dashed circle with } n^\pm \text{]}$$

Source: The author, 2022.

1.4 Free Energy

The free energy is an important quantity that can tell us about the different phases of matter. The free energy is defined by

$$\mathcal{F} = -\frac{T}{V} \log Z , \quad (82)$$

where Z is the (grand) partition function. We will compute the contributions to the free energy up to the $O(\lambda^2)$, which will correspond to all the Feynman diagrams that contribute to the vacuum until three-loops. Our theory is described by the following Lagrangian density,

$$\mathcal{L} = \partial_\mu \phi \partial^\mu \phi^* - \bar{m}^2 |\phi|^2 - \frac{1}{3!} \bar{\lambda} (\phi \phi^*)^2 + \Delta \mathcal{L}, \quad (83)$$

where \bar{m} and $\bar{\lambda}$ are the bare mass and bare coupling constant and $\Delta \mathcal{L}$ includes the counterterms that are needed to render a finite theory. The field can be decomposed in two real scalar fields,

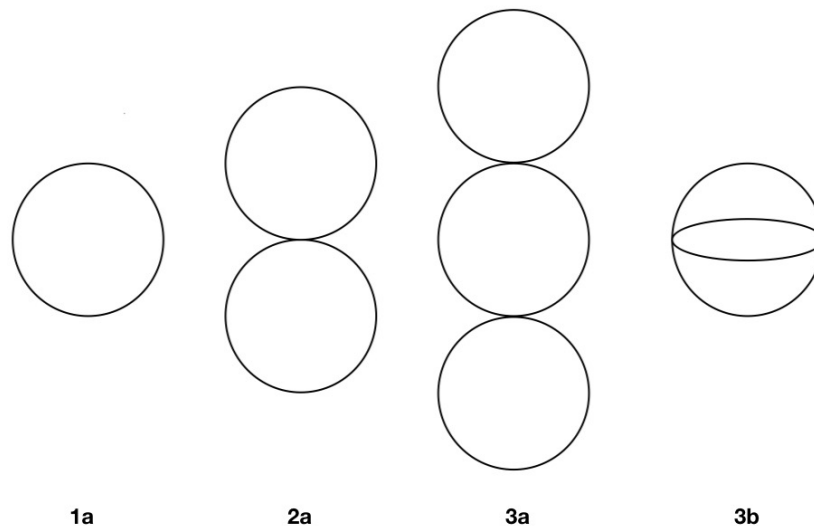
$$\phi = \frac{1}{\sqrt{2}} (\phi_1(x) + i\phi_2(x)) . \quad (84)$$

The free energy can be separated in some sets of diagrams: The vacuum diagrams, the mass diagrams and the vertex diagram (with four external legs). There is a subtle difference in computing those contributions in the physical mass or the in bare parameters. This difference relies in which analysis we expect to do. If one is interested in thermodynamical observables, like entropy, for example, it would be better to study the system by

computing it in the physical mass, since it can be associated with a high-energy scattering, that could be simulated in this laboratory. The other analysis, considering the mass and the coupling functions that runs with the temperature, can only be associated with situations in the early Universe but, for a phase transition analysis, this computation can be very useful.

1.4.1 Vacuum Contributions

All the contributions to the vacuum until second order in perturbation theory $O(\lambda^2)$ at $T = 0$, are quantified by the diagrams shown in Figure 10. As we saw in the Figure 10. - Free energy of a scalar theory at order λ^2



Source: The author, 2022.

previous section, when we impose the KMS condition, thermal contributions arise (or thermal diagrams). Separating the vacuum by loop order (Figure 10), let us compute each on of these terms separately.

$$\mathcal{F} = \mathcal{F}_1 + \mathcal{F}_2 + \mathcal{F}_3 . \tag{85}$$

1.4.1.1 One-loop

First of all, since we are doing the computation diagrammatically, we need to be careful with the divergences,

$$\mathcal{F}_1 = \mathcal{F}_{1a} + \Delta_1 \mathcal{E}_0 , \quad (86)$$

where the above equation, \mathcal{F}_{1a} represents the diagram 1a in the Figure 10 and $\Delta_1 \mathcal{E}_0$ is the counterterm for the zero point energy of the theory, or the vacuum. It is possible to make the analogy between some quantum field theories as a infinite coupled harmonic oscillators, it is expected that, at the zero point energy we find infinities this is the reason why we need the vacuum counter-terms. The calculation of \mathcal{F}_{1a} is done in (42) and it is,

$$\mathcal{F}_{1a} = \frac{\bar{m}^4}{(4\pi)^2} \left(\frac{M}{\bar{m}} \right)^{2\epsilon} e^{\gamma_E \cdot \epsilon} \frac{\gamma_E [\epsilon - 1]}{(1 - \epsilon)} - \frac{8T^4}{\pi^2} h_5^\epsilon(y, r) .$$

The temperature functions are defined in the same convention of Haber and Weldon's work (HABER; WELDON, 1982). Expanding the first term of \mathcal{F}_{1a} in ϵ , taking only the divergent part and summing the vacuum counterterm explicited as defined in the appendix C, we obtain the finite result

$$\mathcal{F}_1 = -\frac{\bar{m}^4}{(4\pi)^2} \left[\frac{3}{4} + \ln \left(\frac{M}{\bar{m}} \right) \right] - \frac{8T^4}{\pi^2} h_5^\epsilon(y, r) , \quad (87)$$

where,

$$h_5^\epsilon(y, r) = -\frac{1}{16} \int_0^\infty x^2 dx \left[\ln (1 - e^{-(\omega-r)}) + (r \rightarrow -r) \right] . \quad (88)$$

To simplify our expressions and align them with other results found in the literature (ANDERSEN, 2000), let us define

$$\ln \left(\frac{M^2}{\bar{m}^2} \right) \equiv \bar{L} , \quad \frac{\bar{\lambda}}{(4\pi)^2} \equiv \bar{\alpha} . \quad (89)$$

Re-writing the one-loop free energy using (89), we then obtain

$$\mathcal{F}_1 = -\frac{\bar{m}^4}{(4\pi)^2} \left[\frac{3}{4} + \frac{\bar{L}}{2} \right] - \frac{8T^4}{\pi^2} h_5^e(y, r), \quad (90)$$

at $\mu = 0$ that is $r = 0$ reproduces the result of Andersen, Braaten and Strickland (ANDERSEN, 2000).

1.4.1.2 Two-Loops

For the free energy at two-loop order, we have a contribution of order λ shown by the term $2a$ in Figure 10. It can be rendered finite by adding to it two types of counterterms: a mass and vacuum counterterm of renormalization (ANDERSEN, 2000).

$$\mathcal{F}_2 = \mathcal{F}_{2a} + \frac{\partial \mathcal{F}_{1a}}{\partial \bar{m}^2} \Delta_1 \bar{m}^2 + \Delta_2 \mathcal{E}_0 \quad (91)$$

where,

$$\mathcal{F}_{2a} = \frac{\bar{\lambda}}{3} I_1^2,$$

and the terms I_n and the counter-terms are explicitly given in the Appendix A and C.

The explicit result for the term \mathcal{F}_{2a} is

$$\mathcal{F}_{2a} = \frac{1}{3} \bar{\lambda} \left[\frac{\bar{m}^2}{(4\pi)^2} \left(\frac{M}{\bar{m}} \right)^{2\epsilon} e^{\gamma_E \cdot \epsilon} \Gamma[-1 + \epsilon] + \frac{T^2}{\pi^2} h_3^e(y, r) \right]^2$$

Expanding in ϵ , we obtain

$$\begin{aligned} \mathcal{F}_{2a} &= \frac{1}{3} \frac{\bar{\lambda} \bar{m}^4}{(4\pi)^4} \left(\frac{M}{\bar{m}} \right)^{4\epsilon} \left[\frac{1}{\epsilon^2} + \frac{2}{\epsilon} + \frac{1}{6} (18 + \pi^2) \right] \\ &+ \frac{2}{3} \frac{\bar{\lambda}}{16\pi^4} \left(\frac{M}{\bar{m}} \right)^{2\epsilon} \left[\left(-\frac{1}{\epsilon} - 1 \right) h_3^e(y, r) \right] \bar{m}^2 T^2 \\ &+ \frac{1}{3} \frac{\bar{\lambda}}{\pi^4} T^4 h_3^e(y, r)^2. \end{aligned} \quad (92)$$

Summing the counter-terms (Appendix C), we have

$$\begin{aligned} \mathcal{F}_2 = & \frac{\bar{\lambda}}{3} \frac{\bar{m}^4}{(4\pi)^4} \left[1 + 4 \ln \left(\frac{M}{\bar{m}} \right) + 4 \ln^2 \left(\frac{M}{\bar{m}} \right) \right] \\ & - \frac{2}{3} \frac{\bar{\lambda} \bar{m}^2 T^2}{16\pi^4} \left[1 + 2 \ln \left(\frac{M}{\bar{m}} \right) \right] h_3^e(y, r) + \frac{1}{3} \frac{\bar{\lambda}}{\pi^4} T^4 h_3^e(y, r)^2 \end{aligned} \quad (93)$$

or

$$\mathcal{F}_2 = \frac{\bar{\alpha}}{3} \left[\frac{\bar{m}^4}{(4\pi)^2} \left(1 + 2\bar{L} + \bar{L}^2 \right) - \frac{2}{\pi^2} \left(1 + \bar{L} \right) \bar{m}^2 T^2 h_3^e(y, r) + \frac{16}{\pi^2} T^4 h_3^e(y, r)^2 \right], \quad (94)$$

which is the renormalized result for the diagram *2a* shown in Figure 10, at $\mu = 0$ that is $r = 0$ reproduces the result of Andersen, Braaten and Strickland (ANDERSEN, 2000).

1.4.1.3 Three Loops

The free energy at second order in λ comes from the three-loop diagrams labeled *3a* and *3b* in Figure 10. These diagrams are rendered finite by both mass, vertex and vacuum counterterms (ANDERSEN, 2000),

$$\begin{aligned} \mathcal{F}_3 = & \mathcal{F}_{3a} + \mathcal{F}_{3b} + \frac{\partial \mathcal{F}_{2a}}{\partial \bar{m}^2} \Delta_1 \bar{m}^2 + \frac{\mathcal{F}_{2a}}{\bar{\lambda}} \Delta_1 \bar{\lambda} + \frac{1}{2} \frac{\partial^2 \mathcal{F}_{1a}}{(\partial \bar{m}^2)^2} (\Delta_1 \bar{m}^2)^2 \\ & + \frac{\partial \mathcal{F}_{1a}}{\partial \bar{m}^2} \Delta_2 \bar{m}^2 + \Delta_2 \mathcal{E}_0. \end{aligned} \quad (95)$$

The explicit expressions for the diagrams *3a* and *3b* are

$$\mathcal{F}_{3a} = -\frac{2}{9} \bar{\lambda}^2 I_1^2 I_2 \quad (96)$$

and

$$\mathcal{F}_{3b} = -\frac{1}{18} \bar{\lambda}^2 I_{ball} \quad (97)$$

By using the results shown in the Appendix A and B, we have that

$$\begin{aligned}
\mathcal{F}_{3a} = & -\frac{2}{9}\bar{\lambda}^2 \left[\frac{\bar{m}^4}{(4\pi)^6} \left(\frac{M}{\bar{m}} \right)^{6\epsilon} \left(\frac{1}{\epsilon^3} + \frac{2}{\epsilon^2} + \frac{3}{\epsilon} + \frac{\pi^2}{4\epsilon} + \frac{\pi^2}{6} \right) + \right. \\
& -\frac{\bar{m}^2 T^2}{128\pi^6} \left(\frac{M}{\bar{m}} \right)^{4\epsilon} \left(\frac{1}{\epsilon^2} + \frac{1}{\epsilon} + \frac{\pi^2}{6} + 1 \right) h_3^e(y, r) + \\
& -\frac{\bar{m}^2 T^2}{32\pi^6} \left(\frac{M}{\bar{m}} \right)^{2\epsilon} \left(\frac{1}{\epsilon} + 1 \right) h_3^e(y, r) h_1^e(y, r) + \frac{\bar{m}^4}{1024\pi^6} \left(\frac{1}{\epsilon^2} + \frac{2}{\epsilon} + \right. \\
& \left. + \frac{\pi^2}{6} + 3 \right) \left(\frac{M}{\bar{m}} \right)^{4\epsilon} h_1^e(y, r) + \frac{T^4}{16\pi^6 \epsilon} \left(\frac{M}{\bar{m}} \right)^{2\epsilon} h_3^e(y, r)^2 + \\
& \left. + \frac{T^4}{4\pi^6} h_3^e(y, r)^2 h_1^e(y, r) \right]. \tag{98}
\end{aligned}$$

The basketball diagram (the term $3b$ in Figure 10) deserves a special attention: we compute this contribution step by step in the Section 1.7 of this chapter. The final result is the following,

$$\begin{aligned}
\mathcal{F}_{3b} = & -\frac{\bar{\lambda}^2}{18} \left\{ \frac{\bar{m}^4}{(4\pi)^6} \left(\frac{M^2}{\bar{m}^2} \right)^{3\epsilon} \left[\frac{2}{\epsilon^3} + \frac{23}{\epsilon^2} + \frac{(35 + \pi^2)}{2\epsilon} + C_2 \right] + \frac{\bar{m}^2}{(4\pi)^4} \left(\frac{M}{\bar{m}} \right)^{4\epsilon} \left[-\frac{6}{\epsilon^2} \right. \right. \\
& \left. \left. - \frac{17}{\epsilon} - \frac{15\mu^2}{2\bar{m}^2} - 4B_1 \right] \left(\frac{T^2}{\pi^2} h_3^e(y, r) \right) + 6 \frac{1}{(4\pi)^2} \left[\left(\frac{M}{\bar{m}} \right)^{2\epsilon} \frac{1}{\epsilon} + 2 \right] \left(\frac{T^4}{\pi^4} h_3^e(y, r)^2 \right) \right. \\
& \left. + \frac{T^4}{(4\pi)^6} \left(6 \mathcal{K}_2 + 4 \mathcal{K}_3 \right) \right\}. \tag{99}
\end{aligned}$$

The counter-terms (Appendix C) required to make (99) finite come not only from the vacuum of the theory, but from the coupling and the mass terms as well. Summing all of them, we can finally write the result for three-loop contributions as

$$\begin{aligned}
\mathcal{F}_3 = & \frac{2\bar{\alpha}^2}{9(4\pi)^2} \left\{ \frac{\bar{m}^4}{4} \left[-C_2 - 6\bar{L}^3 - 19\bar{L}^2 - \frac{43}{2}\bar{L} + \frac{23\pi^2}{12} + 23 + \psi^{(2)}(1) \right] + \right. \\
& \left. -4\bar{m}^2 T^2 \left(6B_1 - 14\bar{L}^2 - 30\bar{L} + \pi^2 + 12 \right) h_3^e(y, r) - 128T^4 (6 + 5\bar{L}) h_3^e(y, r)^2 \right.
\end{aligned}$$

$$\left. -4h_1^e(y, r) \left((\bar{L} + 1)\bar{m}^2 - 16T^2 h_3^e(y, r) \right)^2 + 30T^2 \mu^2 h_3^e(y, r) - \frac{3}{2} \mathcal{K}_2 T^4 - \mathcal{K}_3 T^4 \right\}, \quad (100)$$

where $B_1 = 1.47856$, $C_2 = 39.429$, $\psi^{(2)}(1) = -2.40411$ and

$$\begin{aligned} \mathcal{K}_2 = & -4 \int_0^\infty p^2 dp \frac{n_p^+ + n_p^-}{\omega_p} \int_0^\infty q^2 dq \frac{n_q^+ + n_q^-}{\omega_q} \sum_\sigma \int_{|\bar{p}-\bar{q}|}^{|\bar{p}+\bar{q}|} \frac{A}{pq} dA \times \\ & \times \left(\frac{E_\sigma^2 - A^2 + 4\bar{m}^2}{E_\sigma^2 - A^2} \right)^{1/2} \ln \left[\frac{(E_\sigma^2 - A^2)^{1/2} + (E_\sigma^2 - A^2 - 4\bar{m}^2)^{1/2}}{(E_\sigma^2 - A^2)^{1/2} - (E_\sigma^2 - A^2 - 4\bar{m}^2)^{1/2}} \right], \end{aligned} \quad (101)$$

$$\begin{aligned} \mathcal{K}_3 \equiv & \frac{2}{T^4} \int_0^\infty p dp \frac{n_p^+ + n_p^-}{\omega_p} \int_0^\infty q dq \frac{n_q^+ + n_q^-}{\omega_q} \int_0^\infty r dr \frac{n_r^+ + n_r^-}{\omega_r} \sum_{j,k=\pm 1} \left[f(\omega_{jk}, p+q+r) + \right. \\ & \left. - f(\omega_{jk}, p+q-r) - f(\omega_{jk}, p-q+r) + f(\omega_{jk}, p-q-r) \right], \end{aligned} \quad (102)$$

with $\omega_{jk} = \omega_p + j\omega_q + k\omega_r$ and

$$f(\omega, p) = p \ln \frac{|\bar{m}^2 - \omega^2 + p^2|}{\bar{m}^2} + (\omega^2 - \bar{m}^2)^{1/2} \ln \left| \frac{(\omega^2 - \bar{m}^2)^{1/2} + p}{(\omega^2 - \bar{m}^2)^{1/2} - p} \right|. \quad (103)$$

It is useful to look at the limit $m \rightarrow 0$, corresponding the high temperature expansion of (101) and (102), to obtain

$$\mathcal{K}_2 = -\frac{(4\pi)^4}{72} \left[\ln \left(\frac{4\pi T}{\bar{m}} \right) - \frac{1}{2} - \frac{\zeta'(-1)}{\zeta(-1)} \right],$$

$$\mathcal{K}_3 = \frac{1}{4} \frac{1}{(4\pi)^2} \left[-\frac{1}{3} \frac{\zeta'(-3)}{\zeta(-3)} + \frac{1}{3} \frac{\zeta'(-1)}{\zeta(-1)} - \frac{7}{45} \right] = \frac{14.1723}{32\pi^6}. \quad (104)$$

The constants can be re-organized to write a more compact result,

$$C_3 = -C_2 + \frac{23\pi^2}{12} + 23 + \psi_1^{(2)}, \quad (105)$$

$$C_4 = 6B_1 + \pi^2 + 12 \quad (106)$$

and

$$\mathcal{K}_3 = 1024\pi^6 K_3 = 453.514. \quad (107)$$

Our result then becomes,

$$\begin{aligned} \mathcal{F}_3 = & \frac{2\bar{\alpha}^2}{9(4\pi)^2} \left\{ \frac{\bar{m}^4}{4} \left[-6\bar{L}^3 - 19\bar{L}^2 - \frac{43}{2}\bar{L} + C_3 \right] + \right. \\ & -4\bar{m}^2 T^2 \left(-14\bar{L}^2 - 30\bar{L} + C_4 \right) h_3^e(y, r) - 128T^4 (5 + 6\bar{L}) h_3^e(y, r)^2 \\ & \left. -4h_1^e(y, r) \left((\bar{L} + 1)\bar{m}^2 - 16T^2 h_3^e(y, r) \right)^2 + 30T^2 \mu^2 h_3^e(y, r) - \frac{3}{2}K_2 T^4 - K_3 T^4 \right\} \quad (108) \end{aligned}$$

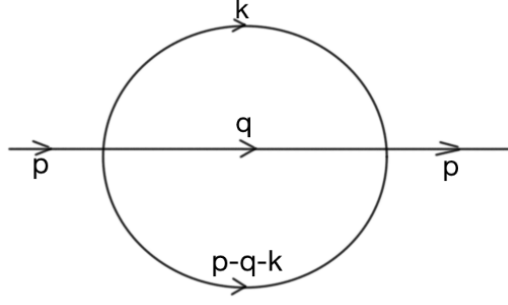
All of those contributions came from the vacuum of our theory, at $\mu = 0$ that is $r = 0$ reproduces the result of Andersen, Braaten and Strickland (ANDERSEN, 2000). To evaluate the total free energy, we need to compute the bare parameters in terms of the physical parameters. For that we will need to investigate both contributions, to the mass and to the coupling constant.

1.5 Setting Sun

In order to establish the free energy of the theory, we will need the calculation of the diagrams that contribute to the mass and coupling of the fields. One of them needs to be evaluated off-shell, since all contributions to the effective potential are off-shell (WEINBERG, 2013). This diagram is called "setting sun" diagram, represented by the Figure 11 that can be read as the following integral,

$$Ssun(p) = C_S i^2 \lambda^2 \int_{k,q} \frac{1}{(k^2 - m^2 + i\epsilon)} \frac{1}{(q^2 - m^2 + i\epsilon)} \frac{1}{((p - k - q)^2 - m^2 + i\epsilon)}. \quad (109)$$

Figure 11. - The setting sun diagram, a Feynman diagram with two loops and two external legs



Source: The author, 2022.

where C_S is the symmetry factor of the diagram. For the complex scalar field theory we have $C_S = 2/9$.

1.5.1 Non-thermal Contribution

The calculation of the setting sun diagram is rather difficult, because a naive introduction of the Feynman parameters results in divergences in its evaluation (KLEINERT, 1990; T'HOOFT; VELTMAN, 1972). The problem is solved by lowering the degree of divergence through partial integration (KLEINERT, 1990; T'HOOFT; VELTMAN, 1972). Using the following identity.

$$1 = \frac{1}{2d} \left(\frac{\partial k^\mu}{\partial k^\mu} + \frac{\partial q^\mu}{\partial q^\mu} \right), \quad (110)$$

where $d = 4 - 2\epsilon$. Inserting this identity into (109) and performing a partial integration, in which the surface term is discarded, we obtain a sum of two integrals,

$$Ssun(p) = \frac{i^2 \lambda^2}{d-3} [3m^2 \xi(p) + \chi(p)], \quad (111)$$

where

$$\xi(p) = \int \frac{d^4 k}{(2\pi)^4} \frac{d^4 q}{(2\pi)^4} \frac{1}{(k^2 + m^2)} \frac{1}{(q^2 + m^2)} \frac{1}{((p+k+q+i\mu)^2 + m^2)^2}, \quad (112)$$

and

$$\chi(p) = -\frac{p^\mu}{2} \frac{\partial}{\partial p^\mu} \int \frac{d^4 k}{(2\pi)^4} \frac{d^4 q}{(2\pi)^4} \frac{1}{(k^2 + m^2)} \frac{1}{(q^2 + m^2)} \frac{1}{((p + k + q + i\mu)^2 + m^2)}. \quad (113)$$

Let us start dealing with $\xi(p)$. For that, we make the change of variables $q' \rightarrow p + i\mu + q + k$ and $dq' = dq$. Next we introduce the Feynman parameters (Appendix A),

$$A = k^2 + m^2, \quad (114)$$

and

$$B = (p + i\mu + q + k)^2 + m^2. \quad (115)$$

Working out the denominator of (113) with the Feynman parameters, we have

$$xA + (1-x)B = k^2 + (p + i\mu + q)^2 + 2(p + i\mu + q)k + m^2 - x(p + i\mu + q)^2 - 2x(p + i\mu + q)k. \quad (116)$$

Performing the exchange of variables $k + r \rightarrow k'$ (where we did it $r = (p + i\mu + q)$), $dk = dk'$ and suming $x^2 r^2 - x^2 r'^2$ to construct $(k' - xr)^2 + x(1-x)r^2 + m^2$, we obtain the result

$$\begin{aligned} \xi(p) &= \int \frac{d^4 q}{(2\pi)^4} \frac{1}{((q_4)^2 + \vec{q}^2 + m^2)^2} \times \\ &\times \int_0^1 dx \int \frac{d^4 k'}{(2\pi)^4} \frac{1}{((k' - xr)^2 + x(1-x)r^2 + m^2)^2}. \end{aligned} \quad (117)$$

Now, imposing the dimensional regularization in the \overline{MS} scheme, we obtain that Eq. (117) becomes

$$\xi(p) = \left(\frac{e^{\gamma_E} M^2}{4\pi} \right)^\epsilon \int \frac{d^d q}{(2\pi)^d} \frac{1}{(q^2 + m^2)^2}$$

$$\times \int_0^1 dx \int \frac{d^d k'}{(2\pi)^d} \frac{1}{((k' - xr)^2 + x(1-x)r^2 + m^2)^2}, \quad (118)$$

where M is the renormalization constant and γ_E is the Euler-Mascheroni constant. Making $q' - xr \rightarrow q''$, $dq' = dq''$, $x(1-x)r^2 + m^2 \rightarrow \Delta$, and using the integration result written in the Appendix A, we can easily integrate Eq. (118).

$$\begin{aligned} \xi(p) &= \frac{\Gamma(2 - d/2)}{\Gamma(2)} \left(\frac{e^{\gamma_E} M^2}{4\pi} \right)^{2\epsilon} \frac{1}{(4\pi)^{d/2}} \int_0^1 dx \int \frac{d^d q}{(2\pi)^d} \frac{1}{(q^2 + m^2)^2} \\ &\times \left(\frac{1}{x(1-x)r^2 + m^2} \right)^{2-d/2}. \end{aligned} \quad (119)$$

Now, to perform the integrals in (119), we use the Feynman parameters one more time (Appendix A), factorizing the $x(1-x)$ term, we obtain

$$\begin{aligned} \xi(p) &= \frac{\Gamma(4 - d/2)}{\Gamma(2)} \left(\frac{e^{\gamma_E} M^2}{4\pi} \right)^{2\epsilon} \frac{1}{(4\pi)^{d/2}} \int_0^1 dx [x(1-x)]^{d/2-2} \times \\ &\times \int_0^1 dy \int \frac{d^d q}{(2\pi)^d} \frac{y(1-y)^{1-d/2}}{[y(q^2 + m^2) + (1-y)((p - i\mu - q)^2 + \frac{m^2}{x(1-x)})]^{4-d/2}}. \end{aligned} \quad (120)$$

Working the denominator of expression above,

$$(yA + (1-y)B) = q^2 - 2(p - i\mu)q(1-y) + (1-y)(p - i\mu)^2 + \left[y + \frac{1-y}{x(1-x)} \right] m^2, \quad (121)$$

and summing $(1-y)^2(p - i\mu)^2 - (1-y)^2(p - i\mu)^2$, we have

$$(yA + (1-y)B) = [q - (1-y)(p - i\mu)]^2 + (1-y)y(p - i\mu)^2 + \left[y + \frac{1-y}{x(1-x)} \right] m^2. \quad (122)$$

Now, the integral is quite easy. Doing $q - (1 - y)(p - i\mu) \rightarrow q'$ and denoting by Δ the rest of the above equation, using the results from Appendix A, we find

$$\begin{aligned} \xi(p) &= \frac{\Gamma(4 - d/2)}{\Gamma(2)} \left(\frac{e^{\gamma_E} M^2}{4\pi} \right)^\epsilon \frac{1}{(4\pi)^{d/2}} \int_0^1 dx [x(1-x)]^{d/2-2} \\ &\times \int_0^1 dy y (1-y)^{1-d/2} \frac{1}{(4\pi)^{d/2}} \frac{\Gamma(4-d)}{\Gamma(4-d/2)} \left(\frac{1}{\Delta} \right)^{4-d}. \end{aligned} \quad (123)$$

Simplifying and setting $d \rightarrow 4 - 2\epsilon$,

$$\begin{aligned} \xi(p) &= \frac{\Gamma(2\epsilon) e^{2\gamma_E \epsilon}}{\Gamma(2)} \left(\frac{M^2}{m^2} \right)^{2\epsilon} \frac{1}{(4\pi)^4} \int_0^1 dx [x(1-x)]^{-\epsilon} \times \\ &\times \int_0^1 dy y (1-y)^{-1+\epsilon} \frac{1}{[(1-y)y \frac{(p-i\mu)^2}{m^2} + (y + \frac{1-y}{x(1-x)})]^{2\epsilon}}. \end{aligned} \quad (124)$$

Then, expanding the denominator until $O(\epsilon)$:

$$\begin{aligned} \xi(p) &= \frac{\Gamma(2\epsilon) e^{2\gamma_E \epsilon}}{\Gamma(2)} \left(\frac{M^2}{m^2} \right)^{2\epsilon} \frac{1}{(4\pi)^4} \left[\frac{\Gamma(1-\epsilon)^2}{\Gamma(2-2\epsilon)} \frac{\Gamma(\epsilon)}{\Gamma(2+\epsilon)} + \right. \\ &\left. -2\epsilon \int_0^1 dx [x(1-x)]^{-\epsilon} \int_0^1 dy y (1-y)^{-1+\epsilon} \ln \left(y - \frac{\mu^2(1-y)y}{m^2} + \frac{1-y}{x(1-x)} \right) \right]. \end{aligned} \quad (125)$$

Let us begin analyzing the first line of (125). When we add it to (111), we have

$$l_1 = \frac{-3\lambda^2 m^2 \Gamma(2\epsilon) e^{2\gamma_E \epsilon}}{(1-\epsilon)\Gamma(2)} \left(\frac{M^2}{m^2} \right)^{2\epsilon} \frac{1}{(4\pi)^4} \left[\frac{\Gamma(1-\epsilon)^2}{\Gamma(2-2\epsilon)} \frac{\Gamma(\epsilon)}{\Gamma(2+\epsilon)} \right]. \quad (126)$$

Expanding the above result for $\epsilon \rightarrow 0$,

$$l_1 \approx -\frac{3\lambda^2 m^2}{2(4\pi)^4} \left\{ \frac{1}{\epsilon^2} + \frac{1}{\epsilon} \left[2 \ln \left(\frac{M^2}{m^2} \right) + 3 \right] + \ln \left(\frac{M^2}{m^2} \right) \left(3 + \ln \left(\frac{M^2}{m^2} \right) \right) + \frac{\pi^2}{12} + \frac{9}{2} \right\}. \quad (127)$$

This result contemplates the off-shell computation without chemical potential (that is for $\mu = 0$). Now, we need to recover some information for μ . Let us start by analyzing the second term of (125) and adding it to equation (111),

$$l_2 = \frac{3\lambda^2 m^2}{(1-2\epsilon)} \frac{\Gamma(2\epsilon) e^{2\gamma_E \epsilon}}{\Gamma(2)} \left(\frac{M^2}{m^2}\right)^{2\epsilon} \frac{2\epsilon}{(4\pi)^4} \int_0^1 dx [x(1-x)]^{-\epsilon} \times \\ \times \int_0^1 dy y(1-y)^{-1+\epsilon} \ln \left(y - \frac{\mu^2(1-y)y}{m^2} + \frac{1-y}{x(1-x)} \right) \Bigg]. \quad (128)$$

The environment contributions, that came from the Bose-Einstein integrals, have a limited range for $m \geq |\mu|$ (we will discuss a little about that in the next chapter). But for the vacuum contributions we have a different range that is $m \geq \mu$, where $m = \mu$ is the condition to the Bose-Einstein condensation. This allow us to expand the logarithm term in Eq. (128) up to $O(\mu^2)$ (for high orders we have very small contributions since they come μ^2/m^4 , what become neglectable),

$$l_2 = \frac{3\lambda^2 m^2}{(1-2\epsilon)} \frac{\Gamma(2\epsilon) e^{2\gamma_E \epsilon}}{\Gamma(2)} \left(\frac{M^2}{m^2}\right)^{2\epsilon} \frac{2\epsilon}{(4\pi)^4} \int dx dy \left\{ \frac{\mu^2(x-1)xy^2((1-x)x)^{-\epsilon}(1-y)^\epsilon}{m^2(x^2y - xy + y - 1)} + \right. \\ \left. + y((1-x)x)^{-\epsilon}(1-y)^{\epsilon-1} \log \left(\frac{1-y}{(1-x)x} + y \right) \right\}. \quad (129)$$

As a standard procedure, taking the limit $\epsilon \rightarrow 0$ and integrating in dx and dy , we have

$$l_2 = \frac{\lambda^2}{(4\pi)^4} \left[-\frac{\mu^2}{2} + 6.51586m^2 \right]. \quad (130)$$

The final answer is (summing $l_1 + l_2$),

$$l_1 + l_2 \approx -\frac{3\lambda^2 m^2}{2(4\pi)^4} \left\{ \frac{1}{\epsilon^2} + \frac{1}{\epsilon} \left[2 \ln \left(\frac{M^2}{m^2} \right) + 3 \right] + \ln \left(\frac{M^2}{m^2} \right) \left(3 + \ln \left(\frac{M^2}{m^2} \right) \right) \right\} + \\ + \frac{\mu^2}{3m^2} - 4.34391 + \frac{\pi^2}{12} + \frac{9}{2} \Bigg\}. \quad (131)$$

This is the off-shell result for the setting sun diagram, for non-zero chemical potential, without the term $\chi(p)$ in (113). For the term $\chi(p)$ we have already calculated this contribution by using the Feynman parameters. The result is

$$\begin{aligned} \chi(p) = & -\frac{p^\mu}{2} \left(\frac{e^{\gamma_E M^2}}{4\pi} \right)^{2\epsilon} \frac{\Gamma(3-d)}{(4\pi)^{d/2}} \frac{\partial}{\partial p^\mu} \left\{ \int_0^1 dx [x(1-x)]^{d/2-2} \times \right. \\ & \left. \times \int_0^1 dy (1-y)^{1-d/2} \frac{1}{(4\pi)^{d/2}} \left[(1-y)y(p-i\mu)^2 + \left(y + \frac{1-y}{x(1-x)} \right) m^2 \right]^{d-3} \right\}. \end{aligned} \quad (132)$$

The notation p^μ means $p^\mu = (p_4, \vec{p})$. The whole point here is to identify the external momenta as,

$$p^\mu = (|p_4|, \vec{p}), \quad (133)$$

so, what is written inside the brackets is in fact this p^μ . Making the derivative of (125),

$$\begin{aligned} \chi(p) = & p^2 \left(\frac{e^{\gamma_E M^2}}{4\pi} \right)^{2\epsilon} \frac{(3-d)\Gamma(3-d)}{(4\pi)^d} \left\{ \int_0^1 dx [x(1-x)]^{d/2-2} \times \right. \\ & \left. \times \int_0^1 dy y(1-y)^{2-d/2} \left[(1-y)y(p-i\mu)^2 + \left(y + \frac{1-y}{x(1-x)} \right) m^2 \right]^{d-4} \right\}, \end{aligned} \quad (134)$$

where, $p^2 = p^\mu p_\mu = (|p_4|, \vec{p})^2$ and $(3-d)\gamma_E(3-d) = \gamma_E(4-d)$. Now, we need to choose how to evaluate the contribution on-shell. The choice will be $p_4 = 0$, in other words, $p^2 = \vec{p}^2$ (static frame).

$$\begin{aligned} \chi(p) = & (+\vec{p}^2) \left(\frac{e^{\gamma_E M^2}}{4\pi} \right)^{2\epsilon} \frac{\Gamma(2\epsilon)}{(4\pi)^{4-2\epsilon}} \left\{ \int_0^1 dx [x(1-x)]^{-\epsilon} \times \right. \\ & \left. \times \int_0^1 dy y(1-y)^\epsilon \left[(1-y)y(\vec{p}^2 - \mu^2) + \left(y + \frac{1-y}{x(1-x)} \right) m^2 \right]^{-2\epsilon} \right\} \end{aligned} \quad (135)$$

which, when simplifying, gives

$$\chi(p) = (+\vec{p}^2) \left(\frac{M^2}{m^2} \right)^{2\epsilon} \frac{\Gamma(2\epsilon) e^{2\epsilon\gamma_E}}{(4\pi)^4} \int_0^1 dx [x(1-x)]^{-\epsilon} \int_0^1 dy y(1-y)^\epsilon$$

$$\left\{ 1 - 2\epsilon \ln \left[y(1-y) \frac{(-\mu^2 + \vec{p}^2)}{m^2} + \left(y + \frac{1-y}{x(1-x)} \right) \right] \right\}. \quad (136)$$

Here, we cannot do the same approximation we did for $\xi(p)$. The reason is quite simple: The momenta dependency. Since we have an external momentum, we can factorize it and treat the argument of the logarithm function as small. We can separate Eq (136) in two parts $\chi(p) = \chi_1(p) + \chi_2(p)$ and replacing this in (111), the equation will be $l_3(p)$ and the second line denoted by $l_4(p)$, where $l_3(p)$ is explicitly given by

$$l_3(p) = \frac{i^2 \lambda^2}{d-3} \chi_1(p)$$

$$= \frac{-\lambda^2 \vec{p}^2}{(1-2\epsilon)} \left(\frac{M^2}{m^2} \right)^{2\epsilon} \frac{\Gamma(2\epsilon) e^{2\epsilon\gamma_E}}{(4\pi)^4} \int_0^1 dx [x(1-x)]^{-\epsilon} \int_0^1 dy y(1-y)^\epsilon, \quad (137)$$

where here, we need to be careful. Proceeding like Kleinert (see Quantum Field Theory and particle physics, Kleinert (1996), page 541), we have

$$l_3(p) = \frac{-\lambda^2 \vec{p}^2}{(1-2\epsilon)} \left(\frac{M^2}{m^2} \right)^{2\epsilon} \frac{\Gamma(2\epsilon) e^{\epsilon\gamma_E}}{(4\pi)^4} \lim_{\epsilon \rightarrow 0} \left\{ \frac{\Gamma(1-\epsilon)^2 \Gamma(1-\epsilon)}{\Gamma(2-2\epsilon) \Gamma(3-\epsilon)} \right\} \quad (138)$$

Taking this limit, the term in the parenthesis will be a constant 1/2; the rest of the terms can be expanded for $\epsilon \rightarrow 0$, giving

$$l_3(p) = \frac{-\lambda^2}{(4\pi)^4} \left[\frac{p^2}{4} \left(\log \left(\frac{M^2}{m^2} \right) + 2 \right) + \frac{p^2}{4\epsilon} \right] \quad (139)$$

with the choice $p = im$, we have

$$l_3(im) = \frac{\lambda^2}{(4\pi)^4} \left[\frac{m^2}{4} \left(\log \left(\frac{M^2}{m^2} \right) + 2 \right) + \frac{m^2}{4\epsilon} \right]. \quad (140)$$

Now, considering the term $l_4(p) = i^2 \lambda^2 \chi_2(p)/(d-3)$, we obtain

$$l_4(p) = \frac{-\lambda^2 \bar{p}^2}{(1-2\epsilon)} \left(\frac{M^2}{m^2} \right)^{2\epsilon} \frac{\Gamma(2\epsilon) e^{2\epsilon\gamma_E}}{(4\pi)^4} \left\{ \int_0^1 dx [x(1-x)]^{-\epsilon} \int_0^1 dy y(1-y)^\epsilon \times \right. \\ \left. \times (-2\epsilon) \ln \left[y(1-y) \frac{(-\mu^2 + \bar{p}^2)}{m^2} + \left(y + \frac{1-y}{x(1-x)} \right) \right] \right\}. \quad (141)$$

Separating the logarithm term in (141) as

$$l_4(p) = \frac{-\lambda^2 \bar{p}^2}{(1-2\epsilon)} \left(\frac{M^2}{m^2} \right)^{2\epsilon} \frac{\Gamma(2\epsilon) e^{2\epsilon\gamma_E}}{(4\pi)^4} \int_0^1 dx [x(1-x)]^{-\epsilon} \int_0^1 dy y(1-y)^\epsilon \times \\ (-2\epsilon) \left\{ \log \left[\frac{m^2}{yp^2(x(1-x))} + \frac{m^2}{p^2(1-y)} - \frac{\mu^2}{p^2} + 1 \right] + \log \left[\frac{y(1-y)}{m^2} \right] + \log [p^2] \right\}, \quad (142)$$

and using the approximation $\ln(1+z) \approx z$, we obtain

$$l_4(p) = \frac{-\lambda^2 \bar{p}^2}{(1-2\epsilon)} \left(\frac{M^2}{m^2} \right)^{2\epsilon} \frac{\Gamma(2\epsilon) e^{2\epsilon\gamma_E}}{(4\pi)^4} \int_0^1 dx [x(1-x)]^{-\epsilon} \int_0^1 dy y(1-y)^\epsilon \times \\ -2\epsilon \left\{ \frac{m^2}{yp^2(x(1-x))} + \frac{m^2}{p^2(1-y)} - \frac{\mu^2}{p^2} + \log \left[\frac{y(1-y)}{m^2} \right] + \log [p^2] \right\}. \quad (143)$$

All of the integrals in (143) can be evaluated analytically. We can neglect the first two terms of the second line, since they remain proportional to ϵ in the end of the computations. Doing that, we have:

$$l_4(p) = \frac{-\lambda^2 \bar{p}^2}{(1-2\epsilon)} \left(\frac{M^2}{m^2} \right)^{2\epsilon} \frac{\Gamma(2\epsilon) e^{2\epsilon\gamma_E}}{(4\pi)^4} \int_0^1 dx [x(1-x)]^{-\epsilon} \int_0^1 dy y(1-y)^\epsilon \times \\ -2\epsilon \left\{ -\frac{\mu^2}{p^2} + \log [y(1-y)] + \log \left[\frac{p^2}{m^2} \right] \right\}. \quad (144)$$

Let us now use the identity:

$$\ln [y(1 - y)] + \ln \left[\frac{p^2}{m^2} \right] = \log \left[\frac{y(1 - y)p^2}{m^2} \right]. \quad (145)$$

When applying in the limits of integration in (144) this term does not contain any singularities (see (KLEINERT, 1996), page 540) and can be neglected. So what remains is the chemical potential contribution. Summing into the divergent part, we have

$$l_4(p) = \frac{-\lambda^2}{(4\pi)^4} \left[\frac{p^2}{4} \left(\log \left(\frac{M^2}{m^2} \right) + 2 \right) + \frac{p^2}{4\epsilon} + \frac{\mu^2}{2} \right]. \quad (146)$$

Now, we can write the on-shell and off-shell results, for the setting sun diagram. Taking the choice $p = im$, we have for the on-shell result:

$$Ssun(-m^2) \approx -\frac{3\lambda^2 m^2}{2(4\pi)^4} \left\{ \frac{1}{\epsilon^2} + \frac{1}{\epsilon} \left[2 \ln \left(\frac{M^2}{m^2} \right) + \frac{17}{6} \right] + 2 \ln \left(\frac{M^2}{m^2} \right) \left[\frac{17}{6} + \ln \left(\frac{M^2}{m^2} \right) \right] + \frac{5\mu^2}{6m^2} + B_1 \right\}, \quad (147)$$

where $B_1 = 1.47856$. The off-shell result, on the other hand, gives

$$Ssun(0) \approx -\frac{3\lambda^2 m^2}{2(4\pi)^4} \left\{ \frac{1}{\epsilon^2} + \frac{1}{\epsilon} \left[2 \ln \left(\frac{M^2}{m^2} \right) + 3 \right] + \ln \left(\frac{M^2}{m^2} \right) \left(3 + \ln \left(\frac{M^2}{m^2} \right) \right) + \frac{\mu^2}{3m^2} + B_0 \right\}, \quad (148)$$

where $B_0 = 0.978557$.

Now, for a complex scalar theory, we need to compute for all possible permutations due to the Feynman rules,

$$\begin{aligned} & -\frac{2\lambda^2}{9} \frac{1}{8} \int_k \int_q \left[G(k_4 + i\mu) G(q_4 + i\mu) G(k_4 + q_4 + i\mu) + \right. \\ & \left. + G(k_4 + i\mu) G(q_4 + i\mu) G(k_4 + q_4 - i\mu) + \right. \end{aligned}$$

$$\begin{aligned}
& +G(k_4 + i\mu)G(q_4 - i\mu)G(k_4 + q_4 + i\mu) + \\
& +G(k_4 - i\mu)G(q_4 + i\mu)G(k_4 + q_4 + i\mu) + \\
& +G(k_4 - i\mu)G(q_4 - i\mu)G(k_4 + q_4 + i\mu) + \\
& +G(k_4 + i\mu)G(q_4 - i\mu)G(k_4 + q_4 - i\mu) + \\
& +G(k_4 - i\mu)G(q_4 + i\mu)G(k_4 + q_4 + i\mu) + \\
& +G(k_4 - i\mu)G(q_4 - i\mu)G(k_4 + q_4 - i\mu) \Big]. \tag{149}
\end{aligned}$$

By using the translation property (46), which was discussed in Section 1.2.3 we can rewrite the propagators,

$$\begin{aligned}
Ssun(p) = & \frac{-2\lambda^2}{9} \frac{1}{8} \int_k \int_q \Big[3G(k_4)G(q_4)G(k_4 + q_4 + i\mu) + \\
& +3G(k_4)G(q_4)G(k_4 + q_4 - i\mu) + \\
& +G(k_4)G(q_4)G(k_4 + q_4 + 3i\mu) + \\
& +G(k_4)G(q_4)G(k_4 + q_4 - 3i\mu) \Big].
\end{aligned}$$

The same procedure is addressed in the literature as the Silver Blaze property (GERGELY, 2014), which makes a shift in the temporal coordinate of the momenta $p_4 \rightarrow p_4 - i\mu$. Since we already have calculated the propagators off-shell, the result with the correct symmetry factor for the complex scalar field is,

$$\begin{aligned}
Ssun(0) = & \frac{-2\lambda^2}{9} \frac{1}{8} \left\{ \frac{9m^2}{(4\pi)^4} \left\{ \frac{1}{\epsilon^2} + \frac{1}{\epsilon} \left[2 \ln \left(\frac{M^2}{m^2} \right) + 3 \right] + \ln \left(\frac{M^2}{m^2} \right) \left(3 + \ln \left(\frac{M^2}{m^2} \right) \right) \right. \right. \\
& + \left. \frac{\mu^2}{3m^2} + C_0 \right\} + \frac{3m^2}{(4\pi)^4} \left\{ \frac{1}{\epsilon^2} + \frac{1}{\epsilon} \left[2 \ln \left(\frac{M^2}{m^2} \right) + 3 \right] + \ln \left(\frac{M^2}{m^2} \right) \left(3 + \ln \left(\frac{M^2}{m^2} \right) \right) \right. \\
& \left. \left. + \frac{9\mu^2}{3m^2} + C_0 \right\} \right\}. \tag{150}
\end{aligned}$$

Simplifying,

$$S_{Sun}(0) = \frac{-2\lambda^2}{9} \left\{ \frac{\lambda^2 m^2}{(4\pi)^4} \left\{ -\frac{3}{2\epsilon^2} - \frac{3}{2\epsilon} \left(2 \ln \left(\frac{M^2}{m^2} \right) + 3 \right) - 9 \ln \left(\frac{M^2}{m^2} \right) - 3 \ln^2 \left(\frac{M^2}{m^2} \right) - \frac{3\mu^2}{2m^2} - C_0 \right\} \right\}, \quad (151)$$

where $C_0 = 9.45154$. The result above is the off-shell result for the setting sun. The on-shell result is,

$$S_{Sun}(-m^2) = \frac{-2\lambda^2}{9} \frac{m^2}{(4\pi)^4} \left\{ -\frac{3}{2\epsilon^2} - \frac{3}{2\epsilon} \left[2 \ln \left(\frac{M^2}{m^2} \right) + \frac{17}{6} \right] - \frac{6}{2} \ln \left(\frac{M^2}{m^2} \right) \left[\frac{17}{6} \ln \left(\frac{M^2}{m^2} \right) \right] - \frac{3\mu^2}{m^2} + C_1 \right\}, \quad (152)$$

where $C_1 = -7.82654$. The off-shell (151) result at $\mu = 0$ reproduces the same result of Gergely Markó, Urko Reinosa, and Zsolt Szép (MARKÓ, 2012), and the on-shell (152) at $\mu = 0$ reproduces the result of Andersen, Braaten and Strickland (ANDERSEN, 2000).

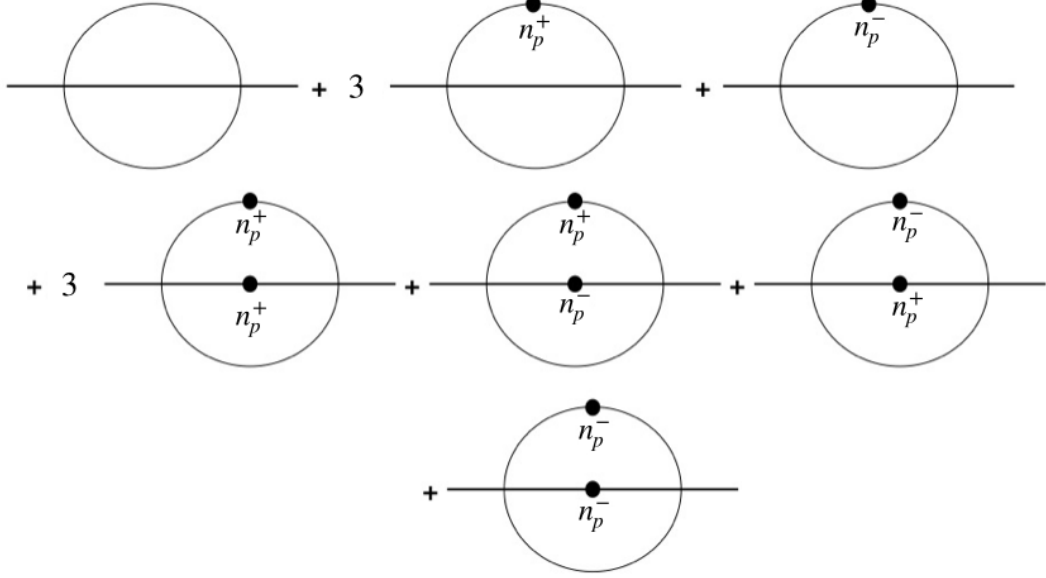
1.6 Thermal Setting Sun

Now, let us investigate the computation of the thermal contributions for the setting sun diagram. Applying the Keldysh prescription (Figure 5) as discussed in Section 1.2.3, we can write the setting sun diagram as follows,

$$I_{Sun}(p_0, \vec{p}) = I'_0 + 3(I_1'^+ + I_1'^-) + 3(I_1'^{-+} + I_1'^{-} + I_1'^{+-} + I_1'^{-}). \quad (153)$$

where the I'_0 is just the non-thermal contribution, which we have already computed above. The other terms are the thermal contributions. The superscript I^{-+} stand for the sign of the chemical potential in the Bose-Einstein (BE) distribution. We will write their expressions explicitly, but first let us represent diagrammatically. Figure 12 shows diagrammatically the thermal contributions to the setting sun diagram. In momentum

Figure 12. - Pictorial representation of the setting sun diagram at finite temperature and chemical potential



Source: The author, 2022.

space-time, we have explicitly,

$$\begin{aligned}
 I_{Sun}(k_0, \vec{k}) &= \int_p \int_q \frac{i}{p^2 - m^2} \frac{i}{q^2 - m^2} \frac{-1}{((k - p - q)^2 - m^2)} \\
 &+ 3 \int_p \int_q \delta(p) n((p_0 - \mu) \text{sgn}(p_0)) \frac{i}{q^2 - m^2} \frac{-1}{(k - p - q)^2 - m^2} \\
 &- 3 \int_p \int_q \delta(p) \delta(q) n((p_0 - \mu) \text{sgn}(p_0)) n((q_0 - \mu) \text{sgn}(q_0)) \frac{1}{(k - p - q)^2 - m^2}. \quad (154)
 \end{aligned}$$

where,

$$\int_p \equiv \int \frac{d^4 p}{(2\pi)^4}. \quad (155)$$

Since the first term was already evaluated (the first term corresponds to the $T = 0$ contribution), we only have to deal with the other two integrals, that involves the one and two Bose-Einstein (BE) factors, respectively.

1.6.1 Off-Shell Contributions

There is a difference in considering $k = im$, or $k = 0$ for the thermal contributions. We will start with the off-shell contributions.

1.6.1.1 One Bose-Einstein Contribution

The one Bose-Einstein integral can be identified as the eye diagram (a bubble with two external legs) plus the thermal factor, shown in Figure 12,

$$3(I_1^+ + I_1^-) = -3 \int_p \int_q \delta(p) n((p_0 - \mu) \text{sgn}(p_0)) \frac{i}{q^2 - m^2} \frac{1}{(k - p - q)^2 - m^2}. \quad (156)$$

First, let us take the off-shell contribution,

$$\begin{aligned} 3(I_1^+ + I_1^-) \Big|_{\text{off-shell}} &= 3 \left(\frac{e^{\gamma_E} M^2}{4\pi} \right)^{2\epsilon} \int \frac{d^{4-2\epsilon} p}{(2\pi)^{4-2\epsilon}} \delta(p) n((p_0 - \mu) \text{sgn}(p_0)) \\ &\times \int_0^1 dx \frac{\Gamma[\epsilon]}{(4\pi)^{2-\epsilon}} \frac{1}{(x(x-1)p^2 + m^2)^\epsilon}. \end{aligned} \quad (157)$$

After we integrate the frequencies, it becomes $n^+(\omega_p)$ and we will write n_p^+ . The delta functions are,

$$\delta(p) \equiv 2\pi \delta(p^2 - m^2) = 2\pi \frac{1}{2\omega_p} (\delta(p_0 + \omega_p) + \delta(p_0 - \omega_p)), \quad (158)$$

where $\omega_p^2 = \vec{p}^2 + m^2$. Integrating in p_0 and expanding the last term of (157) that depends on ϵ , we have

$$3(I_1^+ + I_1^-) \Big|_{k=0} = \frac{3}{(2\pi)^4} \left(\frac{M^2}{m^2} \right)^\epsilon \left[\frac{T^2 h_3^e}{\epsilon} \right] - \frac{3T^2 h_3^e}{(2\pi)^4} \left(\frac{\pi}{\sqrt{3}} - 2 \right). \quad (159)$$

1.6.1.2 Two Bose-Einstein Contribution

The two Bose-Einstein contributions are finite and given by the following expression,

$$3(I_1'^{- -} + I_1'^{- +} + I_1'^{+ -} + I_1'^{- -}) = -3 \int_p \int_q \delta(p) \delta(q) n((p_0 - \mu) \text{sgn}(p_0)) n((q_0 - \mu) \text{sgn}(q_0))$$

$$\times \frac{1}{(k - p - q)^2 - m^2}. \quad (160)$$

As before, we first evaluate it first off-shell ($k = 0$), opening the integrals and integrating in the four momenta,

$$3(I_1'^{- -} + I_1'^{- +} + I_1'^{+ -} + I_1'^{- -}) = -3 \int \frac{d^{d-1}p}{(2\pi)^{d-1}} \frac{n_p^+ + n_p^-}{2\omega_p}$$

$$\times \int \frac{d^{d-1}q}{(2\pi)^{d-1}} \frac{n_q^+ + n_q^-}{2\omega_q} 2 \sum_{\sigma=\pm 1} \left[\frac{1}{\omega_\sigma^2 - A^2 - m^2} \right], \quad (161)$$

where, $A^2 \equiv |\vec{p} + \vec{q}|^2$ and $\omega_\sigma^2 = (\omega_p + \sigma\omega_q)^2$, with $\sigma = \pm 1$. Now, we have to integrate the angle between p and q ,

$$3(I_1'^{- -} + I_1'^{- +} + I_1'^{+ -} + I_1'^{- -}) = -\frac{3}{4} \frac{4}{(2\pi)^4} \int dp p^2 \frac{n_p^+ + n_p^-}{2\omega_p}$$

$$\times \int dq q^2 \frac{n_q^+ + n_q^-}{2\omega_q} \sum_{\sigma=\pm 1} \int_{-1}^1 dt \left[\frac{1}{\omega_\sigma^2 - p^2 - q^2 - 2pqt - m^2} \right]$$

Integrating in dt and making the sum in σ ,

$$3(I_1'^{- -} + \dots) = -\frac{3}{8} \frac{1}{(2\pi)^4} \int pdp \frac{n_p^+ + n_p^-}{\omega_p} \int qdq \frac{n_q^+ + n_q^-}{\omega_q} \log \left[\frac{-3m^2 - 4(p^2 - pq + q^2)}{-3m^2 - 4(p^2 + pq + q^2)} \right].$$

This integral is not analytical, therefore and we will define this result as,

$$G^{2BE}(0, \vec{0}) \equiv \int pdp \frac{n_p^+ + n_p^-}{\omega_p} \int qdq \frac{n_q^+ + n_q^-}{\omega_q} \log \left[\frac{-3m^2 - 4(p^2 - pq + q^2)}{-3m^2 - 4(p^2 + pq + q^2)} \right].$$

(162)

where $G^{2BE}(0, \vec{0})$ stands for the off-shell contribution. The complete answer, without any approximation is,

$$\begin{aligned}
I_{Sun}(0) = & \frac{-2\lambda^2}{9} \left\{ \frac{\lambda^2 m^2}{(4\pi)^4} \left\{ -\frac{3}{2\epsilon^2} - \frac{3}{2\epsilon} \left(2 \ln \left(\frac{M^2}{m^2} \right) + 3 \right) - 9 \ln \left(\frac{M^2}{m^2} \right) + \right. \right. \\
& \left. \left. - 3 \ln^2 \left(\frac{M^2}{m^2} \right) - \frac{3\mu^2}{2m^2} - C_0 \right\} + \right. \\
& \left. - \frac{2\lambda^2}{9} \left\{ \frac{3}{(2\pi)^4} \left(\frac{M^2}{m^2} \right)^\epsilon \left[\frac{T^2 h_3^e}{\epsilon} \right] - \frac{3T^2 h_3^e}{(2\pi)^4} \left(\frac{\pi}{\sqrt{3}} - 2 \right) - \frac{3}{8} \frac{1}{(2\pi)^4} G^{2BE}(0, \vec{0}) \right\} \right\}, \quad (163)
\end{aligned}$$

where $C_0 = 9.45154$.

1.6.1.3 Off-Shell High-T Expansion

To solve $G^{2BE}(0, \vec{0})$ analytically, we will consider only the contributions that are relevant in the $T \gg m$ regime. For that reason, we need to separate $G^{2BE}(0, \vec{0})$ in two different regions of integration: the high momenta $p \geq \Lambda$ and low momenta $p \leq \Lambda$ regions. Let us begin with the high momenta region $p \geq \Lambda$. For this region, we have the liberty to make $m \rightarrow 0$

$$G^{2BE}(0, \vec{0}) \Big|_{p \geq \Lambda} = -\frac{3 \times 2}{2(2\pi)^4} \int_{\Lambda}^{\infty} dp \frac{1}{e^{\beta p} - 1} \int_0^p dq \frac{1}{e^{\beta q} - 1} \log \left[\frac{p^2 - pq + q^2}{p^2 + pq + q^2} \right],$$

where the the factor 2 appears because we divide the integral in two regions. Making $\beta p = x$, $\beta q = y$ and summing and subtracting a $1/y$ term to suppress the UV divergence,

$$\begin{aligned}
G^{2BE}(0, \vec{0}) \Big|_{p \geq \Lambda} = & -\frac{3T^2}{(2\pi)^4} \int_0^{\infty} dx \frac{1}{e^x - 1} \int_0^x dy \left(\frac{1}{e^y - 1} - \frac{1}{y} \right) \log \left[\frac{|x^2 - xy + y^2|}{|x^2 + xy + y^2|} \right] + \\
& -\frac{3T^2}{(2\pi)^4} \int_{\Lambda\beta}^{\infty} dx \frac{1}{e^x - 1} \int_0^x dy \left(\frac{1}{y} \right) \log \left[\frac{|x^2 - xy + y^2|}{|x^2 + xy + y^2|} \right].
\end{aligned}$$

Note that in the first integral we made $\Lambda\beta \rightarrow 0$, because it was already finite, since we subtracted the remaining infinity. By solving numerically the first integral and integrating

the second one, we have

$$G^{2BE}(0, \vec{0}) \Big|_{p \geq \Lambda} = -\frac{3T^2}{(2\pi)^4} (0.523151) - \frac{3T^2}{(2\pi)^4} \frac{\pi^2}{6} \log \left(\frac{\Lambda}{T} \right). \quad (164)$$

For the low-momenta limit, we can't simply throw away the mass, because we have divergences associated with those terms. In this regime, we will set the approximation $n^\pm \approx \frac{T}{\omega \pm \mu}$,

$$G^{2BE}(0, \vec{0}) \Big|_{p \leq \Lambda} = -\frac{3T^2 \times 2}{2(2\pi)^4} \int_0^\Lambda \frac{p dp}{\omega_p^2 - \mu^2} \int_0^p \frac{q dq}{\omega_q^2 - \mu^2} \log \left[\frac{1 + \frac{4}{3} \left(\frac{p^2 - pq + q^2}{m^2} \right)}{1 + \frac{4}{3} \left(\frac{p^2 + pq + q^2}{m^2} \right)} \right]. \quad (165)$$

By making $p/m \equiv x$, $q/m \equiv y$ and $\mu/m \equiv r$,

$$G^{2BE}(0, \vec{0}) \Big|_{p \leq \Lambda} = -\frac{3T^2}{(2\pi)^4} \int_0^{\Lambda/m} \frac{x dx}{1 + x^2 - r^2} \int_0^x \frac{y dy}{1 + y^2 - r^2} \times \log \left[\frac{1 + \frac{4}{3}(x^2 - xy + y^2)}{1 + \frac{4}{3}(x^2 + xy + y^2)} \right], \quad (166)$$

and proceeding a last substitution $y = xt$, we can separate the problematic part from the logarithm,

$$G^{2BE}(0, \vec{0}) \Big|_{p \leq \Lambda} = -\frac{3T^2}{(2\pi)^4} \int_0^1 dt \int_0^{\Lambda/m} \frac{tx^3 dx}{(1 + x^2 - r^2)(1 + x^2 t^2 - r^2)} \left\{ \log \left[\frac{4x^2 + 3/(1 - t + t^2)}{4x^2 + 3/(1 + t + t^2)} \right] + \log \left[\frac{1 - t + t^2}{1 + t + t^2} \right] \right\}. \quad (167)$$

By taking out the problematic part of the logarithm function, the first integral with respect the first log term, is finite. The second demands a little care, subtracting the infinite like before

$$G^{2BE}(0, \vec{0}) \Big|_{p \leq \Lambda} = -\frac{3T^2}{(2\pi)^4} \int_0^1 dt \int_0^{\Lambda/m} \frac{tx^3 dx}{(1 + x^2 - r^2)} \left(\frac{1}{x^2 t^2} \right) \log \left[\frac{1 - t + t^2}{1 + t + t^2} \right] +$$

$$-\frac{3T^2}{(2\pi)^4} \int_0^1 dt \int_0^{\Lambda/m} \frac{tx^3 dx}{(1+x^2-r^2)} \left(\frac{1}{(1+x^2t^2-r^2)} - \frac{1}{x^2t^2} \right) \log \left[\frac{1-t+t^2}{1+t+t^2} \right]. \quad (168)$$

The first line of (168) is trivial, the second demands a few additional manipulation,

$$\begin{aligned} & -\frac{3T^2}{(2\pi)^4} \int_0^1 dt \int_0^{\Lambda/m} \frac{tx^3 dx}{x^2t^2} \left(\frac{r^2-1}{(1+x^2t^2-r^2)(1+x^2-r^2)} \right) \log \left[\frac{1-t+t^2}{1+t+t^2} \right] \\ &= \frac{3T^2}{(2\pi)^4} \int_0^1 \frac{dt}{t} \log \left[\frac{1-t+t^2}{1+t+t^2} \right] \int_0^{\Lambda/m} \frac{xdx}{1-t^2} \left(\frac{1}{(1+x^2-r^2)} - \frac{t^2}{(1+x^2t^2-r^2)} \right) \end{aligned} \quad (169)$$

$$= \frac{3T^2}{(2\pi)^4} \int_0^1 \frac{dt}{t-t^3} \log \left[\frac{1-t+t^2}{1+t+t^2} \right] \frac{1}{2} \ln \left(\frac{1+x^2-r^2}{1+x^2t^2-r^2} \right) \Big|_0^{\Lambda/m} \quad (170)$$

where,

$$\begin{aligned} \frac{1}{2} \ln \left(\frac{1+x^2-r^2}{1+x^2t^2-r^2} \right) \Big|_0^{\Lambda/m} &= \frac{1}{2} \left[\ln(1+\Lambda^2/m^2-r^2) - \ln(1+t^2\Lambda^2/m^2-r^2) \right] \\ &= \frac{1}{2} \left[-\ln t^2 + \ln \left(1 + \frac{m^2-m^2r^2}{\Lambda^2} \right) - \ln \left(1 + \frac{m^2-m^2r^2}{t^2\Lambda^2} \right) \right] \approx -\ln t. \end{aligned} \quad (171)$$

In the above equation, we take the limit $\Lambda \rightarrow \infty$. Finally,

$$\begin{aligned} G^{2BE}(0, \vec{0}) \Big|_{T \gg m} &= -\frac{3T^2}{(2\pi)^4} \int_0^1 \frac{\ln t}{t-t^3} dt \log \left[\frac{1-t+t^2}{1+t+t^2} \right] - \frac{3}{6} \frac{T^2\pi^2}{(2\pi)^4} \left[\frac{1}{2} \log \left(\frac{m^2-\mu^2}{T^2} \right) \right. \\ & \quad \left. - \frac{1}{2} \log \left(\frac{\Lambda^2}{T^2} \right) \right]. \end{aligned} \quad (172)$$

Summing the high momenta with the low momenta contributions we have

$$\begin{aligned}
G_{T \gg m}^{2BE}(0, \vec{0}) &\approx -\frac{3 T^2 \pi^2}{6 (2\pi)^4} \left[\frac{1}{2} \log \left(\frac{m^2 - \mu^2}{T^2} \right) \right] - \frac{3T^2}{(2\pi)^4} \int_0^1 \frac{\ln t}{t - t^3} dt \log \left[\frac{1 - t + t^2}{1 + t + t^2} \right] \\
&- \frac{3T^2}{(2\pi)^4} \int_0^\infty dx \frac{x}{e^x - 1} \int_0^1 dt \left(\frac{1}{e^{xt} - 1} - \frac{1}{xt} \right) \log \left[\frac{|1 - t + t^2|}{|1 + t + t^2|} \right] \\
&- \frac{3T^2}{(2\pi)^4} \int_0^1 dt \int_0^\infty \frac{tx^3 dx}{(1 + x^2 - r^2)(1 + x^2 t^2 - r^2)} \log \left[\frac{4x^2 + 3/(1 - t + t^2)}{4x^2 + 3/(1 + t + t^2)} \right]. \quad (173)
\end{aligned}$$

The above result is in agreement with the term found by Parwani (PARWANI, 1992), in the limit $\mu \rightarrow 0$ (the same thing as $r \rightarrow 0$, since $r = \mu/m$) and multiplied by the symmetry factor $1/6$ (symmetry factor for a real scalar field). The first and the second integral in (173) are evaluated numerically. The last one needs a different treatment because of the r dependence. For that, we will expand it in terms of r until order $O(r^{12})$

$$\begin{aligned}
R(r) &= 0.135541 + 0.10529r^2 + 0.0874081r^4 + 0.0753038r^6 + \\
&+ 0.0664521r^8 + 0.0596447r^{10} + 0.0542177r^{12}. \quad (174)
\end{aligned}$$

In this order, we have very good agreement with the exact numerical result. In fact, the error is 0.00002%, when comparing the numerical with the approximation (174). Our final expression for the two Bose-Einstein off-shell contribution to the setting sun diagram is,

$$3(I_1'^{--} + I_1'^{-+} + \dots) \Big|_{k=0} = \frac{T^2}{64\pi^2} \left[\log \left(\frac{m^2 - \mu^2}{T^2} \right) \right] + \frac{3T^2}{16\pi^4} \left[2.73381 + R(r) \right]. \quad (175)$$

Now, we can write the complete non-thermal and thermal contributions, off-shell, with the right symmetry factor for a $\lambda|\phi|^4$ theory, result for the setting sun diagram,

$$I_{Sun}^{T \gg m}(0) = \frac{-2\lambda^2}{9} \left\{ \frac{\lambda^2 m^2}{(4\pi)^4} \left\{ -\frac{3}{2\epsilon^2} - \frac{3}{2\epsilon} \left(2 \ln \left(\frac{M^2}{m^2} \right) + 3 \right) - 9 \ln \left(\frac{M^2}{m^2} \right) + \right. \right.$$

$$\begin{aligned}
& -3 \ln^2 \left(\frac{M^2}{m^2} \right) - \frac{3\mu^2}{2m^2} - C_0 \Big\} + \\
& - \frac{2\lambda^2}{9} \left\{ \frac{3}{(2\pi)^4} \left(\frac{M^2}{m^2} \right)^\epsilon \left[\frac{T^2 h_3^\epsilon}{\epsilon} \right] - \frac{3T^2 h_3^\epsilon}{(2\pi)^4} \left(\frac{\pi}{\sqrt{3}} - 2 \right) \right\} + \\
& + \frac{T^2}{64\pi^2} \left[\log \left(\frac{m^2 - \mu^2}{T^2} \right) \right] + \frac{3T^2}{16\pi^4} \left[2.73381 + R(r) \right] \Big\} , \tag{176}
\end{aligned}$$

where $C_0 = 9.45154$. The above result is consistent with the known literature and brings new information about the chemical potential. In the case $\mu = 0$ retrieves the results of (PARWANI, 1992) and (MARKÓ, 2012).

1.6.2 On-Shell Setting sun Diagram

Let us now evaluate the on-shell thermal contributions for the setting sun diagram. Starting with the term with one Bose-Einstein factor.

1.6.2.1 One Bose-Einstein

The one Bose-Einstein momentum integral term can be identified as the eye diagram plus the thermal factor, shown in Figure 12 and given by

$$3(I_1^{'+} + I_1'^{-}) = -3 \int_p \int_q \delta(p) n((p_0 - \mu) \text{sgn}(p_0)) \frac{i}{q^2 - m^2} \frac{1}{(k - p - q)^2 - m^2}. \tag{177}$$

Since we are interested in the correction for the mass spectrum, we will take the real part in the contribution for one Bose-Einstein on-shell. Taking it on-shell and, as shown before, applying the Feynman parameters (Appendix A) and using the regularization formulas in the Appendix A, we have

$$\begin{aligned}
3(I_1^{'+} + I_1'^{-}) &= \frac{3}{2} \left(\frac{e^{\gamma_E} M^2}{4\pi} \right)^{2\epsilon} \int \frac{d^{4-2\epsilon} p}{(2\pi)^{4-2\epsilon}} \delta(p) n((p_0 - \mu) \text{sgn}(p_0)) \\
&\times \int_0^1 dx \frac{\gamma_E[\epsilon]}{(4\pi)^{2-\epsilon}} \frac{1}{(x(x-1)(m^2 + p^2) + m^2)^\epsilon} \Big|_{k=(0,im)}. \tag{178}
\end{aligned}$$

The equation (178) has real and imaginary parts. We recall that the imaginary part is associated with the decay of the field, while the real part gives the contribution for the mass spectrum of the theory.

$$3(I_1'^+ + I_1'^-)|_{\vec{k}=im} = \frac{3T^2 h_3}{(2\pi)^4} \left[\frac{1}{\epsilon} + 2 + \ln\left(\frac{M^2}{m^2}\right) \right] + \frac{3T^2 h_3^\epsilon}{(2\pi)^4} \left(2 - \frac{\pi}{2} \right). \quad (179)$$

1.6.2.2 Two Bose-Einstein

The contribution with two Bose-Einstein factors is finite and given by the following expression,

$$\begin{aligned} 3(I_1'^{- -} + I_1'^{- +} + I_1'^{+ -} + I_1'^{- -}) &= -3 \int_p \int_q \delta(p) \delta(q) n^{(\mu)}((p_0 - \mu) \text{sgn}(p_0)) \\ &\times n^{(\mu)}((q_0 - \mu) \text{sgn}(q_0)) \frac{1}{(k - p - q)^2 - m^2}, \end{aligned} \quad (180)$$

which, when taking on-shell $k = (0, im)$ and opening the integrals and integrating in the four momenta, we obtain

$$\begin{aligned} 3(I_1'^{- -} + I_1'^{- +} + I_1'^{+ -} + I_1'^{- -}) &= -3 \int \frac{d^{d-1}p}{(2\pi)^{d-1}} \frac{n_p^+ + n_p^-}{2\omega_p} \\ &\times \int \frac{d^{d-1}q}{(2\pi)^{d-1}} \frac{n_q^+ + n_q^-}{2\omega_q} 2 \sum_{\sigma} \left[\frac{1}{\omega_{\sigma}^2 - A^2 - m^2} \right], \end{aligned}$$

where we have defined, $A^2 \equiv (-im + \vec{p} + \vec{q}) \cdot (-im + \vec{p} + \vec{q})^*$ and $\omega_{\sigma}^2 = (\omega_p + \sigma\omega_q)^2$, with $\sigma = \pm 1$. Now, we have to integrate the angle between p and q ,

$$\begin{aligned} 3(I_1'^{- -} + I_1'^{- +} + I_1'^{+ -} + I_1'^{- -}) &= -\frac{3}{(2\pi)^4} \int_0^{\infty} dp p^2 \frac{n_p^+ + n_p^-}{\omega_p} \\ &\times \int_0^{\infty} dk k^2 \frac{n_k^+ + n_k^-}{\omega_k} \sum_{\sigma} \int_{-1}^1 \frac{dt}{\omega_{\sigma}^2 - p^2 - q^2 - 2pqt - m^2}. \end{aligned}$$

Integrating in t and summing in σ in the frequencies, we get

$$3(I_1'^{--} + I_1'^{-+} + I_1'^{+-} + I_1'^{--}) = \frac{-3}{2(2\pi)^4} G^{2BE}(0, im), \quad (181)$$

where,

$$G^{2BE}(0, im) = \int_0^\infty dp p \frac{n_p^+ + n_p^-}{\omega_p} \int_0^\infty dk k \frac{n_k^+ + n_k^-}{\omega_k} \times \\ \times \ln \left[\frac{4m^2(2p^2 + 3pq + 2q^2) + 5m^4 + 4(p+q)^2(p^2 + q^2)}{4m^2(2p^2 - 3pq + 2q^2) + 5m^4 + 4(p-q)^2(p^2 + q^2)} \right]. \quad (182)$$

The complete answer when summing Eqs. (152), (179) and (181) without any approximation is,

$$I_{Sun}(-m^2) = \frac{-2\lambda^2}{9} \frac{m^2}{(4\pi)^4} \left\{ -\frac{3}{2\epsilon^2} - \frac{3}{2\epsilon} \left[2 \ln \left(\frac{M^2}{m^2} \right) + \frac{17}{6} \right] - \frac{6}{2} \ln \left(\frac{M^2}{m^2} \right) \left[\frac{17}{6} + \right. \right. \\ \left. \left. \ln \left(\frac{M^2}{m^2} \right) \right] - \frac{3\mu^2}{m^2} + C_1 \right\} \\ - \frac{2\lambda^2}{9} \left\{ \frac{3T^2 h_3}{(2\pi)^4} \left[\frac{1}{\epsilon} + 2 + \ln \left(\frac{M^2}{m^2} \right) \right] + \frac{3T^2 h_3^\epsilon}{(2\pi)^4} \left(2 - \frac{\pi}{2} \right) - \frac{3}{2(2\pi)^4} G^{2BE}(im) \right\}, \quad (183)$$

where $C_1 = -7.82654$. The above result is also known in literature (JONES; PARKIN, 2001), but for the High-T expansion, the new thing here is the analytical evaluation of the one Bose-Einstein factor, that is, the result in terms of the thermal function.

1.6.2.3 On-Shell High-T Expansion

Let us now consider the on-shell contribution for the setting sun diagram in the high temperature approximation. We have two ways of computing an analytical approximation for the on-shell approximation. The first is setting the logarithm part of $G^{2BE}(im)$ to $m \rightarrow 0$ (i.e., considering the high temperature approximation),

$$G^{2BE}(0, im) \Big|_{T \gg m} \approx 2 \int_0^\infty \frac{kdk}{\omega_k} (n_k^+ + n_k^-) \int_0^\infty \frac{qdq}{\omega_q} (n_q^+ + n_q^-) \ln \left| \frac{k+q}{k-q} \right|, \quad (184)$$

and next dividing the region of integration, introducing a cutoff Λ . For $k \leq 0$ one can make the approximation $n_k^\pm = T/(\omega_k \pm \mu)$ to simplify the integration,

$$G^{2BE}(0, im) \Big|_{k \leq 0} \approx 16T^2 \int_0^\Lambda \frac{k dk}{\omega_k^2 - \mu^2} \int_0^k \frac{q dq}{\omega_q^2 - \mu^2} \ln \left| \frac{k+q}{k-q} \right|. \quad (185)$$

We now write $q = kt$ and subtract off a $1/(k^2 t^2)$ factor from the $1/(\omega_k^2 - \mu^2)$ term, such that we can isolate the logarithmic piece:

$$\begin{aligned} G^{2BE}(0, im) \Big|_{k \leq 0} &= 16T^2 \int_0^\Lambda dk \frac{k^3}{k^2 + m^2 + \mu^2} \int_0^1 dt \frac{t}{k^2 t^2} \ln \left| \frac{1+t}{1-t} \right| + \\ &+ 16T^2 \int_0^\Lambda dk \frac{k^3}{k^2 + m^2 + \mu^2} \int_0^1 t dt \left(\frac{1}{k^2 t^2 + m^2 + \mu^2} - \frac{1}{k^2 t^2} \right) \ln \left| \frac{1+t}{1-t} \right|. \end{aligned} \quad (186)$$

Solving the first line of (186) and defining as Gl_1 ,

$$Gl_1 = 2T^2 \pi^2 \left[\ln \left(\frac{\Lambda^2}{T^2} \right) - \ln \left(\frac{m^2 - \mu^2}{T^2} \right) \right]. \quad (187)$$

To compute the second line of (186), we first change the order of integration to obtain

$$\begin{aligned} &16T^2 \int_0^1 t dt \ln \left(\frac{1+t}{1-t} \right) \int_0^\Lambda dk \frac{k^3}{k^2 t^2} \frac{-\Omega^2 + \mu^2}{(k^2 t^2 + \Omega^2 - \mu^2)(\Omega^2 - \mu^2 + k^2)} \\ &= 16T^2 \int_0^1 \frac{dt}{t} \ln \left(\frac{1+t}{1-t} \right) \int_0^\Lambda dk \frac{dk}{1-t^2} \left(\frac{k}{(\Omega^2 - \mu^2 + k^2)} - \frac{kt^2}{(\Omega^2 - \mu^2 + k^2 t^2)} \right) \\ &= 16T^2 \int_0^1 dt \ln \left(\frac{1+t}{1-t} \right) \frac{1}{t-t^3} \frac{1}{2} \ln \left(\frac{\Omega^2 - \mu^2 + k^2}{\Omega^2 - \mu^2 + k^2 t^2} \right)^\Lambda \\ &= 16T^2 \int_0^1 dt \ln \left(\frac{1+t}{1-t} \right) \frac{1}{t-t^3} \frac{1}{2} \left[\ln(\Omega^2 - \mu^2 + \Lambda^2) - \ln(\Omega^2 - \mu^2 + \Lambda^2 t^2) \right] \\ &= 16T^2 \int_0^1 dt \ln \left(\frac{1+t}{1-t} \right) \frac{1}{t-t^3} \frac{1}{2} \left[\ln(\Omega^2 - \mu^2 + \Lambda^2) - \ln(\Omega^2 - \mu^2 + \Lambda^2 t^2) \right] \\ &= 16T^2 \int_0^1 dt \ln \left(\frac{1+t}{1-t} \right) \frac{1}{t-t^3} \frac{1}{2} \left[\ln \Lambda^2 + \ln \left(\frac{\Omega^2 - \mu^2}{\Lambda^2} + 1 \right) \right. \\ &\quad \left. - \ln \Lambda^2 - \ln \left(\frac{\Omega^2 - \mu^2}{\Lambda^2} + t^2 \right) \right]. \end{aligned}$$

In the limit $\Lambda \rightarrow \infty$ we can define the second line of (186) as Gl_2

$$Gl_2 = 16T^2 \int_0^1 dt \ln \left(\frac{1+t}{1-t} \right) \frac{\ln t}{t-t^3}. \quad (188)$$

Collecting all $k \leq 0$ terms, Eqs. (187) and (188) (summing $Gl_1 + Gl_2$) we have that

$$G^{2BE}(im) \Big|_{k \leq 0} = 4\pi^2 T^2 \left[\frac{1}{2} \ln \left(\frac{\Lambda^2}{T^2} \right) - \frac{1}{2} \ln \left(\frac{\Omega^2 - \mu^2}{T^2} \right) + \frac{4}{\pi^2} \int_0^1 dt \ln \left(\frac{1+t}{1-t} \right) \frac{\ln t}{t-t^3} \right]. \quad (189)$$

For $k \geq 0$ we can set $m = 0$, because we don't have any $\ln m$ singularities,

$$\begin{aligned} G^{2BE}(im) \Big|_{k \geq 0} &= 16 \int_{\Lambda}^{\infty} dk \frac{1}{(e^{\beta k} - 1)} \int_0^k dq \frac{1}{(e^{\beta q} - 1)} \ln \left(\frac{q+k}{q-k} \right) \\ &= 16T^2 \int_{\Lambda/T}^{\infty} dx \frac{1}{(e^x - 1)} \int_0^x dy \frac{1}{(e^y - 1)} \ln \left(\frac{x+y}{x-y} \right). \end{aligned}$$

Adding and subtracting a $1/y$ term,

$$\begin{aligned} G^{2BE}(im) \Big|_{k \geq 0} &= 16T^2 \int_{\Lambda/T}^{\infty} dx \frac{1}{(e^x - 1)} \int_0^x dy \frac{1}{y} \ln \left(\frac{x+y}{x-y} \right) \\ &+ 16T^2 \int_{\Lambda/T}^{\infty} dx \frac{1}{(e^x - 1)} \int_0^x dy \left[\frac{1}{(e^y - 1)} - \frac{1}{y} \right] \ln \left(\frac{x+y}{x-y} \right). \end{aligned} \quad (190)$$

First let us define

$$G^{2BE}(im) \Big|_{k \geq 0} \equiv I_{k \geq 0}^1 + I_{k \geq 0}^2. \quad (191)$$

Solving the first line in equation (190),

$$I_{k \geq 0}^1 = 4\pi^2 T^2 \left[-x + \ln(-1 + e^x) \right]_{\Lambda/T}^{\infty}$$

$$\approx 4\pi^2 T^2 \left[-\ln\left(\frac{\Lambda}{T}\right) \right] + O(\Lambda) . \quad (192)$$

To solve the second line of equation (190), we can just set $\Lambda = 0$, since the integral is finite,

$$I_{k \geq 0}^2 = 16T^2 \int_0^\infty dx \frac{1}{(e^x - 1)} \int_0^x dy \left[\frac{1}{(e^y - 1)} - \frac{1}{y} \right] \ln \left(\frac{x+y}{x-y} \right).$$

Making $y = xt$,

$$I_{k \geq 0}^2 = 16T^2 \int_0^1 dt \int_0^\infty dx \frac{x}{e^x - 1} \left[\frac{1}{(e^{xt} - 1)} - \frac{1}{xt} \right] \ln \left(\frac{1+t}{1-t} \right) + O(\Lambda) . \quad (193)$$

Collecting all the $k \geq 0$ results, Eqs. (192) and (193), we have that

$$\begin{aligned} G^{2BE}(im) \Big|_{k \geq 0} &= 4\pi^2 T^2 \left[-\frac{1}{2} \ln\left(\frac{\Lambda^2}{T^2}\right) + \frac{4}{\pi^2} \int_0^1 dt \int_0^\infty \frac{xdx}{e^x - 1} \left[\frac{1}{(e^{xt} - 1)} - \frac{1}{xt} \right] \right. \\ &\quad \left. \times \ln \left(\frac{1+t}{1-t} \right) \right]. \end{aligned} \quad (194)$$

Finally, we can write the high- T approximation for $G^{2BE}(im)$ in the form

$$G^{2BE}(im) \Big|_{T \gg m} \approx 4\pi^2 T^2 \left[-\frac{1}{2} \ln \left(\frac{m^2 - \mu^2}{T^2} \right) - 1.50699 \right], \quad (195)$$

where we have evaluated numerically the finite integrals.

Following the same logic, Jones and Parkin (JONES; PARKIN, 2001) have used a little different approximation. They make use of the imaginary time formalism (or Matsubara formalism) and set approximations not only for the two BE term, but for the one BE as well. Their result is,

$$3(I_1'^{-} + I_1'^{+} + \dots) \Big|_{k=im} = \frac{T^2}{(8\pi^2)^2} \ln^2 \left(\frac{1+r}{1-r} \right) + \frac{T^2 r^2}{(2\pi)^4} (\ln 2 - 1/2) +$$

$$-\frac{3T^2}{128\pi^2} \ln\left(\frac{\Omega^2 - \mu^2}{T^2}\right) - \frac{3T^2}{(8\pi)^2} (1.50699) \Big\}. \quad (196)$$

The difference between Jones and Parkin's pioneering result (197) and ours (196) is that they handle all contributions in the high-T approximation and we establish analytic expressions for them, which can be evaluated at both limits ($T \gg m$ and $T \ll m$). In our computation it is possible to take the high-temperature or the low-temperature limit, for the one BE terms. Summing Eqs. (152), (179) and (195), the complete setting sun diagram in the high temperature approximation ($T \gg m$) is,

$$\begin{aligned} I_{Sun}(-m^2) = & \frac{-2\lambda^2}{9} \frac{m^2}{(4\pi)^4} \left\{ -\frac{3}{2\epsilon^2} - \frac{3}{2\epsilon} \left[2 \ln\left(\frac{M^2}{m^2}\right) + \frac{17}{6} \right] - \frac{6}{2} \ln\left(\frac{M^2}{m^2}\right) \left[\frac{17}{6} + \right. \right. \\ & \left. \left. \ln\left(\frac{M^2}{m^2}\right) \right] - \frac{3\mu^2}{m^2} + C_1 \right\} \\ & - \frac{2\lambda^2}{9} \left\{ \frac{3T^2 h_3}{(2\pi)^4} \left[\frac{1}{\epsilon} + 2 + \ln\left(\frac{M^2}{m^2}\right) \right] + \frac{3T^2 h_3^e}{(2\pi)^4} \left(2 - \frac{\pi}{2} \right) + \right. \\ & \left. - \frac{12\pi^2 T^2}{2(2\pi)^4} \left[-\frac{1}{2} \ln\left(\frac{m^2 - \mu^2}{T^2}\right) - 1.50699 \right] \right\}, \quad (197) \end{aligned}$$

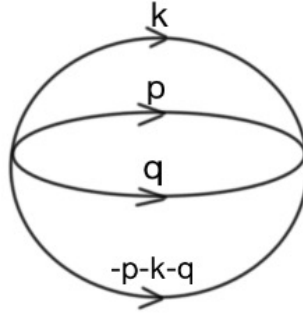
where $C_1 = -7.82654$. Once again, the above result is known in the literature (JONES; PARKIN, 2001), but in this work, we can analytically treat the one BE factor, that is, the only term that needed an approximation was the two Bose-Einstein factor, for the others we can use the high temperature expansion of the thermal functions (Appendix B).

1.7 Basketball Diagram

Let us now evaluate the basketball diagram of Figure 13. We start with the with no BE factors, the term vacuum contribution for this diagram.

1.7.1 I_0 Term

Figure 13. - The basketball diagram



Source: The author, 2022.

The diagram in Figure 13 can be read as follow

$$Basket = C_S i^2 \lambda^2 \int_{p,k,q} \frac{1}{(p^2 - m^2)} \frac{1}{(k^2 - m^2)} \frac{1}{(q^2 - m^2)} \frac{1}{((-p - k - q)^2 - m^2)} \quad (198)$$

where C_S is the symmetry factor, which for our model is $C_S = 1/18$, λ is the coupling constant of the theory and the integral measure means

$$\int_{p,k,q} \equiv \int \frac{d^4 p}{(2\pi)^4} \frac{d^4 k}{(2\pi)^4} \frac{d^4 q}{(2\pi)^4} . \quad (199)$$

Defining I_0 as,

$$I_0 \equiv \int_{p,k,q} \frac{1}{(p^2 - m^2)} \frac{1}{(k^2 - m^2)} \frac{1}{(q^2 - m^2)} \frac{1}{((-p - k - q)^2 - m^2)},$$

that was calculated by Andersen, Strickland and Braaten in (ANDERSEN, 2000). Since we have divergent integrals, we need to do some regularization process. We choose to

work with dimensional regularization in the \overline{MS} scheme.

$$I_0 = \left(\frac{e^{\gamma_E} M^2}{4\pi} \right)^{3\epsilon} \int \frac{d^d k}{(2\pi)^d} \frac{d^d q}{(2\pi)^d} \frac{d^d p}{(2\pi)^d} \frac{1}{(k^2 + m^2)} \frac{1}{(q^2 + m^2)} \frac{1}{(p^2 + m^2)}$$

$$\times \frac{1}{((p+k+q)^2 + m^2)},$$

where M is just a scale parameter that came from the regularization procedure and $d = 4 - 2\epsilon$. Using the Feynman parameters (Appendix A), where $A \equiv (k^2 + m^2)$, $B \equiv (q^2 + m^2)$, $C \equiv (p^2 + m^2)$ and $D \equiv ((p+k+q)^2 + m^2)$ and expressing in terms of Bessel functions the propagators in (198)

$$\mathcal{I}_0 = \frac{m^4}{(4\pi)^6} \left(\frac{e^{\gamma_E} M^2}{m^2} \right)^{3\epsilon} \frac{32}{\gamma_E(2-\epsilon)} \int_0^\infty dt t^{-t+2\epsilon} K_{1-\epsilon}^4(2t)$$

where,

$$K_{1-\epsilon}(2t) = \frac{\gamma_E(1-\epsilon)t^{-1+\epsilon}}{2} + \frac{\gamma_E(1-\epsilon)\gamma_E(\epsilon)}{2} \sum_{j=0} \left(\frac{t^{2j+1+\epsilon}}{(j+1)!\gamma_E(j+1+\epsilon)} \right. \\ \left. - \frac{t^{2j+1-\epsilon}}{j!\gamma_E(2+j-\epsilon)} \right).$$

Putting $d = 4 - 2\epsilon$ and integrating in dt we obtain the following result for the above expression,

$$\mathcal{I}_0 \approx \frac{m^4}{(4\pi)^6} \left(\frac{M^2}{m^2} \right)^{3\epsilon} \left[\frac{2}{\epsilon^3} + \frac{23}{3\epsilon^2} + \frac{(35 + \pi^2)}{2\epsilon} + 39.429 \right]. \quad (200)$$

Next we will show step by step the derivation of the thermal and chemical contributions for the basketball diagram.

1.8 Thermal Basketball

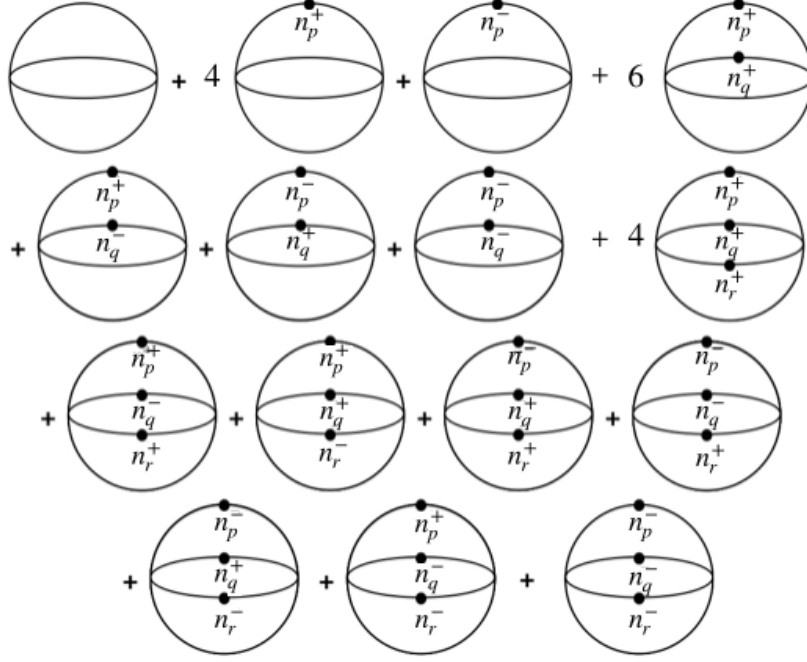
Applying the real-time propagator in the Keldysh formulation (which was explained in the end of the subsection 1.2.3) and after some algebra we can eliminate the four delta product, after that we identify the terms that have the step functions and when

integrated in p_0 will be vanish. With this we can find

$$\begin{aligned}
 I_{ball} = & \mathcal{I}_0 + 4(\mathcal{I}_1^+ + \mathcal{I}_1^-) + 6(\mathcal{I}_2^{++} + \mathcal{I}_2^{+-} + \mathcal{I}_2^{--} + \mathcal{I}_2^{-+}) + 4(\mathcal{I}_3^{+++} + \mathcal{I}_3^{---} + \\
 & + \mathcal{I}_3^{--+} + \mathcal{I}_3^{+-} + \mathcal{I}_3^{+--} + \mathcal{I}_3^{-++} + \mathcal{I}_3^{+--} + \mathcal{I}_3^{++-}) , \tag{201}
 \end{aligned}$$

where the subscript number means the quantity of BE factors and the superscript means the BE with the sign of the chemical potential. These terms with BE factors will give the thermal contribution, for the basketball diagram for the complex scalar complex field. It is important to note that, if we set $\mu = 0$ we recover the same result obtained in (ANDERSEN, 2000). Remembering that, the terms with four BE cancel in the Keldysh prescription and we do not have any pinch singularities. That would come along these terms. The above expression Eq. (201), can be better understood diagrammatically, as shown in Figure 14.

Figure 14. - Pictorial representation of the basketball contributions



Legend: The first diagram is the standard basketball diagram at $T = 0$,
the others are representing the thermal contributions.

Source: The author, 2022.

The thermal contribution with one BE factor can be expressed as

$$\begin{aligned} \mathcal{I}_1^\pm &= \left[\left(\frac{e^{\gamma_E} M^2}{4\pi} \right)^\epsilon \int \frac{d^{4-2\epsilon} p}{(2\pi)^{4-2\epsilon}} n((p_0 - \mu) \text{sgn}(p_0)) 2\pi \delta(p^2 - m^2) \right] \left(\frac{e^{\gamma_E} M^2}{4\pi} \right)^{2\epsilon} \\ &\times \int \frac{d^{4-2\epsilon} q}{(2\pi)^{4-2\epsilon}} \int \frac{d^{4-2\epsilon} r}{(2\pi)^{4-2\epsilon}} \frac{1}{q^2 - m^2} \frac{1}{r^2 - m^2} \frac{1}{(p + q + r)^2 - m^2}. \end{aligned} \quad (202)$$

It is important to note that, the integral above has only one BE, corresponding to a thermal integral times the setting sun diagram which is evaluated at $T = 0$ and on-shell,

$$\begin{aligned} \mathcal{I}_2^\pm &= \left[\left(\frac{e^{\gamma_E} M^2}{4\pi} \right)^\epsilon \int \frac{d^{4-2\epsilon} p}{(2\pi)^{4-2\epsilon}} n((p_0 - \mu) \text{sgn}(p_0)) 2\pi \delta(p^2 - m^2) \right] \\ &\times \left[\left(\frac{e^{\gamma_E} M^2}{4\pi} \right)^\epsilon \int \frac{d^{4-2\epsilon} q}{(2\pi)^{4-2\epsilon}} n((q_0 - \mu) \text{sgn}(q_0)) 2\pi \delta(q^2 - m^2) \right] \end{aligned}$$

$$\times \left(\frac{e^{\gamma_E M^2}}{4\pi} \right)^\epsilon \int \frac{d^{4-2\epsilon} r}{(2\pi)^{4-2\epsilon}} \frac{1}{r^2 - m^2} \frac{1}{(p+q+r)^2 - m^2}. \quad (203)$$

The above term can be represented by two thermal integrals times the eye diagram,

$$\begin{aligned} \mathcal{I}_3^\pm &= \left[\left(\frac{e^{\gamma_E M^2}}{4\pi} \right)^\epsilon \int \frac{d^{4-2\epsilon} p}{(2\pi)^{4-2\epsilon}} n((p_0 - \mu) \operatorname{sgn}(p_0)) 2\pi \delta(p^2 - m^2) \right] \\ &\times \left[\left(\frac{e^{\gamma_E M^2}}{4\pi} \right)^\epsilon \int \frac{d^{4-2\epsilon} q}{(2\pi)^{4-2\epsilon}} n((q_0 - \mu) \operatorname{sgn}(q_0)) 2\pi \delta(q^2 - m^2) \right] \\ &\times \left(\frac{e^{\gamma_E M^2}}{4\pi} \right)^\epsilon \int \frac{d^{4-2\epsilon} r}{(2\pi)^{4-2\epsilon}} n((r_0 - \mu) \operatorname{sgn}(r_0)) 2\pi \delta(r^2 - m^2) \frac{-1}{(p+q+r)^2 - m^2} \end{aligned} \quad (204)$$

where the last integral in (204) will be the only true challenge that we need to solve, since the others are well solved in literature.

1.8.1 One Bose-Einstein factor

Let us begin with the easiest part, the term that contains only one BE factor:

$$\begin{aligned} 4(\mathcal{I}_1^+ + \mathcal{I}_1^-) &= 4(\text{Settingsun}) \times \left[\left(\frac{e^{\gamma_E M^2}}{4\pi} \right)^\epsilon \int \frac{d^{4-2\epsilon} p}{(2\pi)^{4-2\epsilon}} n((p_0 - \mu) \operatorname{sgn}(p_0)) \right. \\ &\left. \times 2\pi \delta(p^2 - m^2) \right]. \end{aligned} \quad (205)$$

Using that,

$$\delta(p^2 - m^2) = \frac{1}{2\omega_p} [\delta(p_0 - \omega_p) + \delta(p_0 + \omega_p)],$$

and integrating in the p_0 , we have

$$\int \frac{d^{4-2\epsilon} p}{(2\pi)^{4-2\epsilon}} n((p_0 - \mu) \operatorname{sgn}(p_0)) 2\pi \delta(p^2 - m^2) = \int \frac{d^{3-2\epsilon} p}{(2\pi)^{3-2\epsilon}} \frac{n_p^+ + n_p^-}{2\omega_p}.$$

Evaluating for the limit $\epsilon \rightarrow 0$

$$\frac{1}{2\pi^2} \int \frac{p^2 dp}{1} \frac{n_p^+ + n_p^-}{2\omega_p} \equiv \frac{1}{2\beta^2\pi^2} [h_3(y, r) + h_3(y, -r)].$$

But,

$$n_p^+ = \frac{1}{e^{\beta(\omega_p + \mu)} - 1}, \quad \omega_p = \sqrt{p^2 + m^2}.$$

which leave us with,

$$\frac{1}{2\beta^2\pi^2} [h_3(y, r) + h_3(y, -r)] = \frac{T^2}{\pi^2} h_3^\epsilon(y, r), \quad y \equiv \beta \cdot m, \quad r \equiv \mu/m.$$

Finally, the contribution with one BE factor reads

$$4(\mathcal{I}_1^+ + \mathcal{I}_1^-) = 4(\text{Settingsun}) \times \frac{T^2}{\pi^2} h_3^\epsilon(y, r).$$

Using the result for the setting sun (152) calculated in the previous section (noting that $\beta = 1/T$), we obtain

$$4(\mathcal{I}_1^+ + \mathcal{I}_1^-) = \frac{m^2}{(4\pi)^4} \left(\frac{M}{m}\right)^{4\epsilon} \left[-\frac{6}{\epsilon^2} - \frac{17}{\epsilon} - \frac{12\mu^2}{m^2} + 4C_1 \right] \times \frac{T^2}{\pi^2} h_3^\epsilon(y, r), \quad (206)$$

where $C_1 = -7.82654$.

1.8.2 Two Bose-Einstein factors

For the terms \mathcal{F}_2^\pm with two BE factors, the procedure is the same. We have to collect the terms that have, at least, one BE sign in common, making possible to write just one expression for those terms,

$$6(\mathcal{I}_2^{++} + \mathcal{I}_2^{+-} + \mathcal{I}_2^{--} + \mathcal{I}_2^{-+}) = 6 \left[\int \frac{d^{3-2\epsilon} p}{(2\pi)^{3-2\epsilon}} \frac{n_p^+ + n_p^-}{2\omega_p} \right. \\ \left. \times \int \frac{d^{3-2\epsilon} q}{(2\pi)^{3-2\epsilon}} \frac{n_q^+ + n_q^-}{2\omega_q} \right] \times \left(\text{Eyediagram} \right). \quad (207)$$

For the thermal part we can take the limit $\epsilon \rightarrow 0$, leaving us with

$$6(\mathcal{I}_2^{++} + \mathcal{I}_2^{+-} + \mathcal{I}_2^{-+} + \mathcal{I}_2^{--}) = \frac{3}{2} \left[\frac{1}{(4\pi)^2} \left(\frac{M}{m} \right)^{2\epsilon} \frac{4T^4}{\epsilon \pi^4} (h_3^e(y, r))^2 - \int \frac{d^3p}{(2\pi)^3} \frac{n_p^+ + n_p^-}{\omega_p} \right. \\ \left. \times \int \frac{d^3q}{(2\pi)^3} \frac{n_q^+ + n_q^-}{\omega_q} \sum_{i,j} \int_0^1 \ln \left(\frac{m^2 + x(1-x)(\omega_{i,j}^2 - A^2)}{m^2} \right) dx \right], \quad (208)$$

where $A \equiv |\vec{p} + \vec{q}|$ and $\omega_{ij} = i \cdot \omega_p + j \cdot \omega_q$. The above integral in x , give us

$$\sum_{i,j} \int_0^1 \ln \left(\frac{m^2 + x(1-x)(\omega_{i,j}^2 - A^2)}{m^2} \right) dx = \left\{ -2 \right. \\ \left. + \sum_{i,j} \left(\frac{\omega_{ij}^2 - A^2 + 4m^2}{\omega_{ij}^2 - A^2} \right)^{1/2} \ln \left[\frac{(\omega_{ij}^2 - A^2)^{1/2} + (\omega_{ij}^2 - A^2 - 4m^2)^{1/2}}{(\omega_{ij}^2 - A^2)^{1/2} - (\omega_{ij}^2 - A^2 - 4m^2)^{1/2}} \right] \right\}. \quad (209)$$

The above term corresponds to the $A^2 < E^2 - 4m^2$ condition. Integrating the constant term in $(1/pq) \int AdA$, we obtain

$$\frac{8}{(2\pi)^4} \int p^2 dp \frac{n_p^+ + n_p^-}{\omega_p} \int q^2 dq \frac{n_q^+ + n_q^-}{\omega_q} \left[\frac{A^2}{pq} \right]_{|\vec{p}-\vec{q}|}^{|\vec{p}+\vec{q}|} = 8 \frac{T^4}{\pi^4} (h_3^e(y, r))^2, \quad (210)$$

and plugging in our calculations, we have

$$6(\mathcal{I}_2^{++} + \mathcal{I}_2^{+-} + \mathcal{I}_2^{-+} + \mathcal{I}_2^{--}) = \frac{6}{(4\pi)^2} \left(\left(\frac{M}{m} \right)^{2\epsilon} \frac{1}{\epsilon} + 2 \right) \frac{T^4}{\pi^4} h_3^e(y, r)^2 + \frac{6}{(4\pi)^4} \mathcal{K}_2. \quad (211)$$

Now, the problem remains in solving \mathcal{K}_2 , where we choose the follow substitution

$$\frac{d}{dt'}(A^2) = \frac{d}{dt'}(p^2 + q^2 + 2pqt') = 2A \frac{dA}{dt'} = 2pq,$$

where $t' \equiv \cos \theta_{p,q}$ and

$$dt' = \frac{A}{pq} dA.$$

Plugging these definitions, we can obtain the term \mathcal{K}_2 , as

$$\begin{aligned} \mathcal{K}_2 &= -4 \int_0^\infty p^2 dp \frac{n_p^+ + n_p^-}{\omega_p} \int_0^\infty q^2 dq \frac{n_q^+ + n_q^-}{\omega_q} \sum_\sigma \int_{|\bar{p}-\bar{q}|}^{|\bar{p}+\bar{q}|} \frac{A}{pq} dA \\ &\times \left(\frac{\omega_\sigma^2 - A^2 + 4m^2}{\omega_\sigma^2 - A^2} \right)^{1/2} \ln \left[\frac{(\omega_\sigma^2 - A^2)^{1/2} + (E_\sigma^2 - A^2 - 4m^2)^{1/2}}{(\omega_\sigma^2 - A^2)^{1/2} - (\omega_\sigma^2 - A^2 - 4m^2)^{1/2}} \right], \end{aligned} \quad (212)$$

where $\omega_\sigma = \omega_p + \sigma\omega_q$. Summing the frequencies $\omega_p + \omega_q$ and $\omega_p - \omega_q$ (note that here, we've already multiplied by 2, since the summations will give the same answer), making the integral in dA and taking the limit $m \rightarrow 0$,

$$\mathcal{K}_2 = -\frac{(4\pi)^4}{72} \left[\ln \left(\frac{4\pi T}{m} \right) - \frac{1}{2} - \frac{\zeta'(-1)}{\zeta(-1)} \right], \quad (213)$$

which reproduce the result obtained in (ANDERSEN, 2000).

1.8.3 Three Bose-Einstein factors

For the last term \mathcal{F}_3^\pm with three BE factors, we will proceed in the same way. By putting all the pieces together and using the Dirac delta function to integrate over the time component of the momenta. After that, we can set $\epsilon \rightarrow 0$,

$$\begin{aligned} 4(\mathcal{I}_3^{+++} + \mathcal{I}_3^{---} + \dots) &= 4 \int \frac{d^3p}{(2\pi)^3} \frac{n_p^+ + n_p^-}{2\omega_p} \int \frac{d^3q}{(2\pi)^3} \frac{n_q^+ + n_q^-}{2\omega_q} \\ &\times \int \frac{d^3r}{(2\pi)^3} \frac{n_r^+ + n_r^-}{2\omega_r} \sum_{i,k,j}^{1,-1} \frac{-1}{(\omega_{ijk})^2 + m^2} \\ &= \frac{1}{(2\pi)^6} \int_0^\infty p^2 dp \frac{n_p^+ + n_p^-}{\omega_p} \int_0^\infty \int_{-1}^1 q^2 dq dt' \frac{n_q^+ + n_q^-}{\omega_q} \int_0^\infty \int_{-1}^1 r^2 dr dt \frac{n_r^+ + n_r^-}{\omega_r} \times \\ &\times \sum_{i,k,j}^{1,-1} \frac{-1}{(\omega_{ijk})^2 + m^2}, \end{aligned} \quad (214)$$

where, t and t' are different angles. The frequencies are defined as,

$$\omega_{ijk} = i \cdot \omega_p + j \cdot \omega_q + k \cdot \omega_r, \quad (215)$$

where $i, j, k = \pm$. Defining $\vec{A} \equiv \vec{p} + \vec{q}$, we can make the integral over the first angle $t \equiv \cos \theta_{r,A}$, where $\theta_{r,A}$ is the angle between \vec{r} and \vec{A} ,

$$\begin{aligned} \int_{-1}^1 dt \frac{-1}{\omega_{ijk}^2 + |A + \vec{r}|^2 + m^2} &= \int_{-1}^1 dt \frac{-1}{\omega_{ijk}^2 + (A^2 + r^2 + Art) + m^2} \\ &= \frac{1}{Ar} \arctan \left[\frac{2Ar}{A^2 - \omega_{ijk}^2 + m^2 + r^2} \right] \\ &= \frac{1}{2Ar} \left[\ln \left(1 + \frac{2Ar}{A^2 - \omega_{ijk}^2 + m^2 + r^2} \right) - \ln \left(1 - \frac{2Ar}{A^2 - \omega_{ijk}^2 + m^2 + r^2} \right) \right] \\ &= \frac{1}{2Ar} \left[\ln \left(\frac{A^2 - \omega_{ijk}^2 + m^2 + r^2 + 2Ar}{A^2 - \omega_{ijk}^2 + m^2 + r^2 - 2Ar} \right) \right]. \end{aligned}$$

Now, instead of integrating the next angle t' , we will perform the following replacement $dt' = d \cos \theta_{p,q} = AdA/(pq)$,

$$\begin{aligned} \int_{|p-q|}^{|p+q|} \frac{AdA}{pq} \frac{1}{2Ar} \left[\ln \left(\frac{A^2 - \omega_{ijk}^2 + m^2 + r^2 + 2Ar}{A^2 - \omega_{ijk}^2 + m^2 + r^2 - 2Ar} \right) \right] \\ = \frac{1}{2pqr} \int_{|p-q|}^{|p+q|} dA \ln \left(\frac{A^2 - \omega_{ijk}^2 + m^2 + r^2 + 2Ar}{A^2 - \omega_{ijk}^2 + m^2 + r^2 - 2Ar} \right). \end{aligned} \quad (216)$$

The integral result will be,

$$\begin{aligned} \int_{|p-q|}^{|p+q|} dA \ln \left(\frac{A^2 - \omega_{ijk}^2 + m^2 + r^2 + 2Ar}{A^2 - \omega_{ijk}^2 + m^2 + r^2 - 2Ar} \right) &= f(\omega_{ijk}, p + q + r) + \\ &- f(\omega_{ijk}, p + q - r) - f(\omega_{ijk}, p - q + r) + f(\omega_{ijk}, p - q - r), \end{aligned} \quad (217)$$

where,

$$f(\omega, p) = p \ln |m^2 - \omega^2 + p^2| + (\omega^2 - m^2)^{1/2} \ln \left| \frac{(\omega^2 - m^2)^{1/2} + p}{(\omega^2 - m^2)^{1/2} - p} \right|. \quad (218)$$

The above result, allow us to define a useful quantity,

$$\begin{aligned} \mathcal{K}_3 \equiv & \frac{2}{T^4} \int_0^\infty p dp \frac{n_p^+ + n_p^-}{\omega_p} \int_0^\infty q dq \frac{n_q^+ + n_q^-}{\omega_q} \int_0^\infty r dr \frac{n_r^+ + n_r^-}{\omega_r} \sum_{j,k=\pm 1} \left[f(\omega_{jk}, p+q+r) \right. \\ & \left. - f(\omega_{jk}, p+q-r) - f(\omega_{jk}, p-q+r) + f(\omega_{jk}, p-q-r) \right]. \end{aligned} \quad (219)$$

If we limit the region of integration by $r < q < p$ and set $\mu = 0$ the constant factor 2 become 96, since we will have 8 plus 3! multiplying the integral, which gives us the same result found by the authors of (ANDERSEN, 2000). The result is still not complete, we have to sum all the frequencies ω^2 , we will proceed as follows,

$$\sum_{i,k,j}^{1,-1} (i * \omega_p + j * \omega_q + k * \omega_r)^2 = 2 \sum_{k,j}^{1,-1} (\omega_p + j * \omega_q + k * \omega_r)^2. \quad (220)$$

After that, we expand in a Taylor series until first order with respect to the mass. Taking this result, summing the others answers corresponding to the choices $(-p, -q, r)$, $(-p, q, -r)$, $(p, -q, -r)$ and multiplying all by 2, we have the final finite term of this integration, which is

$$\begin{aligned} & = 2 \times 2 \left[(p+q+r) \ln(p+q+r) - (-p+q+r) \ln(-p+q+r) \right. \\ & \left. - (p-q+r) \ln(p-q+r) - (p+q-r) \ln(p+q-r) \right]. \end{aligned} \quad (221)$$

Let us make a reflection about the result above. As one can see, there is no IR divergent term, what suggests that there will be no cutoff dependence and even more, no chemical potential. Since we do not have IR term, we just need to consider the high momenta regime or the hard momenta (when $m \rightarrow 0$ and $\mu \rightarrow 0$). Plugging the result in the

equation (214) we can calculate it numerically. This had been done by Frenkel and Sá in (FRENKEL; SAA; TAYLOR, 1992). In order to give an analytical answer, we will proceed as indicated by Arnold and Zhai in (ARNOLD; ZHAI, 1994). Taking all the pieces until now, we have

$$\begin{aligned}
4(\mathcal{I}_3^{+++} + \mathcal{I}_3^{---} + \dots) &= \frac{32}{(2\pi)^6} \int dp \frac{1}{e^{\beta p} - 1} \int dq \frac{1}{e^{\beta q} - 1} \int dr \frac{1}{e^{\beta r} - 1} \times \\
&\times \left[(p + q + r) \ln(p + q + r) - (-p + q + r) \ln(-p + q + r) + \right. \\
&\left. - (p - q + r) \ln(p - q + r) - (p + q - r) \ln(p + q - r) \right], \tag{222}
\end{aligned}$$

we can easily see that this expression can be recovered from

$$4(\mathcal{I}_3^{+++} + \mathcal{I}_3^{---} + \dots) \Big|_{m,\mu=0} = \int \frac{d^3 p}{(2\pi)^3} \frac{d^3 q}{(2\pi)^3} \frac{d^3 r}{(2\pi)^3} \frac{n_p n_q n_r}{p q r} \frac{1}{|\vec{p} + \vec{q} + \vec{r}|^2}.$$

Making a Fourier transformation to the coordinate space,

$$\int \frac{d^3 p}{(2\pi)^3} \frac{n_p}{p} e^{i\vec{p}\vec{x}} = \frac{1}{2\pi^2 x} \int_0^\infty dp \frac{\sin(\beta p x)}{e^{\beta p} - 1} = \frac{1}{4\pi x \beta} \left(\cos(\pi x) - \frac{1}{\pi x} \right), \tag{223}$$

leads us to,

$$\begin{aligned}
&\int d^3 x \left[\frac{1}{4\pi x \beta} \left(\coth \pi x - \frac{1}{\pi x} \right) \right]^3 \frac{1}{4\pi x \beta} \\
&= \frac{1}{4} \frac{1}{(4\pi)^2 \beta^4} \int_0^\infty dx \frac{1}{x^2} \left(\coth x - \frac{1}{x} \right)^3 \\
&= \frac{1}{4} \frac{1}{(4\pi)^2 \beta^4} \left[-\frac{1}{3} \frac{\zeta'(-3)}{\zeta(-3)} + \frac{1}{3} \frac{\zeta'(-1)}{\zeta(-1)} - \frac{7}{45} \right], \tag{224}
\end{aligned}$$

and then

$$4(\mathcal{I}_3^{+++} + \mathcal{I}_3^{---} + \dots) \approx \frac{14.1723}{32\pi^6 \beta^4}. \tag{225}$$

After all of this, we can write the final answer for the basketball diagram, by summing Eqs. (200), (206), (211) and (219), to obtain

$$I_{ball} = \mathcal{I}_0 + 4(\mathcal{I}_1^+ + \mathcal{I}_1^-) + 6(\mathcal{I}_2^{++} + \mathcal{I}_2^{+-} + \mathcal{I}_2^{-+} + \mathcal{I}_2^{--}) + 4(\mathcal{I}_3^{+++} + \mathcal{I}_3^{--+} + \mathcal{I}_3^{-++} + \mathcal{I}_3^{+--} + \mathcal{I}_3^{+-+} + \mathcal{I}_3^{+--}) ,$$

which gives,

$$\begin{aligned} I_{ball} = & \frac{m^4}{(4\pi)^6} \left(\frac{M^2}{m^2} \right)^{3\epsilon} \left[\frac{2}{\epsilon^3} + \frac{23}{3\epsilon^2} + \frac{(35 + \pi^2)}{2\epsilon} + C_2 \right] + \frac{m^2}{(4\pi)^4} \left(\frac{M}{m} \right)^{4\epsilon} \left[-\frac{6}{\epsilon^2} \right. \\ & \left. - \frac{17}{\epsilon} - \frac{12\mu^2}{m^2} + 4C_1 \right] \left(\frac{T^2}{\pi^2} h_3^\epsilon(y, r) \right) + 6 \frac{1}{(4\pi)^2} \left[\left(\frac{M}{m} \right)^{2\epsilon} \frac{1}{\epsilon} + 2 \right] \left(\frac{T^4}{\pi^4} h_3^\epsilon(y, r)^2 \right) \\ & + \frac{T^4}{(4\pi)^6} \left(6 \mathcal{K}_2 + 4 \mathcal{K}_3 \right) , \end{aligned} \quad (226)$$

where $C_1 = -7.82654$, $C_2 = 39.429$. In the high temperature limit $T \gg m$,

$$\mathcal{K}_2 \rightarrow -\frac{(4\pi)^4}{72} \left[\ln \left(\frac{4\pi T}{m} \right) - \frac{1}{2} - \frac{\zeta'(-1)}{\zeta(-1)} \right] , \quad \mathcal{K}_3 \rightarrow 453.514 . \quad (227)$$

The above result brings of new the chemical potential and it is in agreement with the literature (ANDERSEN, 2000), in the case $\mu = 0$ we recover the result of (ANDERSEN, 2000). Before we continue, another calculation is needed: the computation of the bare parameters in terms of the physical ones.

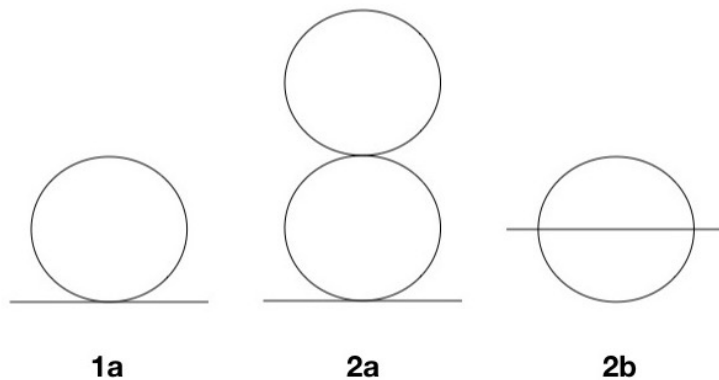
1.9 Physical Parameters

For a complete/correct description of the free energy we need to compute the bare mass and coupling, otherwise, the contributions calculated above just represent the vacua of the theory.

1.9.1 Physical Mass

Any physical mass should not depend on the temperature (or chemical potential), meaning that, for a scalar particle (the Higgs particle for example), we should be able to use the parameters that are used to compute the Higgs in the LHC, since we have a $\lambda\phi^4$ potential, that is the same potential for the Higgs particle in the Standard Model of Particle Physics.

Figure 15. - Self-energy contributions to the scalar field at $T=0$



Source: The author, 2022.

A mass of a particle is given by the location of the pole in the propagator (LEHMANN, 1955). If $\Sigma(p^2)$ is the self-energy function, then

$$p^2 + \bar{m}^2 + \Sigma(p^2) = 0 \quad \text{at} \quad p^2 = -m^2 . \quad (228)$$

Until two loops, the contributions to $\Sigma(p^2)$ that establish the mass of the theory are shown in the Figure 15. We will compute these contributions order by order in perturbation theory.

1.9.1.1 One-Loop Contribution

The one-loop contribution does not depend on any external momenta and it is given by,

$$\Sigma_1 = \Sigma_{1a} + \Delta_1 \bar{m}^2 , \quad (229)$$

where the tadpole term is,

$$\Sigma_{1a} = \frac{2\bar{\lambda}}{3} I_1 \Big|_{T=0, \mu=0},$$

and $\Delta_1 \bar{m}^2$ is the counterterm (see Appendix C). Summing up the counter-term (Appendix C) we have the one-loop contribution,

$$\Sigma_1 = -\frac{2\bar{\lambda}}{3} \frac{\bar{m}^2}{(4\pi)^2} \left(1 + 2 \ln \left(\frac{M}{\bar{m}} \right) \right). \quad (230)$$

1.9.1.2 Two-Loop Contributions

The two loops contributions to $\Sigma(p^2)$ are more complicated, because of the setting sun diagram, diagram 2b from Figure 15, which has an external momenta and need to be integrated on-shell

$$\Sigma_2(p^2) = \Sigma_{2a} + \Sigma_{2b}(p^2) + \frac{\partial \Sigma_{1a}}{\partial \bar{m}} \Delta_1 \bar{m}^2 + \frac{\Sigma_{1a}}{\bar{\lambda}} \Delta_1 \bar{\lambda} + \Delta_2 \bar{m}^2, \quad (231)$$

and the last two terms in Eq. (231) are the counterterms required to make Σ_2 finite. The tadpole with one-loop insertion is given by the term 2a shown in Figure 15 and it is

$$\Sigma_{2a} = -\frac{4\bar{\lambda}^2}{9} I_1 I_2 \Big|_{T=0}.$$

Using the expressions for I_1 and I_2 in the Appendix C, we have that

$$\Sigma_{2a} = -\frac{4\bar{\lambda}^2}{9} \left[\frac{\bar{m}^2}{(4\pi)^2} \left(\frac{M}{\bar{m}} \right)^{2\epsilon} e^{\gamma_E \cdot \epsilon} \gamma_E [-1 + \epsilon] \right] \times \left[\frac{1}{(4\pi)^2} \left(\frac{M}{\bar{m}} \right)^{2\epsilon} e^{\gamma_E \cdot \epsilon} \gamma_E [\epsilon - 1] (\epsilon - 1) \right].$$

The remaining is the setting sun diagram, already calculated in Section 1.5. The answer for the on-shell contribution is,

$$\begin{aligned} \Sigma_{2b}(-\bar{m}^2) &= \frac{\bar{m}^2 \bar{\lambda}^2}{3(4\pi)^4} \left\{ \frac{1}{\epsilon^2} + \frac{1}{\epsilon} \left[2 \ln \left(\frac{M^2}{\bar{m}^2} \right) + \frac{17}{6} \right] + 2 \ln \left(\frac{M^2}{\bar{m}^2} \right) \left[\frac{17}{6} + \right. \right. \\ &\left. \left. + \ln \left(\frac{M^2}{\bar{m}^2} \right) \right] + \frac{3\mu^2}{\bar{m}^2} + C_1 \right\}, \end{aligned}$$

where $C_1 = -7.82654$. Since we are interested in the physical mass, which means the mass of the field in the vacuum, we have to set $\mu = 0$. Summing up all of the counter-terms, we can write an expression for the physical mass m in terms of the bare mass \bar{m} . By inverting this expression, we can write \bar{m} in terms of m :

$$m^2 = \bar{m}^2 + \Sigma(P^2) , \quad (232)$$

such that,

$$m^2 = \bar{m}^2 - \frac{2}{3}\alpha \bar{m}^2(1 + \bar{L}) + \frac{2}{9}\alpha^2\bar{m}^2\left(\frac{13}{2}\bar{L}^2 + \frac{31}{4}\bar{L} - \frac{\pi^2}{4} - \frac{2}{3} + \frac{1}{3}C_1\right) . \quad (233)$$

Taking into account the constants, we can have a more compact answer,

$$m^2 = \bar{m}^2 - \frac{2}{3}\alpha \bar{m}^2(1 + \bar{L}) + \frac{2}{9}\alpha^2\bar{m}^2\left(\frac{13}{2}\bar{L}^2 + \frac{31}{4}\bar{L} + B_2\right) , \quad (234)$$

where,

$$B_2 = -\frac{\pi^2}{4} - \frac{2}{3} + \frac{1}{3}C_1 . \quad (235)$$

Inverting the expression (234), we obtain

$$\bar{m}^2 = m^2 + \frac{2}{3}\alpha m^2(1 + L) + \frac{2}{9}\alpha^2 m^2\left(\frac{13}{2}L^2 + \frac{31}{4}L + B_2\right) , \quad (236)$$

which gives us the bare mass \bar{m} expressed in terms of the physical mass m . The above results can be found in many textbooks, in special we indicate the Hagen Kleinert book about scalar theories (KLEINERT; SCHULTE-FROHLINDE'S, 2001).

1.9.2 Physical Coupling

A good way to define the coupling is using some renormalization condition for a scattering $2 \rightarrow 2$ process. The amplitude should be $-\bar{\lambda}$ at the threshold $p = (\bar{m}, 0)$ (on-shell at $\mu = 0$). It is often useful to express scattering amplitudes in terms of the Mandelstam variables,

$$s = (p + p')^2 = (k + k')^2, \quad t = (k - p)^2 = (k' - p')^2; \quad u = (k' - p)^2 = (k - p')^2.$$

Each channel (it is we how denominate the variables above) represents a possible configuration for a $2 \rightarrow 2$ process. For any process, s is the square of the total initial 4-momentum. The definitions of t and u appear to be interchangeable (by renaming $k \rightarrow k'$); it is conventional to define t as the squared difference of the initial and final momenta of the most similar particles. The renormalization condition for the vertex interaction follows by setting $\bar{\lambda}$ equal to the magnitude of the scattering amplitude at zero momentum, which means that at the threshold $s = 4\bar{m}^2$ and $t = u = 0$. By applying that,

$$\lambda = \bar{\lambda} - [G^{(4)}(\bar{m}^2) + 2G^{(4)}(0)] , \quad (237)$$

where,

$$G^{(4)}(p^2) = -\frac{5\bar{\lambda}^2}{9} \int \frac{d^4k}{(2\pi)^4} \frac{1}{k^2 + \bar{m}^2} \frac{1}{(k+p)^2 + \bar{m}^2} . \quad (238)$$

By using dimensional regularization and applying the Feynman parameters (3.4.1), we can easily obtain that

$$G^{(4)}(p^2) = -\frac{5\bar{\lambda}^2}{9} \left(\frac{M^2 e^{\gamma_E}}{4\pi} \right)^\epsilon \int_0^1 dx \int \frac{d^d k}{(2\pi)^d} \frac{1}{[k^2 - x(1-x)p^2 + \bar{m}^2]^2} . \quad (239)$$

Applying the formulas of Appendix C,

$$G^{(4)}(p^2) = -\frac{5\bar{\lambda}^2}{9(4\pi)^2} \left(\frac{M^2}{\bar{m}^2} \right)^\epsilon \gamma_E(\epsilon) e^{\gamma_E \epsilon} \int_0^1 dx \left[\frac{\bar{m}^2}{\bar{m}^2 - x(1-x)p^2} \right]^\epsilon , \quad (240)$$

and expanding to $O(\epsilon^0)$ and summing the counterterm (Appendix C), we obtain

$$\lambda = \bar{\lambda} - \frac{5\bar{\lambda}^2}{9(4\pi)^2} \left[3 \ln \left(\frac{M^2}{\bar{m}^2} \right) + 2 \right] . \quad (241)$$

Inverting (241) and putting in the notation of Eq. (89), we have

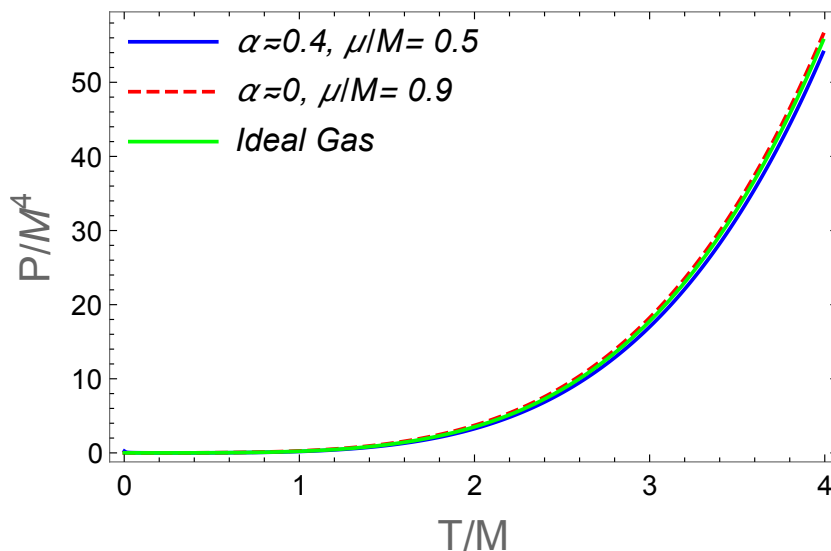
$$\bar{\alpha} = \alpha + \frac{5}{9} \alpha^2 (3L + 2) . \quad (242)$$

The above result also can be found in literature (KLEINERT; SCHULTE-FROHLINDE'S, 2001).

2 PERTURBATIVE ANALYSES

Plugging the bare mass and the bare coupling in the two and three-loop contributions, we can compute the free energy of our theory and since we are interested in the thermal free energy, thus we will discard the vacuum ($T = 0$) contributions. The one-loop free energy is just the thermal part of equation (90). Since the one loop vacuum contribution is the ring diagram (diagram 1a from Figure 10), the bare mass is calculated only until one-loop (the tadpole diagram). The one-loop result gives us the ideal gas contribution ($\mathcal{F}_{IdealGas} = -\pi^2 T^4/45$). For one-loop there is no need to consider the corrections that came from the coupling. A simple way to see that is to compare the ideal gas free energy with the one loop computation expanded in the physical mass until α order and the one loop computation until α^0 .

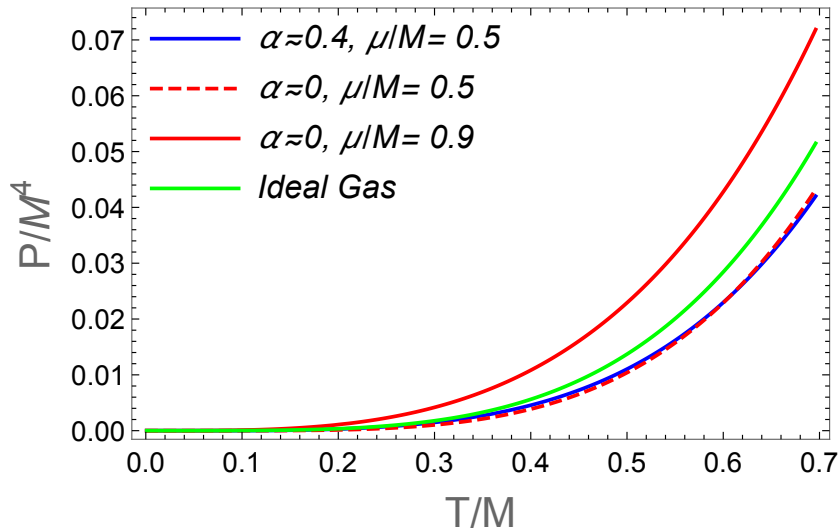
Figure 16. - One-loop pressure P varying with T



Legend: The blue and red curves are the free-energy with the mass and coupling corrections. The green is the ideal gas pressure.

Source: The author, 2022.

In a numerical computation, we do not need to consider any expansion for the temperature functions, we just compute the thermal integral numerically. The same holds for different values of α and μ . This is shown in the Figure 16. For small (or high) temperature values, the ideal gas still is a good approximation.

Figure 17. - One-Loop Pressure P varying with T 

Legend: The blue and red curves are the free energy with the mass and coupling corrections, the green is the ideal gas pressure.

Source: The author, 2022.

Even when we look more closely (see Figure 17), we do not have too much difference between the computations considering α (the blue curve and the dashed red are matching). Then, we conclude that the α corrections are irrelevant for one-loop approximation. However, when the chemical potential μ is taken into account (see the red curves of Figure 17), there is a difference. In this order, it is possible to write down an analytical expression for both limits, small and high T .

For small temperature, we have

$$P_{T \ll m} \approx T \left(\frac{mT}{2\pi} \right)^{3/2} e^{-m/T} (e^{\mu/T} + e^{-\mu/T}) . \quad (243)$$

The sign at the exponential inside the parenthesis, stands for particle $+\mu$ and antiparticle $-\mu$. Note that by setting $\mu = 0$ in (243), we recover the usual result for the ideal gas, in the $T \ll m$ regime.

For high temperatures,

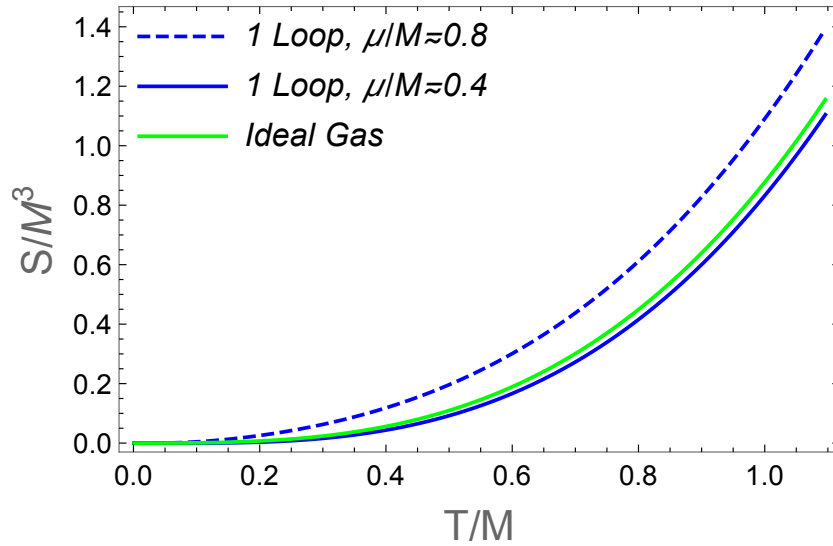
$$P_{T \gg m} \approx \frac{\pi^2 T^4}{45} - \frac{m^2 T^2}{12} + \frac{\mu^2 m^2}{8\pi^2} + \frac{\mu^2 T^2}{6} - \frac{\mu^4}{24\pi^2} . \quad (244)$$

At the above approximation, we consider only the even terms of the high-temperature expansion. The ideal gas takes only the first term of the expansion (in $\mu = 0$ case). In order to recover information about the chemical potential, we need to consider other terms of the expansion. A good approximation, that already gives us relevant information about the charge and the number of particles, is

$$P_{T \gg m} \approx \frac{\pi^2 T^4}{45} + \frac{\mu^2 T^2}{6}. \quad (245)$$

The advantage to work in a thermal field theory is that we are able to compute the pressure, the entropy and any desired thermodynamic quantity, not only with respect to the temperature but with respect to the chemical potential and others quantities as well.

Figure 18. - One-loop entropy S varying with the temperature T



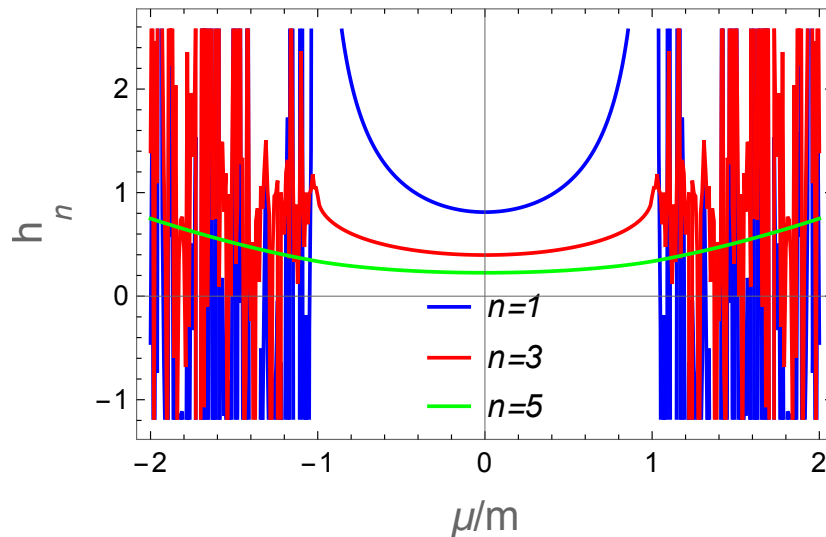
Legend: The blue curve is the one loop approximation and the green curve is the ideal gas entropy. For curves we take $T = 0.2$, $M = T$ and $m^2 = M^2$.

Source: The author, 2022.

The Figure 18 shows how the entropy, defined as $S = \partial P / \partial T$, changes for different values of the chemical potential. A difference begins at $T/M \approx 0.2$. We are able to see that because the chemical potential become more sensible for small values of T . An important thing to notice here is the range of $\mu/M \in [0, 1]$; all of our analysis will be following this range. The explanation for that relies at the convergence of the thermal integrals. The Bose-Einstein integrals only give a convergent result if $|\mu| \leq m$. A simple

way to visualize that is doing the numerical analysis of those integrals.

Figure 19. - Bose-Einstein integrals h 's varying with μ



Legend: The blue curve is the h_1 , the red curve is h_3 and h_5 the green curve . For all curves we take $T = M$ and $m = M$.

Source: The author, 2022.

From Figure 19 it is clear that only h_5 has some convergent result for $\mu \geq m$. However, even when $\mu > m$, the function h_5 (explicitly given in the Appendix A) does not have a physical answer because, for those regions, the free energy assumes a complex value. A natural question arises: What does it happen with the pressure (or other thermodynamical quantity) as we increase the order of perturbation theory? We know that, in the equilibrium, when there is no time evolution of the system, those quantities should converge. We investigate that next.

2.1 Two and Three loops Free energy

We saw that, for one loop, it is enough to consider terms until $O(\alpha^0)$, which means that, for two loops, we will only have terms until $O(\alpha)$ and for three loops, until $O(\alpha^2)$. By taking all the vacuum contributions (90), (94), (108), replacing the bare mass (236) and the bare coupling (241), expanding to order $O(\alpha^2)$ and subtracting the non-thermal contributions, we find the three-loop free energy for the complex scalar field in the physical

mass,

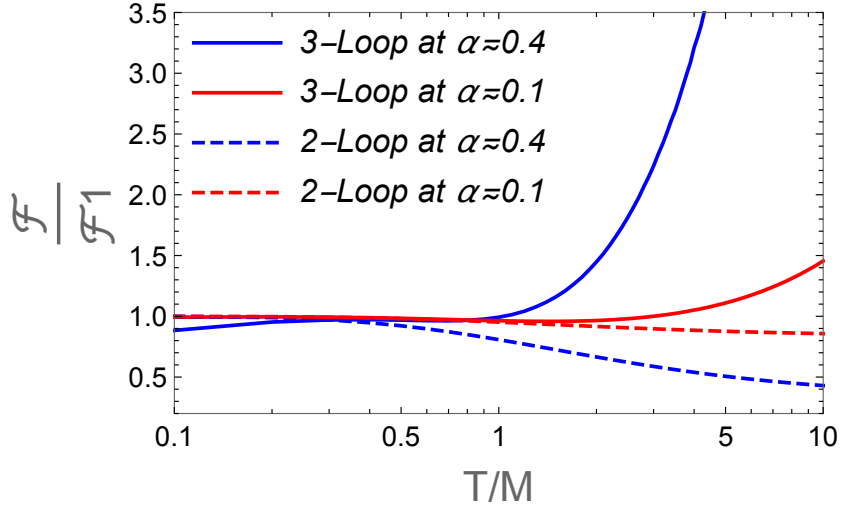
$$\mathcal{F}_{Thermal} = \mathcal{F}^{\mu, T \neq 0} - \mathcal{F}^{\mu, T=0}, \quad (246)$$

where $\mathcal{F} = \mathcal{F}_{1-loop} + \mathcal{F}_{2-loop} + \mathcal{F}_{3-loop}$. Finally,

$$\mathcal{F}_{Thermal} = -\frac{8}{\pi^2} \left[h_5^e - \frac{2\alpha h_3^{e2}}{3} + \frac{\alpha^2}{3} \left(\frac{16h_3^{e2}}{9} - \frac{\mu^2 h_3^e}{4T^2} + \frac{16h_1^e h_3^{e2}}{3} + \frac{K_2}{8 * 16} + \frac{K_3}{8 * 24} \right) \right] T^4. \quad (247)$$

The above result is completely new, which is, the perturbative free energy computed in the physical parameters up to $O(\alpha^2)$ (or $O(\lambda^2)$) for a complex scalar ϕ^4 field theory. The known result in the literature is for a non-complex scalar ϕ^4 field theory (ANDERSEN, 2000). Before computing the pressure $P = -\mathcal{F}$, let us evaluate the impact of the high order thermal contributions against the one-loop contribution, by plotting $\mathcal{F}/\mathcal{F}_1$ for two and three-loops.

Figure 20. - Thermal Free energy normalized by the one-loop free energy, for $\alpha = 0.1$ and $\alpha = 0.4$



Legend: The dashed and solid lines are the two and three-loop approximation.

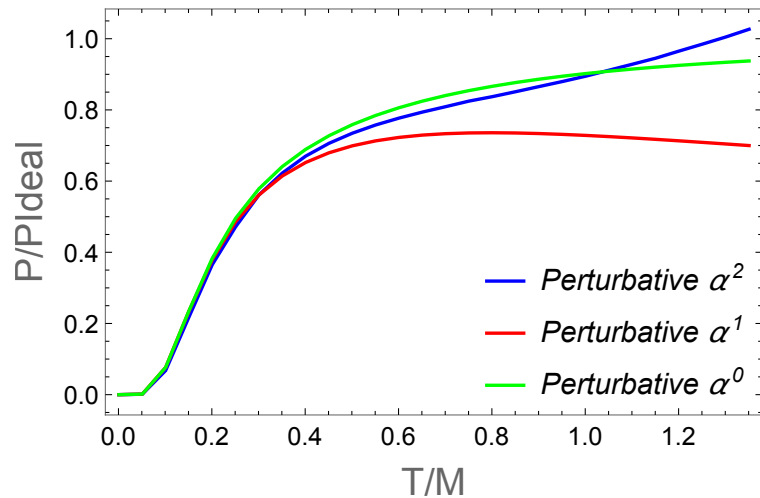
Source: The author, 2022.

The effect of the interaction on the free energy, which is the negative of the pressure, is illustrated in Figure 20. An important thing to notice here is that, even with

the consideration of the chemical potential, the impact of the one-loop diagram in the high order ones, is quite the same as $\mu = 0$. The reason for that is, at high orders of perturbation theory the soft contributions, that is, the $p < T$ contributions become less relevant, if compared with the hard $p > T$ contributions. This is in agreement with the hard thermal loop technique (BRAATEN; PISARSKI, 1990). The only difference appears in the three-loop contribution, where the chemical potential makes the curve start closer to 1.0 but not exactly in 1.0. For $\mu = 0$, the result is the same as in Andersen, Braaten and Strickland work (ANDERSEN, 2000). We normalize the free energy to the one-loop with the same physical mass, which gives \mathcal{F}_1 in Eq. (247). We plot in Figure 20 $\mathcal{F}/\mathcal{F}_1$ as a function of T (setting $m = M$) on a logarithmic scale for two different values of the physical coupling constant: $\alpha = 0.1$ and $\alpha = 0.4$, which corresponds to $\lambda = 15.7914$ and $\lambda = 63.1655$, respectively. The dashed lines are the free energies truncated at α and the solid lines are the free energies truncated at α^2 . It is usual to use $\lambda \equiv g^2$, that looks like a strong fine-structure constant $\alpha = \lambda/(4\pi)^2 = g^2/(4\pi)^2$. We will use this definition in a further analysis.

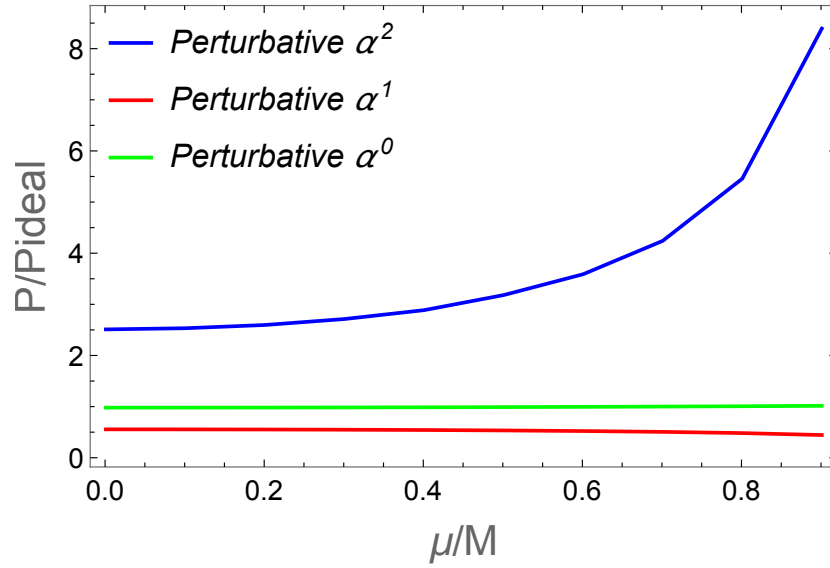
Only with the above analysis (i.e., whether it is converging), we cannot know exactly if the perturbative computation is making sense or not. The only clue we observe is a big difference between α and α^2 order, for values that are closer to ≈ 0.4 . Let us refine our analysis by plotting the pressure for our model.

Figure 21. - Thermal pressure ($P \equiv P_{T \neq 0} - P_{T=0}$) as a function of the temperature T , at $\mu/M = 0.5$, for $\alpha = 0.4$, normalized by the ideal gas pressure P_{ideal}



As one can see in Figure 21, for small values of T like $T/M = 0.6$, we already have a non-converging result. Since we are in the thermodynamic equilibrium, this non-convergence indicates a break down in the perturbation computations. The same problem is shown varying the chemical potential, see Figure 22. The blue curve show a very different behavior from the others, with the temperature fixed at $T/M = 4$.

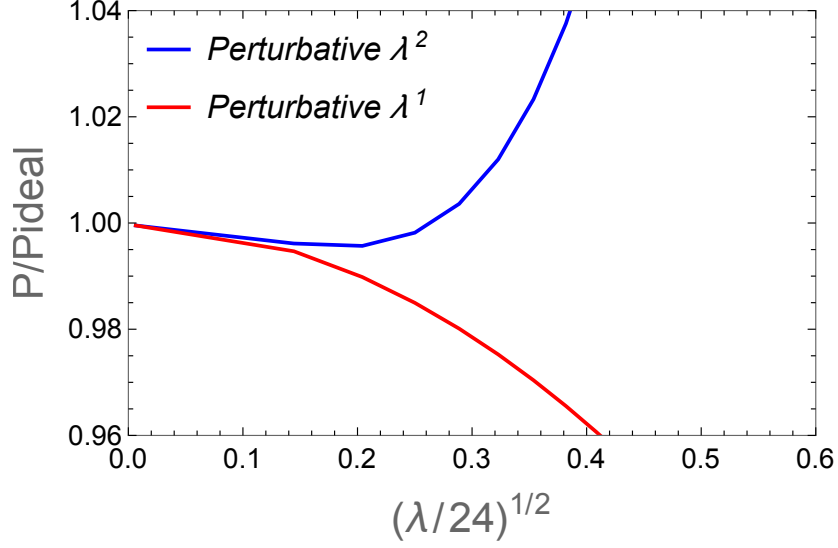
Figure 22. - Thermal pressure ($P \equiv P_{T \neq 0} - P_{T=0}$) as a function of the chemical potential μ , at $T/M = 4$, for $\alpha = 0.4$, normalized by the ideal gas pressure P_{ideal}



Source: The author, 2022.

A final and conclusive analysis is the thermodynamical observable (that shows us this problem), varying with the coupling, since this non convergence in the pressure emerges from considering contributions at high orders in λ . Based on that, we can have a clue about when the theory start to break.

Figure 23. - The normalized thermal pressure at $\mu/M = 0.5$, $T/M = 20$ and $m^2 = M^2$ varying with the coupling λ



Source: The author, 2022.

From Figure 23, it is clear that the perturbation theory gets broken when we consider couplings with values higher than 0.1. The reader should not mistake the regimes the of analysis. In Figure 21, we are considering a rather large coupling ($\alpha = 0.4$), which changes the regime of high-T. As we increase the coupling, what used to be small-T, becomes high-T. A nice way to understand this, is considering the first thermal contribution of the tadpole (first diagram of the self-energy contributions, Figure 15) and the first crossed thermal contribution (proportional to $h_1 \times h_2$) that comes from the tadpole plus a bubble (second diagram of the self-energy contributions, Figure 15), in the high temperature approximation:

$$\delta m_\beta^2 (1) \approx \frac{\lambda T^2}{18}, \quad \delta m_\beta^2 (2) \approx \frac{\lambda^2 T^3}{216\pi \sqrt{m^2 - \mu^2}}. \quad (248)$$

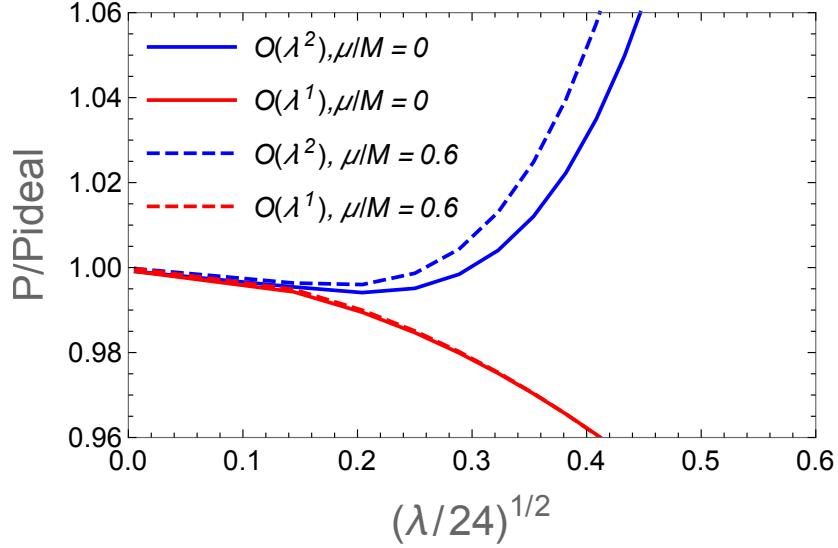
Comparing both approximations,

$$\delta m_\beta^2 (2) / \delta m_\beta^2 (1) = \frac{\lambda T^2}{12\pi \sqrt{m^2 - \mu^2}}, \quad (249)$$

we need to be careful for a larger values of λ , the perturbation theory can break for small values of T since $T/M \gg 1$.

Our concern relies on theories at weak couplings. Considering the $\lambda|\phi|^4$ theory as a weak coupled theory in a thermal bath, for high values of the temperature, the theory loses the perturbative reliability, as we discussed above. The result of Figure 23 was calculated at $\mu = 0$ by Krein, Ramos and Farias (FARIAS; RAMOS; KREIN, 2008). A good observation is the following,

Figure 24. - The normalized thermal pressure at $\mu/M = 0.6$ and $\mu/M = 0$. $T/M = 20$ and $m^2 = M^2$ varying with the coupling $\sqrt{\lambda/24}$



Source: The author, 2022.

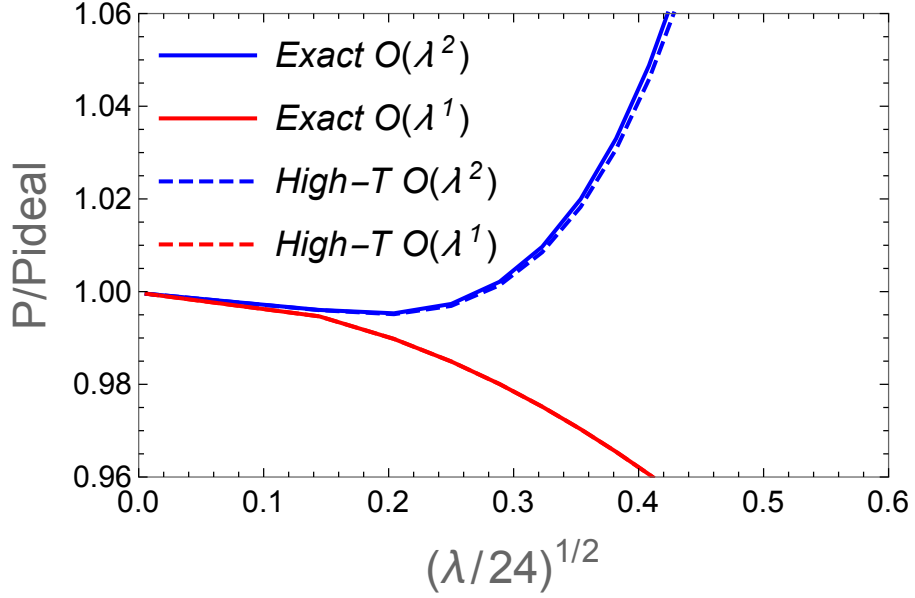
The consideration of the chemical potential (see Figure 24) only starts to make difference, for high orders in the coupling. What is the relevance in considering the chemical potential? A beautiful way to answer that is comparing the exact (numerical) result, with the high temperature approximations, by expanding the h 's functions and evaluating the high order diagrams (from the last sections) in the limit $T \gg m$. Note that, for $T \gg m$ we can use the limit $m \rightarrow 0$ for some diagrams (like for the basketball diagram evaluated in the last section), which makes us loose a small percentage of information about the soft contributions ($p < T$). Even with that, the results are quite the same, see Figure 25. For the thermal functions (the ones that include the Bose-Einstein integrals), we cannot simply take the limit $m \rightarrow 0$. We need to make the correct expansion, as

$$h_3^e(m/T, \mu/m) \approx \frac{\pi^2 T^2}{12} - \frac{m\pi T}{4} \sqrt{1 - \frac{\mu^2}{m^2}} - \frac{m^2}{8} \left(\frac{\mu^2}{m^2} + \log\left(\frac{m}{4\pi T}\right) + \frac{1}{2}(2\gamma - 1) \right),$$

(250)

considering all the information about the chemical potential and the temperature.

Figure 25. - The normalized thermal pressure at $\mu/M = 0.5$, $T/M = 20$ and $m^2 = M^2$ varying with the coupling $\sqrt{\lambda/24}$



Source: The author, 2022.

For small values of T , we do not have too many problems. The perturbation theory is a good and reliable approximation. In order to establish an analytical expression for both regimes, we can apply the approximations (see Appendix B).

For low temperatures:

$$\mathcal{F}_{m \gg T} = -T^4 \left(\frac{m}{2\pi T} \right)^{3/2} \left(e^{\frac{2\mu}{T}} + 1 \right) e^{-\left(\frac{\mu}{T} + \frac{m}{T}\right)} \left\{ 1 - \frac{\alpha^2 \mu^2}{3mT} - \frac{1}{3} \left(\alpha - \frac{8\alpha^2}{9} \right) \sqrt{\frac{2\pi T}{m}} e^{\frac{\mu-m}{T}} + -\frac{1}{3} \left(\alpha - \frac{8\alpha^2}{9} \right) \sqrt{\frac{2\pi T}{m}} e^{-\frac{m+\mu}{T}} \right\}, \quad (251)$$

while for high temperatures:

$$\mathcal{F}_{T \gg m} = \mathcal{F}_{ideal} \left\{ 1 + \left(\frac{10\sqrt{m^2 - \mu^2}}{\pi T} - \frac{5}{3} \right) \alpha + \left[\frac{20\pi T}{9\sqrt{m^2 - \mu^2}} + \frac{20}{9} \right] \left(1 \right. \right.$$

$$\begin{aligned}
& -\frac{6\sqrt{m^2 - \mu^2}}{\pi T} \ln\left(\frac{m}{T}\right) + \left(\frac{100}{9\pi} - \frac{20\gamma_E}{3\pi} + \frac{40 \log(2)}{3\pi} + \frac{20 \log(\pi)}{3\pi}\right) \\
& \times \left. \frac{\sqrt{m^2 - \mu^2}}{T} - 14.8173 \right\} \alpha^2 \Bigg\}, \tag{252}
\end{aligned}$$

where we have neglected terms of $O(m^2/T^2)$, $O(\mu^2/T^2)$ and bigger, due to the hierarchy scale $T \gg m > \mu$. The above expression in the limit $m \rightarrow 0$ (which means for $\mu = 0$) is in agreement with previous results found in the literature (for a \mathcal{Z}_2 theory). This analytical expression does not depend on the regularization scale M . This is the reason why we are working at the physical mass and physical coupling. This situation could be understood as a hypothetical Hadron collider simulation. Let us suppose we have a high energy scattering, where the temperature effects start to become relevant. The pressure and others thermodynamical quantities could be described by this free energy approximation. However, the story is not over! We still need to handle the break down of the perturbation theory. Before we do that, we could think about a different situation, for example: What if the mass of the field thermalizes? What if the field parameters change with the temperature of the environment? Those situations could happen in the early Universe, in the radiation dominated regime for example. It is relevant to see how the quantities behave if they run with T and μ . We start this analysis looking at the thermal mass.

2.2 The Thermal Mass

Now, considering the diagrams of Figure 15 in a thermal environment, which means apply (48) in Eq. (47),

$$\Sigma_1 = \Sigma_{1a} + \Delta_1 \bar{m}^2 \tag{253}$$

the tadpole diagram is (Note that the equation below is written with m instead \bar{m} , all the masses and coupling here and so on in the work are the bare quantities),

$$\Sigma_{1a} = \frac{2\lambda}{3} \int_p \frac{1}{p^2 + m^2} = \frac{2\lambda}{3} I_1 ,$$

where,

$$\begin{aligned}
I_1 &= \left(\frac{e^\gamma M^2}{4\pi} \right)^\epsilon \left[\int \frac{d^{4-2\epsilon} p}{(2\pi)^{4-2\epsilon}} \frac{i}{(k^2 - m^2)} + \int \frac{d^{4-2\epsilon} p}{(2\pi)^{4-2\epsilon}} n^{(\mu)}(p_0 \text{sgn}(p_0 + \mu)) \right. \\
&\quad \left. \times 2\pi \delta(p^2 - m^2) \right] \\
&= \left(\frac{e^\gamma M^2}{4\pi} \right)^\epsilon \int \frac{d^{4-2\epsilon} p}{(2\pi)^{4-2\epsilon}} \frac{-1}{(k^2 + m^2)} + \int \frac{d^3 \vec{p}}{(2\pi)^3} \frac{n^+(\omega_p) + n^-(\omega_p)}{2\omega_p} \\
&= \frac{m^2}{(4\pi)^2} \left(\frac{M}{m} \right)^{2\epsilon} e^{\gamma_E \cdot \epsilon} \gamma_E [-1 + \epsilon] + \frac{T^2}{2\pi^2} \int_0^\infty x^2 dx \frac{n^+(\omega_{x,y}) + n^-(\omega_{x,y})}{2\omega_{x,y}} \\
&= \frac{m^2}{(4\pi)^2} \left(\frac{\mathcal{M}}{m} \right)^{2\epsilon} e^{\gamma_E \cdot \epsilon} \gamma_E [-1 + \epsilon] + \frac{T^2}{\pi^2} h_3^e(y, r). \tag{254}
\end{aligned}$$

Taking the counterterm in the Appendix C, we can calculate the thermal contributions to the self-energy interactions, which are,

$$\Sigma(-m^2) = \Sigma_{1-loop} + \Sigma_{2-loop}(-m^2). \tag{255}$$

The renormalized thermal one-loop contribution will be,

$$\Sigma_{1-loop} = \frac{32}{3} \alpha T^2 h_3^e(y, r) - \frac{2\alpha m^2}{3} - \frac{2}{3} \alpha m^2 L, \tag{256}$$

where $L = \ln(M^2/m^2)$. Note that the counter-terms are the same as the in $T = 0$ case (Appendix C). The two-loop thermal contributions evaluated on-shell are,

$$\Sigma_{2-loop}(-m^2) = \Sigma_{2a} + \Sigma_{2b}(-m^2) + \frac{\partial \Sigma_{1a}}{\partial \bar{m}} \Delta_1 m^2 + \frac{\Sigma_{1a}}{\lambda} \Delta_1 \lambda \Delta_2 m^2. \tag{257}$$

The tadpole with one loop insertion is given by the 2a in figure (Figure 15) is,

$$\Sigma_{2a} = -\frac{16\lambda^2}{9} \frac{1}{4} \int_p \frac{1}{p^2 + m^2} \int_q \frac{1}{(q^2 + m^2)^2} = -\frac{4\lambda^2}{9} I_1 I_2$$

Using the explicit expressions for I_1, I_2 (Appendix A), summing the counterterms (Appendix C) and taking the off-shell result for the setting sun diagram (1.5) we have the

renormalized result,

$$\begin{aligned}
\Sigma_{2-loop}(-m^2) = & -\frac{2\alpha^2 m^2}{3} - \frac{1}{18}\pi^2 \alpha^2 m^2 + \frac{5}{3}\alpha^2 L m^2 + \frac{7}{9}\alpha^2 L^2 m^2 - \frac{2}{9}\alpha^2 C_1 m^2 + \frac{2\alpha^2 \mu^2}{3} \\
& - \frac{8}{3}\alpha^2 G^{2BE}(0, im) + \frac{16}{9}\alpha^2 L m^2 h_1^e(y, r) + \frac{16}{9}\alpha^2 m^2 h_1^e(y, r) - \frac{16}{3}\pi \alpha^2 T^2 h_3^e(y, r) \\
& - \frac{160}{9}\alpha^2 L T^2 h_3^e(y, r) - \frac{256}{9}\alpha^2 T^2 h_1^e(y, r) h_3^e(y, r) .
\end{aligned} \tag{258}$$

Now, we can write the effective mass of the field as³

$$m_{eff}^2(T, \mu) = m^2 + \Sigma(-m^2) \Big|_{T, \mu=0} + \Sigma(-m^2) \Big|_{T, \mu \neq 0} , \tag{259}$$

where we have separated the result of equation (258) in two parts, such that the effective mass is written in terms of the tree-level, the vacuum contributions of the self-energy and the medium contributions,

$$\begin{aligned}
m_{eff}^2(T, \mu) = & m^2 - \frac{2\alpha m^2}{3}(1 + L) + \frac{32\alpha}{3}T^2 h_3^e(y, r) - \frac{2\alpha^2 m^2}{3} - \frac{\pi^2}{18}\alpha^2 m^2 \\
& + \frac{5}{3}\alpha^2 L m^2 + \frac{7}{9}\alpha^2 L^2 m^2 - \frac{2}{9}\alpha^2 C_1 m^2 + \frac{2\alpha^2 \mu^2}{3} + -\frac{8}{3}\alpha^2 G^{2BE}(0, im) \\
& + \frac{16}{9}\alpha^2 m^2 h_1^e(y, r) - \frac{16}{3}\pi \alpha^2 T^2 h_3^e(y, r) - \frac{160}{9}\alpha^2 L T^2 h_3^e(y, r) \\
& - \frac{256}{9}\alpha^2 T^2 h_1^e(y, r) h_3^e(y, r) .
\end{aligned} \tag{260}$$

Subtracting the vacuum contributions, we can define the thermal mass as,

$$\begin{aligned}
m_{Thermal}^2(T, \mu) = & m^2 + \frac{32}{3}\alpha T^2 h_3^e(y, r) + \frac{2\alpha^2 \mu^2}{3} + \frac{8\alpha^2}{3}G^{2BE}(0, im) \\
& - \frac{256}{9}\alpha^2 T^2 h_1^e(y, r) h_3^e(y, r) + \frac{16}{9}\alpha^2 L m^2 h_1^e(y, r) - \frac{1}{9}160\alpha^2 L T^2 h_3^e(y, r)
\end{aligned}$$

³Usually, the convention that is considered for the effective mass (KAPUSTA, 1981) is $m_{eff}^2 = m^2(T, \mu) - \mu^2$.

$$+\frac{16}{9}\alpha^2 m^2 h_1^e(y, r) - \frac{16}{3}\pi\alpha^2 T^2 h_3^e(y, r) . \quad (261)$$

There is an attempt to obtain this result, in the literature, by Jones and Parkin (JONES; PARKIN, 2001). However, there are a couple of differences in their results already explained in Section 1.5. Now, it is relevant to discuss the motivation of the Jones and Parkins work, because in their work, they did the computation of the critical temperature for a $\lambda|\phi|^4$ theory, by calculating the effective mass. In their pioneer work they considered a perturbative and also a nonperturbative approach, using the OPT technique. It appears that the chemical potential of coexistence (called critical point in their pioneer work) found by OPT is too much different than the perturbative critical point, what differs from our analyses. We can show why is different by calculating the critical point with the thermal mass. For a charged scalar field theory, the condition to obtain the minimal energy configuration is $\mu = |m|$ (See chapter 2 of Ref. (KAPUSTA, 2006)),

$$m_{eff}^2 \Big|_{T \neq 0} = m^2 - \mu^2 = 0, \quad (262)$$

which gives us the critical temperature. For our analyzes, this is equivalent to set the thermal mass to zero,

$$\mu^2 = m^2 + \frac{32\alpha}{3}T^2 h_3^e(y, r) \Big|_{T=T_c} + O(\alpha^2) , \quad (263)$$

getting the first-order contribution,

$$\mu^2(T_c) \approx m^2 + \frac{2\lambda T_c^2}{3\pi^2} h_3^e(y, r) \Big|_{T=T_c} , \quad (264)$$

where $\alpha = \lambda^2/(4\pi)^2$. The thermal function is evaluated in the high temperature approximation, once we can have thermal excitations in the condensed phase,

$$\frac{\mu(T_c)}{T_c} = \sqrt{\frac{m^2}{T_c^2} + \frac{\lambda}{18}} . \quad (265)$$

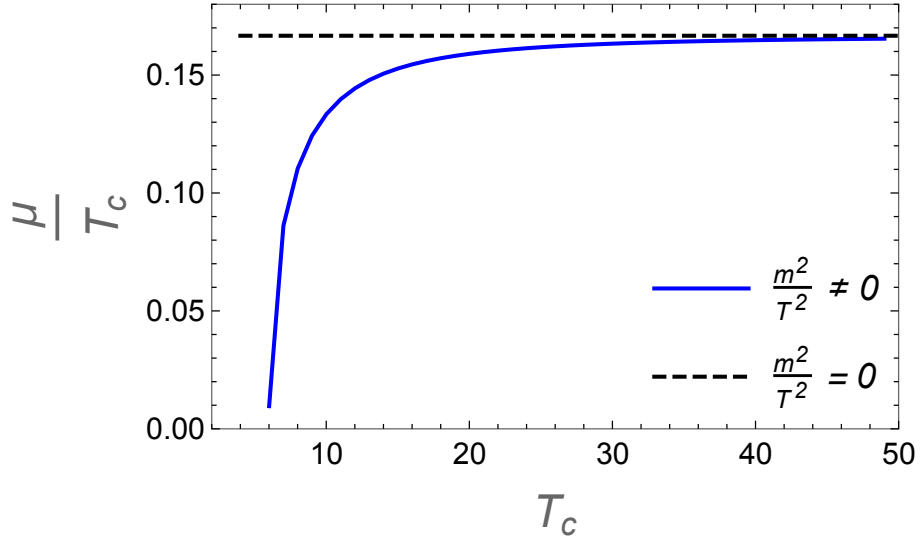
The above expression is the chemical potential of coexistence of the phase transition. We will show that the mass term in (265) is the reason why the nonperturbative computations

of Jones and Parkin seems to be too much different than the perturbative. We can express the critical temperature in terms of μ ,

$$T_c^2(\mu) = \frac{18}{\lambda}(\mu^2 - m^2) . \quad (266)$$

Finally we can show why Jones and Parkin result differs from ours.

Figure 26. - Perturbative critical point



Legend: Without neglecting the mass term (blue curve) and neglecting the mass term (black dashed curve). For the blue curve we set $m^2 = -M^2$, that means we are in the broken phase. For both curves we use $\lambda = 0.5$.

Source: The author, 2022.

As one can see in Figure 26, the perturbative result already reproduces a similar numerical result that Jones and Parkin found, by applying the OPT to the thermal mass (JONES; PARKIN, 2001). Because of the mass term that Jones and Parkin threw away, they lost the information about the broken phase (when setting $m^2 = -1$). In order to make that clear, we will compare the blue curve of Figure 26, which is the equation (265), with the OPT critical point, that came from the optimized thermal mass. Before we start making the nonperturbative analysis or applying the OPT, we should show first why this technique can be so powerful. For the phase transition analysis at one-loop order, we have problems to compute all the contributions.

A complex scalar $\lambda|\phi|^4$ field theory belongs to a well-known universality class of

theories, meaning that the criticality of this theory is described by the same critical exponents of any other scalar theory with $O(N)$ symmetry. These critical exponents have a direct interpretation on statistical physics and they are measured by realistic cases, such as in magnet systems. For $N = 1$ we have one fluctuating spin component in a preferred axis, for $N = 2$ a preferred plane and for $N = 3$ an isotropic three-dimensional set of spins. We have in our case ($U(1)$ symmetry with a $(\phi\phi^*)^2$ interaction), the representation of a relativistic superfluid Bose-Einstein condensation, that has a second-order phase transition (YUKALOV; YUKALOVA, 2014).

2.3 Phase Transition

For the phase transition analysis, it is convenient to compute the thermodynamic potential. This means computing with the bare mass and the bare coupling. Knowing that, we will omit the notation \bar{m} , for economic reasons. But, the reader should not get confused: We are computing in the bare mass and coupling!

2.3.1 The One-Loop Thermodynamic Potential

The thermodynamic potential, that we have computed so far, takes into account only the perturbative behavior of the theory and allows us to separate the interactions by regions, as we showed in section 1.3. The Feynman graph for the one-loop thermodynamic potential, is the same as in Eq. (81) for two fields and with $m^2 \rightarrow m_{H,G}^2(\phi)$ (Eqs. 76). For economic reasons, let us define the thermal effective potential as follows,

$$V_{R-eff}^{T \neq 0} = V_{R-eff}(\phi_c) - \frac{4}{\pi^2} \left[h_5^e(m_H(\phi_c)/T, \mu/m_H(\phi_c)) + h_5^e(m_G(\phi_c)/T, \mu/m_G(\phi_c)) \right], \quad (267)$$

where $V_{R-eff}(\phi_c)$ is given by Eq. (81), and, as before, m_H and m_G denote the Higgs and Goldstone masses defined in Eq. (76). Let us analyze these thermal contributions. As an example, we can expand the first h_5 term in the high temperature expansion,

$$V_{R-eff}^{T \neq 0} \approx V_{R-eff}(\phi_c) - \frac{\pi^2 T^4}{45} - \frac{\mu^2 T^2}{6} + \frac{\mu^4}{24\pi^2} + \frac{m_H^2(\phi_c) T^2}{12} - \frac{\mu^2 m_H^2(\phi_c)}{8\pi^2} +$$

$$\begin{aligned}
& + \frac{\mu^2 m_H(\phi_c) T}{6\pi} \left(1 - \frac{\mu^2}{m_H^2(\phi_c)}\right)^{1/2} - \frac{m_H^3(\phi_c) T}{6\pi} \left(1 - \frac{\mu^2}{m_H^2(\phi_c)}\right)^{1/2} + \\
& - \frac{m_H^4(\phi_c)}{16\pi^2} \ln \left(\frac{m_H(\phi_c)}{4\pi T}\right) + O(m_H^6) + O(m_G^6) .
\end{aligned} \tag{268}$$

Now, we must observe that if we apply

$$\left. \frac{\partial V_{R\text{-}eff(T \neq 0)}^{1\text{-}loop}}{\partial \phi} \right|_{\phi=\xi} = 0 , \tag{269}$$

for the minimum energy configuration, we run into troubles. The difficulty is that T_c is determined by V_{eff}^T at $\phi_c = 0$. But, for small values of ϕ_c , $m_{H,G}^2(\phi_c) < 0$ (since the broken phase happens when $m^2 < 0$). This leads to a physically unacceptable result: A complex critical temperature. The problem is that the terms that become imaginary as $\phi_c \rightarrow 0$, or $T \rightarrow T_c$ are higher order in the coupling constant (order λ^2 and above). Here, it relies the main problem that we can handle with the OPT. In a perturbative description, we need to expand the one-loop result (that is perturbative already) in λ to obtain the physical results. With the OPT, we expand to another parameter and because of that we can retain information about the missing diagrams of the perturbative approach. We can handle the original form of the effective potential. Now, expanding the effective potential in the coupling constant and retaining only the first order correction of order λ , we obtain

$$V_{R\text{-}eff(T \neq 0)}^{O(\lambda)} \approx \frac{m^2}{2} \phi_c^2 - \frac{\mu^2}{2} \phi_c^2 + \frac{\lambda}{4!} \phi_c^4 + \frac{\lambda}{3} \phi_c^2 \left[-\frac{m^2}{(4\pi_c)^2} (1+L) + \frac{T^2}{\pi^2} h_3^\epsilon(y, r) \right] . \tag{270}$$

This is the same as considering the first diagram of Figure 15. Now we can reproduce, approximately, the criticality of the theory. By calculating the minima of our potential Eq.(269), taking the high temperature approximation for h_3 and throwing away the log terms, we can find a well known result for the relativistic superfluid Bose-Einstein condensation,

$$\xi^2(T) \approx -\frac{T^2}{3} - \frac{6}{\lambda} (m^2 - \mu^2) \tag{271}$$

where $\xi(T)$ is $\xi(t) = \langle \phi \rangle$, the thermal average of the scalar field. And the critical temperature, where $\xi(T_c) = 0$, is given by

$$T_c^2 \approx -\frac{18}{\lambda}(m^2 - \mu^2) . \quad (272)$$

For the effective mass computation, we just take

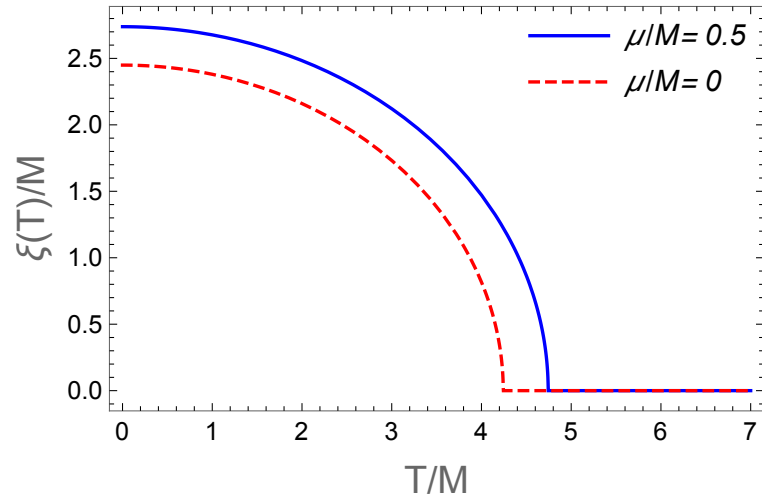
$$m_{eff}^2 = \left. \frac{\partial^2 V_{R-eff(T \neq 0)}^{1-loop}}{\partial \phi^2} \right|_{\phi=0} \quad (273)$$

considering again the high- T approximation for the thermal function h_3^e and throwing away the log terms,

$$m_{eff}^2 \approx m^2 - \mu^2 + \frac{\lambda T^2}{18} . \quad (274)$$

We obtained the same result as in the thermal mass analysis. The Figure 27 shows us how the expectation value changes with the temperature T . Note that there is no discontinuities, as the field ξ assumes the critical temperature. The same holds for the mass of the theory: there isn't any discontinuity, see Figure 28, which seems to characterize the phase transition as second order.

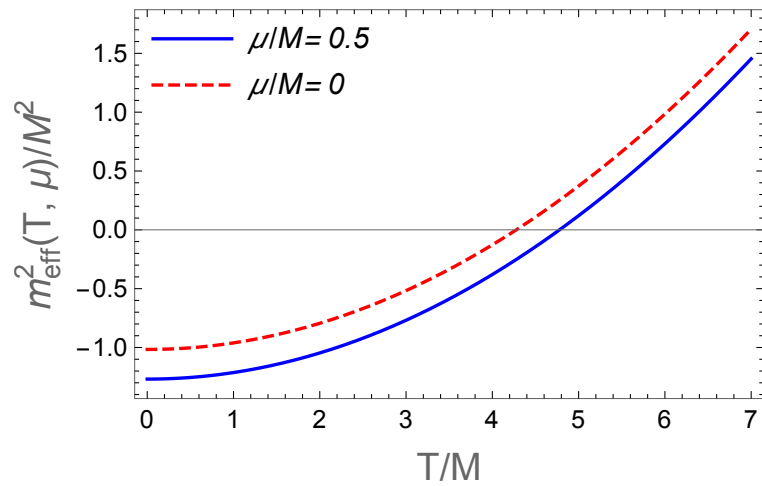
Figure 27. - The scalar field expectation value ξ against T in the minima energy configuration of the theory



Legend: We set $m^2 = -M^2$, that means we are considering the broken phase. For both curves we use $\lambda = 1$.

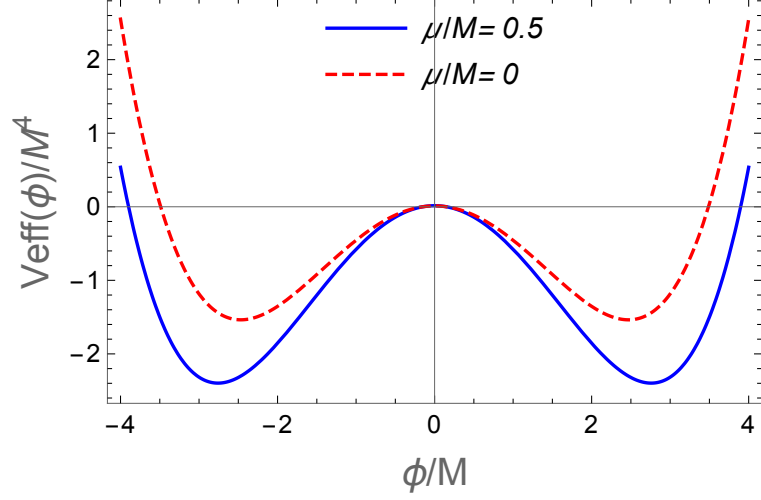
Source: The author, 2022.

Figure 28. - Perturbative critical point, without neglecting the mass term (blue curve) and neglecting the mass term (black dashed curve)



Legend: For the blues curve we set $m^2 = -M^2$, that means the broken phase. For both curves we use $\lambda = 0.5$.

Source: the author, 2022.

Figure 29. - V_{eff} against ϕ showing the vacuum degeneracy, the broken phase

Legend: We set $m^2 = -M^2$, $\lambda = 1$ and $T/M = 0.1$.

Source: The author, 2022.

Plotting the effective potential Eq.(270), we only get one degenerated vacua. Then, Figure 29, Figure 30 and Figure 28 allow us to conclude that the theory may have a second-order phase transition. But, how do we understand this phase transition in terms of a field theory? To answer that, we need to discuss a little bit more about symmetries. The Lagrangian density Eq.(83), is invariant for any $U(1)$ transformation. But, the minimal energy configuration, when $m^2 < 0$, is not invariant. This is called spontaneous symmetry breaking (SSB), which means that the vacua of the theory does not share the same symmetry of the original action or the Lagrangian that defines the theory. To be more specific, the original symmetry $U(1)$ is broken at the lowest energy configuration, what we call the condensate Eq.(271). The ordered phase has two different degrees of freedom: The Higgs and the Goldstone particle. In order to show what this means explicitly, we need to compute the Higgs and the Goldstone masses, re-writing the original fields as

$$\phi = \frac{1}{\sqrt{2}}(\xi_0^2 + \phi_1 + i\phi_2) . \quad (275)$$

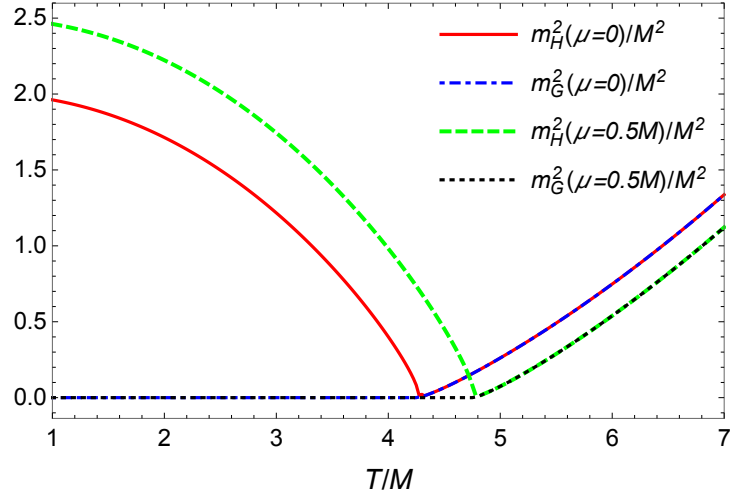
Replacing (275) in the effective potential (270), expanding with respect the desired field and using (273), we have

$$m_1^2 \approx \frac{1}{2}(m^2 - \mu^2) + \frac{T^2\lambda}{36} - \frac{\lambda\mu^2}{24\pi^2} + \frac{\xi_0^2\lambda}{8} , \quad (276)$$

$$m_2^2 \approx \frac{1}{2}(m^2 - \mu^2) + \frac{T^2\lambda}{36} - \frac{\lambda\mu^2}{24\pi^2} + \frac{\xi_0^2\lambda}{24} . \quad (277)$$

Choosing the shifted field to be ϕ_1 , we are choosing m_1 to have $\xi \neq 0$. In other words, ϕ_1 is the Higgs field and ϕ_2 is the Goldstone field.

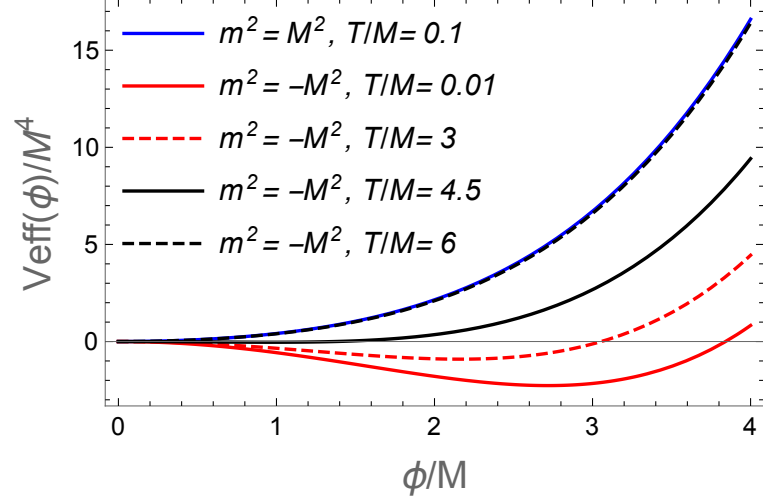
Figure 30. - The physical masses against T



Legend: We set $\langle \phi_{1,2}^2 \rangle = 0$, $\lambda = 1$ and $m^2 = -M^2$ for all curves.

Source: The author, 2022.

Figure 30 shows us the difference at the two physical masses that the theory can assume in the broken phase, with the parameters $\lambda = 1$ and $m^2 = -M^2$. Since we have a second-order phase transition, we have a broken (ordered) and a symmetric phases (disordered). Actually, what happens here is that, above the critical point, the symmetry is restored. This is known as Symmetry Restoration (SR).

Figure 31. - V_{eff} against ϕ showing the symmetry restoration

Legend: We set $\mu/M = 0.5$ and $\lambda = 1$ for all curves.

Source: The author, 2022.

Figure 31 makes clear the SR, once we increase the temperature. The last curve, for $T/M = 6$, matches exactly with the curve in the symmetric phase $m^2 = M^2$. We list many reasons why we need something beyond the standard perturbative approach. We have shown the need for it since we compute high orders of perturbation theory. In the thermal mass, we showed a mistake in the literature that still needs some proof about the use of a resummation technique. Finally, in low orders of perturbation, the effective potential approach already has problems to handle the fully one-loop potential. To fix all those problems, and for further applications, we will apply the Optimized Perturbation Theory (OPT).

3 OPTIMIZED PERTURBATION THEORY

The Optimized Perturbation Theory (OPT) (DUARTE, 2011; FARIAS, 2013; CHIKU; HATSUDA, 1998; POLITZER, 1982), also called linear delta expansion (LDE) (FARIAS; RAMOS; KREIN, 2008; JONES; PARKIN, 2001), has some origins in other methods like the variational method (KLEINERT, 1990), or even the exponential expansion method (EMM) (MILTON, 1987; BENDER, 1989). The central idea about this technique relies in the fact that the path integral, elucidated by Feynman and Wheeler [7], does not converge, in sense that the measure $\int D\phi$ assumes all possible paths, including the discontinued ones. There is a way to compute perturbatively, the correlation functions and obtain some convergent sequence with nonperturbative results. Instead of expanding our interaction term as a Taylor series, we can modify the Taylor expansion itself, multiplying the integrand by some characteristic function or summing a variational parameter in the action. This procedure can cut off areas of field-space for which the ordinary perturbative expansion does not exhibit dominated convergence. This convergence is the main reason why we choose to work with the OPT, you can see that in (SEZNEC; ZINN-JUSTIN, 1979; STEVENSON, 1981; FARIAS; RAMOS; KREIN, 2008; KNEUR, 2002). Let's outline the philosophy behind this method: There are two application paths, the main method starts with inserting an arbitrary non-physical parameter (η for example) into the action, replacing the original action with a modified action of the form ,

$$S_\delta = S_0(\eta) + \delta(S - S_0(\eta)) . \tag{278}$$

The δ is a expansion parameter that gives us control over the perturbation expansions, and it is set to 1 at the end. At any finite order expansion in δ , any quantity computed from (278) will depend on η , which needs to be fixed. We use and optimization principle for that. Now, to do the optimization, we need to find out the best choice of η . There are many ways of doing that (STEVENSON, 1981; KNEUR, 2002; BENGHI, 2021) and we will discuss this issue in the following sections. For the first analysis, we will use the

Principle of Minimal Sensitivity (PMS),

$$\left. \frac{\partial \mathcal{O}_N}{\partial \eta} \right|_{\eta=\bar{\eta}} = 0 . \quad (279)$$

The \mathcal{O}_N represents a physical quantity calculated up to N-th order in delta, δ^N . Since η is an artificial parameter added by hand, the physical quantities should not depend on it. Summing the variational parameter in the mass and multiplying the coupling constant

$$1 : m^2 \rightarrow m^2 + \eta^2(1 - \delta) ,$$

$$2 : \lambda \rightarrow \delta \lambda . \quad (280)$$

The Lagrangian density takes the form,

$$\mathcal{L}^\delta = \mathcal{L}_0(\eta) + \delta[\mathcal{L} - \mathcal{L}_0(\eta)] \quad (281)$$

where, in the case of our problem,

$$\mathcal{L}^\delta = \partial_\mu \phi \partial^\mu \phi^* - \Omega^2 |\phi|^2 - \frac{\delta \lambda}{3!} (\phi \phi^*)^2 + \delta \eta^2 |\phi|^2 + \Delta \mathcal{L}_{ct} , \quad (282)$$

where $\Omega^2 = m^2 + \eta^2$. How does that affect the effective potential? We construct an effective action with (282) and build the effective potential for the model, but now, we will expand with respect to δ instead of λ . Note that, the OPT modify the Feynman diagrams, such that we have the identification (280), modifying the interaction vertex and the propagator. An important point is, all the fields ϕ that appear in these effective potential sections are in fact the background fields ϕ_c , they are constants in our approach.

3.1 OPT Effective Potential at order δ

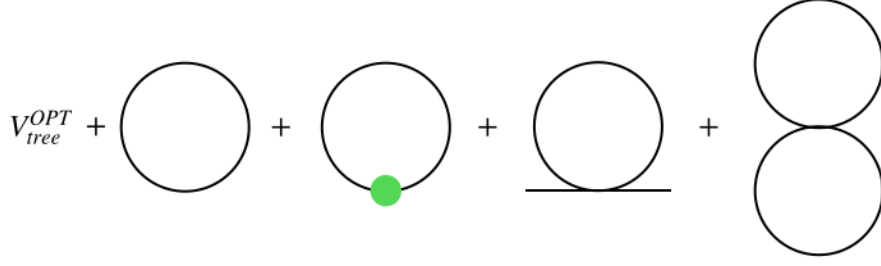
Computing the effective potential and expanding with respect to δ , we find at first order in δ the expression

$$\begin{aligned}
 V_{eff}^{OPT-\delta} &= \frac{\Omega^2}{2}\phi_c^2 - \frac{\mu^2}{2}\phi_c^2 - \frac{\delta\eta^2}{2}\phi_c^2 + \frac{\delta\lambda}{4!}\phi_c^4 + \int_p \ln(p^2 + \Omega^2) - \delta\eta^2\phi_c^2 \int_p \frac{1}{p^2 + \Omega^2} \\
 &+ \frac{\delta\lambda}{3}\phi_c^2 \int_p \frac{1}{p^2 + \Omega^2} + \frac{\delta\lambda}{3} \left[\int_p \frac{1}{p^2 + \Omega^2} \right]^2, \tag{283}
 \end{aligned}$$

where $\Omega^2 \equiv m^2 + \eta^2$. As one can see, the OPT does give additional contributions than the perturbative expansion, in particular already at order δ it includes a two-loop contribution, given by the last term in (283), which is absent in a perturbative expansion at one-loop order. In the following figure below, we show the η dependency, a new mass-like term in tree level and a tadpole with the η as a vertex (the green dot in Figure 32), where

$$\begin{aligned}
 V_{tree}^{OPT} &= V_0 - \frac{\delta\eta^2}{2}\phi_c^2 \\
 &= \frac{\Omega^2}{2}\phi_c^2 - \frac{\mu^2}{2}\phi_c^2 - \frac{\delta\eta^2}{2}\phi_c^2 + \frac{\delta\lambda}{4!}\phi_c^4. \tag{284}
 \end{aligned}$$

All those contributions are proportional to δ , that has to be set equal to one, in the end of the computations ($\delta = 1$).

Figure 32. - OPT effective potential up to order δ , where the green dot is the η insertion

Source: The author, 2022.

There is another way of applying this technique, which is we could simply take the two-loop renormalized effective potential and apply (280).

Let us start by the effective potential. All contributions of Figure 32 have already been computed in the previous sections. Then, the renormalized optimized effective potential is,

$$\begin{aligned}
V_{R-eff}^{OPT-\delta} &= \frac{m^2}{2}\phi_c^2 - \frac{\mu^2}{2}\phi_c^2 + \frac{\eta^2(1-\delta)}{2}\phi_c^2 + \frac{\delta\lambda}{4!}\phi_c^4 - \frac{\delta\Omega^4}{64\pi^2}(2L_\eta+3) - \frac{512T^4}{64\pi^2}h_5^e(y(\eta),r) + \\
&- \frac{\delta\eta^2T^2}{\pi^2}h_3^e(y(\eta),r) + \frac{\delta\eta^2\Omega^2}{16\pi^2}(L_\eta+1) - \frac{\delta\lambda\phi_c^2}{48\pi^2}\left[\Omega^2(L_\eta+1) - 16T^2h_3^e(y(\eta),r)\right] + \\
&+ \frac{\delta\lambda\Omega^4}{768\pi^4}(1+L_\eta)^2 + \frac{\delta\lambda T^2h_3^e(y(\eta),r)}{24\pi^4}\left[8T^2h_3^e(y(\eta),r) - (L_\eta+1)\Omega^2\right], \quad (285)
\end{aligned}$$

where $L_\eta = \ln(M^2/\Omega^2)$ and $y(\eta) = \Omega/T$. Now, applying the PMS Eq.(279), we find

$$\bar{\eta}^2 = \frac{\lambda\phi_c^2}{3} + \frac{\lambda}{24\pi^2}\left[16T^2h_3^e(y(\bar{\eta}),r) - \Omega^2(L_{\bar{\eta}}+1)\right], \quad (286)$$

$$\bar{\phi}_c^2 = \frac{6}{\lambda}(\mu^2 - m^2) - \frac{1}{4\pi^2}\left[16T^2h_3^e(y(\eta),r) - \Omega^2(L_\eta+1)\right]\Bigg|_{\eta=\bar{\eta}}. \quad (287)$$

The two equations above will determine all the dynamics of the optimized theory. The determination of the critical point will be a direct application of these equations. Next

section is devoted to that.

3.1.1 Critical Point in the OPT Approach

Taking the variational parameter $\bar{\eta}$ at $\phi_c = 0$, we have the critical value $\bar{\eta}(T_c)$, which is the optimum $\bar{\eta}$ at $T = T_c$. In the critical temperature,

$$\bar{\eta}^2(T_c) = \frac{\lambda}{24\pi^2} \left\{ 16T_c^2 h_3^e(y(\bar{\eta}), r) \Big|_{T=T_c} + \Omega^2(L_{\bar{\eta}} - 1) \right\}, \quad (288)$$

but, one observes that for $\phi_c = 0$, we also have

$$0 = \frac{6}{\lambda} (\mu^2 - m^2) - \frac{1}{4\pi^2} \left\{ 16T_c^2 h_3^e(y(\bar{\eta}), r) \Big|_{T=T_c} + \Omega^2(L_{\bar{\eta}} - 1) \right\}, \quad (289)$$

$$\implies \bar{\eta}^2(T_c) + m^2 = \mu^2, \quad (290)$$

meaning $\Omega = |\mu|$ is the exact condition for the condensation at order δ . Combining the result above with Eq.(288), we have

$$\frac{\lambda}{24\pi^2} \left\{ 16T_c^2 h_3^e(y(\bar{\eta}(T_c)), r) \Big|_{T=T_c} + \mu^2(L_{\mu} - 1) \right\} + m^2 = \mu^2. \quad (291)$$

For the case $\mu = 0$, the above procedure reproduces exactly the critical temperature of the model (for this case, the thermal integrals are analytical), see (DUARTE, 2011). This result is obtained without throw away the vacuum diagrams, differently than to the one-loop result (270) that is obtained only for $O(\lambda)$ order. Working out the expression (291), we find the critical temperature,

$$T_c^2 = \frac{18}{\lambda} (\mu^2 - m^2) + \frac{3\mu^2}{2\pi^2} \left[\ln \left(\frac{e^{\gamma_E}}{4\pi} \right) + \ln \left(\frac{\mu^2}{M \cdot T_c} \right) \right], \quad (292)$$

where we expand the thermal function and did $\Omega \rightarrow \mu$. Observe that, if $\mu = 0$, we get the same result as (DUARTE, 2011). We also can simplify this expression setting $M \rightarrow Me^{\gamma_E}/4\pi$ (in the \overline{MS} scheme) and $M \rightarrow T$, which gives us

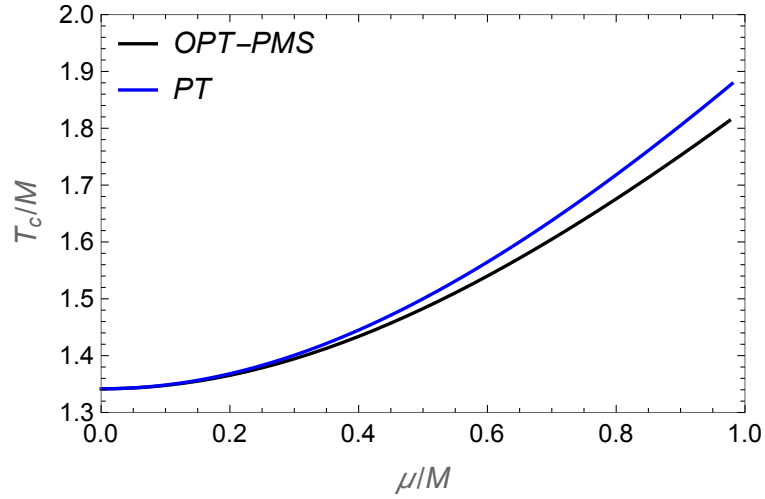
$$T_c^2 = \frac{18}{\lambda} (\mu^2 - m^2) + \frac{3\mu^2}{2\pi^2} \ln \left(\frac{\mu^2}{T_c^2} \right) \quad (293)$$

where the only approximation we needed, was for the Bose-Einstein integrals, since they are not analytical, even when $\Omega = \mu$. The second term of the above equation is very small if compared to the first, so we can write

$$T_c^2|_{OPT} \approx \frac{18}{\lambda}(\mu^2 - m^2) . \quad (294)$$

Equation (291) shows us that the critical temperature is approximately the same as the one found at the $O(\lambda)$ in one-loop computation (272).

Figure 33. - Critical point of the theory, via OPT and perturbation theory, considering $\lambda = 10$



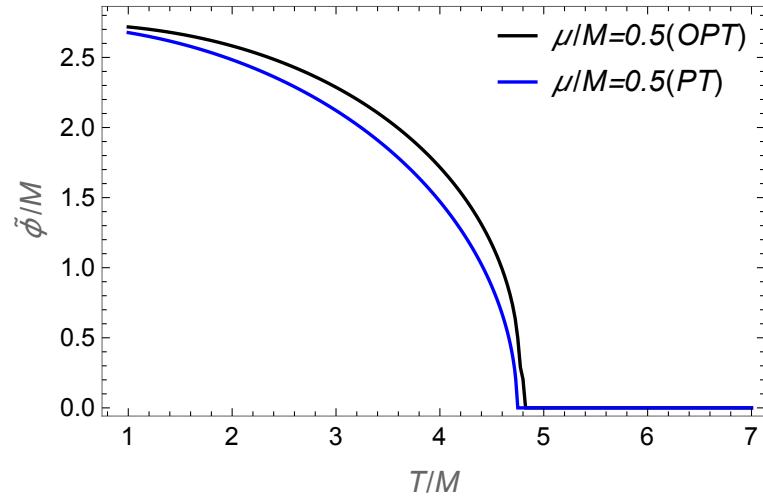
Source: The author, 2022.

Figure 33 shows us that the critical temperature from the OPT matches in a good range of μ with the perturbative approximation, where we set $m^2 = -M^2$ and considered $\lambda = 10$. This result leads us to Jones and Parkin work (JONES; PARKIN, 2001) once again. By this first analysis, the critical temperature should not differ much from the perturbative one.

3.1.2 OPT Phase Transition

Let us continue to analyze the criticality of the theory. The OPT and the perturbative condensate are compared in Figure 34.

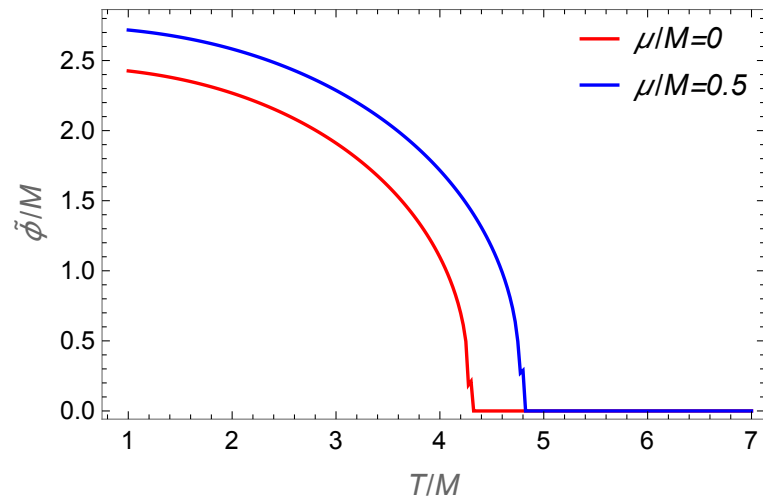
Figure 34. - Comparison between the OPT condensate with the perturbative one, where $m^2 = -M^2$ and $\lambda = 1$



Source: The author, 2022.

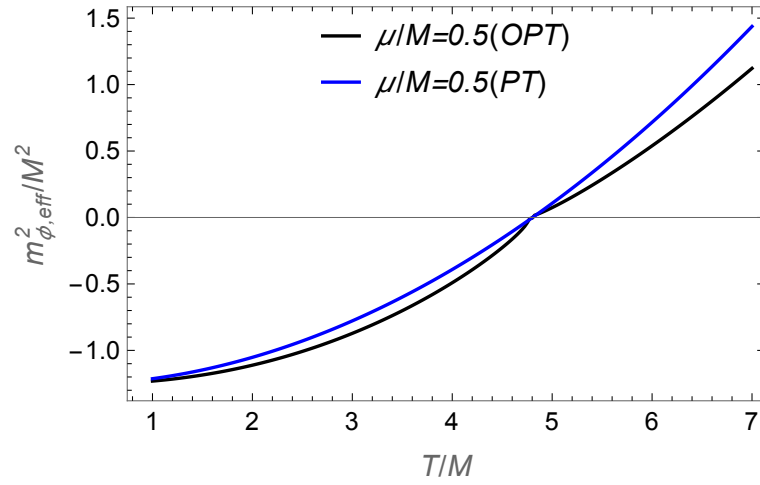
We can see from Figure 34 the difference between the OPT and PT. It seems that the perturbative case have a second-order phase transition and the OPT do not approach zero smoothly, we observe a slight beak for $\bar{\phi} \approx 0.4$. We can see the effect of the chemical potential in the OPT computations in Figure 35, we also note that the beak (around $\bar{\phi} \approx 0.4$) observed in Figure 34 was in fact a discontinuity.

Figure 35. - Comparison between the OPT condensed for $\lambda = 1$, $m^2 = -M^2$



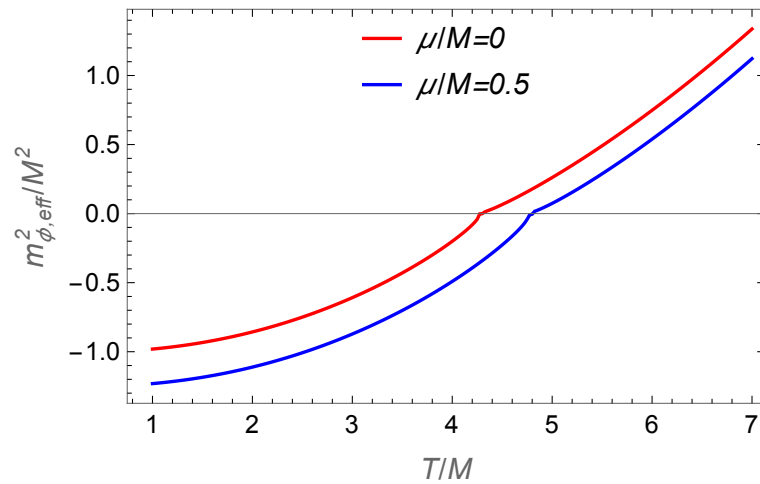
Source: The author, 2022.

Figure 36. - Comparison between the OPT effective mass and the perturbative one, for $\lambda = 1$ and $m^2 = -M^2$



Source: The author, 2022.

Figure 37. - Effective OPT mass with $\lambda = 1$ and $m^2 = -M^2$



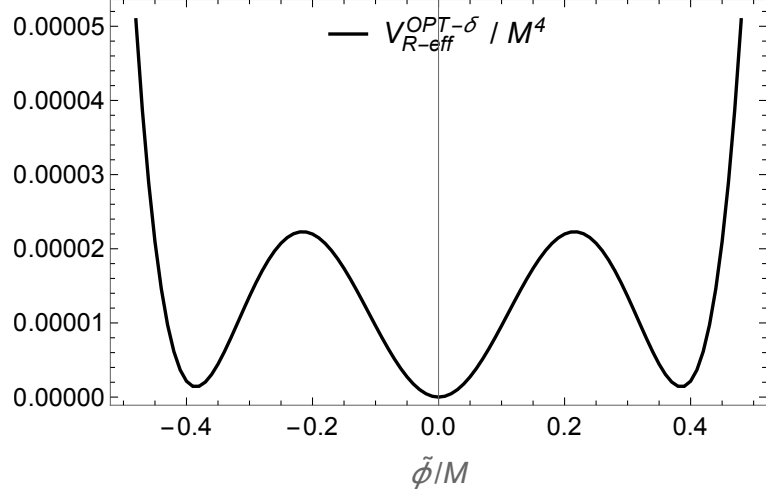
Source: The author, 2022.

The OPT and the perturbative effective masses are compared in Figure 36. The apparent discontinuity in the curves in Figure 36 indicate that the OPT effective potential have a first order phase transition. We can see the difference about considering the chemical potential for OPT, in Figure 36 and Figure 37.

The final piece for the OPT phase transition analysis is the effective potential in the broken phase. There is no need to plot the perturbative result for the broken phase

because the difference, in both results, is very clear. Figure 38 shows a degenerate minima with the origin which is contrary to the behavior seen in Figure 29, indicates that the OPT seems to show a first-order phase transition at order δ .

Figure 38. - Degenerate vacua, an OPT effective potential with three minimum



Legend: The result obtained for $\lambda = 1$ when the temperature is close to T_c in the OPT at order δ .

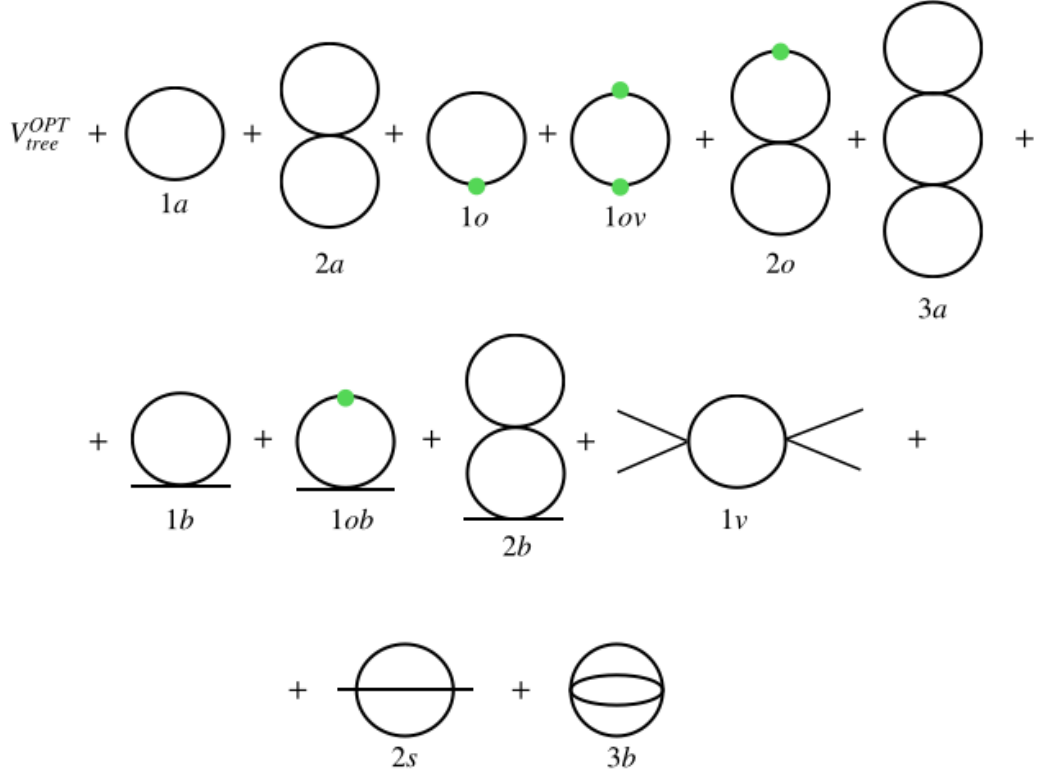
Source: The author, 2022.

This generates a doubt: What is the real phase transition for this model? In the perturbative approach, we found a second-order phase transition. However, with the nonperturbative (the OPT method), we find a first-order. Which one is right? As we discussed, at the end of the thermal mass section, this theory is well known in the literature and to have a second-order phase transition. This problem of a first-order transition is a recurrent problem in literature, not just for the OPT, but for other resummation techniques as well (see (YUKALOV; YUKALOVA, 2014)). The reader could ask if this problem persist for high orders of δ . For that we need to compute more interactions. Next, we carry out the calculations for the effective potential up to order δ^2 .

3.1.2.1 OPT Effective Potential at order δ^2

The OPT effective potential to order δ^2 takes into account more Feynman diagrams as you can see by Figure 39.

Figure 39. - OPT effective potential diagrams until order δ^2 , the green dot is the an η^2 insertion



Source: The author, 2022.

The diagrams $1a, 2a, 3a, 3b$ can be generated straightforward from the free energy calculation (Section 1.4) and the basketball (Section 1.7). The diagrams $1b, 2b, 2s$ from the self-energy calculation (Section 2.2) and the setting sun (Section 1.5). Let us compute the missing pieces of Figure 39, the two OPT insertion

$$1ov = -\frac{1}{2}\delta^2\eta^4 \int \frac{d^4p}{(2\pi)^4} \frac{1}{(p^2 + \Omega^2)^2} = -\frac{1}{2}\delta^2\eta^4 I_2 \tag{295}$$

and the two-loop vacuum diagram with a OPT insertion is,

$$2o = \frac{2}{3}\delta^2\eta^2\lambda \int \frac{d^4p}{(2\pi)^4} \frac{1}{(p^2 + \Omega^2)} \int \frac{d^4q}{(2\pi)^4} \frac{1}{(q^2 + \Omega^2)^2} = \frac{2}{3}\delta^2\eta^2\lambda I_1 I_2 . \tag{296}$$

Taking the counterterms in the Appendix C we have,

$$G_{\text{vacuum}}^{OPT}(\eta^4) = -\frac{\delta^2\eta^4}{16\pi^2} \left[2h_1^e(y, r) + \ln\left(\frac{M}{\Omega}\right) \right], \quad (297)$$

and

$$G_{\text{two-loop}}^{OPT}(\eta^2) = -\frac{\delta^2\eta^2\lambda}{192\pi^4} \left[2h_1^e(y, r) + \ln\left(\frac{M}{\Omega}\right) \right] \left[m^2 \left(2 \ln\left(\frac{M}{\Omega}\right) + 1 \right) - 16T^2 h_3^e(y, r) \right]. \quad (298)$$

The self-energy diagram with one OPT insertion,

$$1ob = \frac{2}{3}\delta^2\eta^2\lambda \int \frac{d^4p}{(2\pi)^4} \frac{1}{(p^2 + \Omega^2)^2} = \frac{2}{3}\delta^2\eta^2\lambda I_2 \quad (299)$$

summing the counterterm,

$$\Delta 1ob = -\frac{4\delta^2\eta^2\lambda}{3 \cdot 32\pi^2\epsilon}; \quad (300)$$

we obtain

$$G_{\text{self-energy}}^{OPT}(\eta^2) = \phi_c^2 \frac{\delta^2\eta^2\lambda}{24\pi^2} \left[2h_1^e(y, r) + \ln\left(\frac{M}{\Omega}\right) \right]. \quad (301)$$

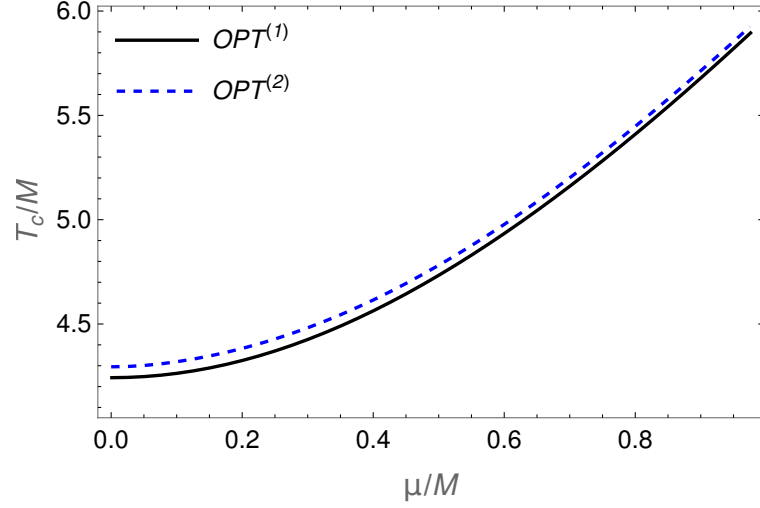
The only calculation we have not done explicitly is the off-shell vertex diagram, but it was done by Benson, Bernstein and Dodelson in Ref. (BENSON, 1991) and the result is,

$$\begin{aligned} G^{(4)}(0, \vec{0}) = & -\frac{\lambda^2\phi_c^4}{288} \left\{ \frac{1}{4\pi^2} \ln\left(\frac{M^2}{\Omega^2}\right) - \frac{2\Omega}{4\mu\pi^2} \arctan\left(\frac{\mu}{\Omega}\right) + \frac{1}{4\pi^2} \left[2 + \ln\left(\frac{M^2}{\Omega^2 - \mu^2}\right) \right] \right\} \\ & + \frac{\lambda^2\phi_c^4}{288} \int_0^\infty \frac{T^2 z^2 dz}{2\pi^2 \omega_z^3} \left[\frac{1}{\mu(\mu - \omega_z)} - 4(\eta_z^-)^2 \omega_z - 4(\eta_z^+)^2 \omega_z \eta_z^- \left(T^3 z^2 + \eta^2 T + 4\eta^2 \mu + 4\mu T^2 z^2 \right. \right. \\ & \left. \left. + 4\mu \omega_z (T - \mu) + m^2 (4\mu + T) - 4\mu^2 T \right) + \frac{1}{\mu(\omega_z + \mu)} \eta_z^+ \left(m^2 (T - 4\mu) + T^3 z^2 + \eta^2 T \right. \right. \\ & \left. \left. - 4\eta^2 \mu - 4\mu \omega_z (\mu + T) - 4\mu T^2 z^2 - 4\mu^2 T \right) \right], \quad (302) \end{aligned}$$

where $\omega_z = \sqrt{\eta^2 + m^2 + T^2 z^2}$, $\eta_z^\pm = 1/(e^{(\omega_z \pm \mu)/T} - 1)$ and η is the variational parameter.

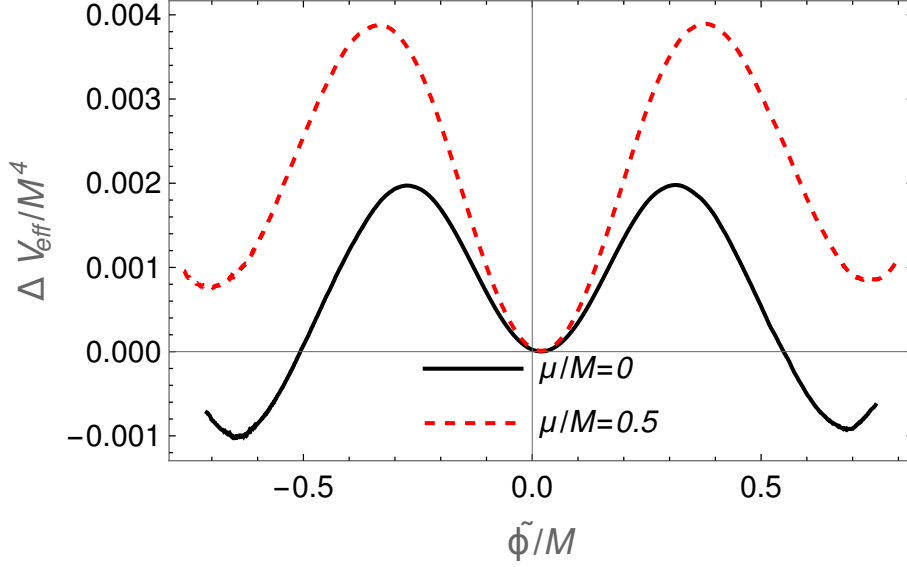
Now, we have all the missing pieces. Note that the critical temperature (Figure 40) receives a little correction due to the computation of these new diagrams as show in Figure 39, but seems like quite the same as the result obtained at order δ .

Figure 40. - Critical point from OPT δ^2 and δ and considering $\lambda = 1$



Source: The author, 2022.

However, the effective potential in the broken phase to order δ^2 share the same problem that the order δ , as one can see in Figure 41 .

Figure 41. - Broken phase OPT effective potential to δ^2 order

Source: The author, 2022.

This problem seems to rely on the prescription, at least, for the Optimized Perturbation Theory. What do we mean about prescription? The determination of the variational parameter η . Here, we do not just use the PMS, but we do minimize the free energy of our system. We could use the PMS in other thermodynamical quantity, like entropy or energy density. Not only what to minimize, but also, how. We could also try another principle, or even better, we could use another tool in order to establish a more rigorous prescription, like the renormalization group equations (RGE) (BENGHI, 2021). All of those possibilities have generated different approaches in the literature.

3.2 OPT Thermal Mass

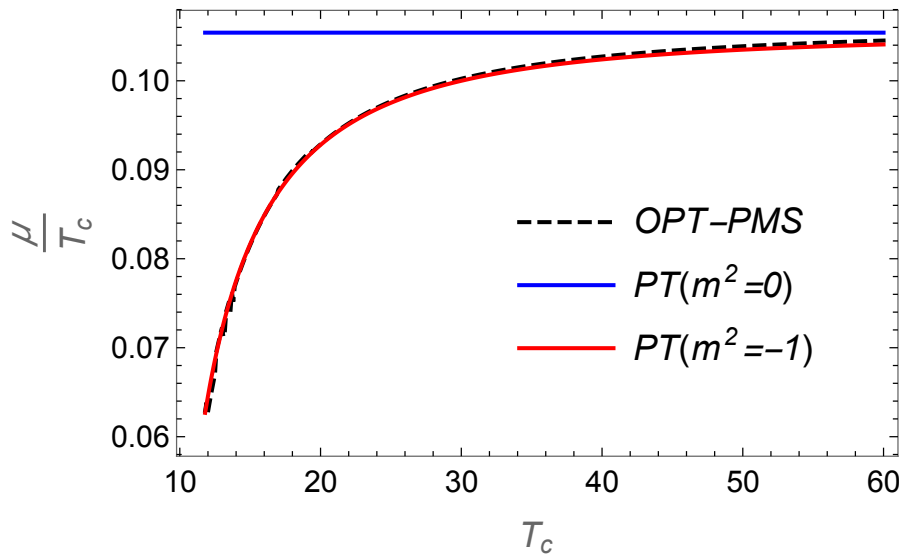
By the analysis of the previous sections, it became clear that the perturbative critical temperature coincides with the OPT result. The only remaining question is if this happens when we minimize the effective mass. To demonstrate that, we take the result (260), re-write the constants in the same notation as Jones and Parkin (JONES; PARKIN, 2001),

$$\alpha = \frac{\lambda}{(4\pi)^2},$$

$$L = \ln \left(\frac{M^2}{m^2} \right), \quad (303)$$

and apply the OPT procedure (280) to obtain the effective mass. Expanding to $O(\delta^2)$ order and applying the PMS (279), we can analyze the OPT critical temperature, via a mass minimization.

Figure 42. - Chemical potential of coexistence and the critical temperature extracted from the effective mass



Legend: The blue and red curves are the perturbative computation for $m^2 = 0$ and $m^2 = -M^2$. The black curve is the OPT result. For all curves we used $\lambda = 0.2$.

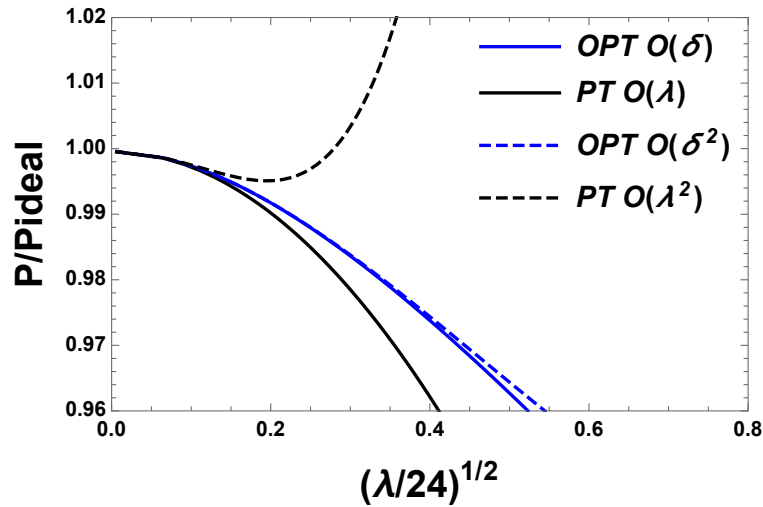
Source: The author, 2022.

In Figure 42, it is clear that Jones and Parkin did not find a result very different from the first-order perturbative. As they threw away the m^2 from the perturbative result, it appears that the OPT gives a very different result, but thanks to their previous analysis we are able to refine this study. Then we confirm our argument and shows that the result given by the minimization of the effective mass is not so different than the perturbative one. We are still studying the possibility to use the variational parameter obtained by the mass minimization in the thermodynamic potential.

3.3 Symmetric Phase

In the symmetric phase, we do not have the same problem about the prescription of η . The PMS applied in the usual way already provides us a convergent result, which allow us to go beyond the usual perturbation theory.

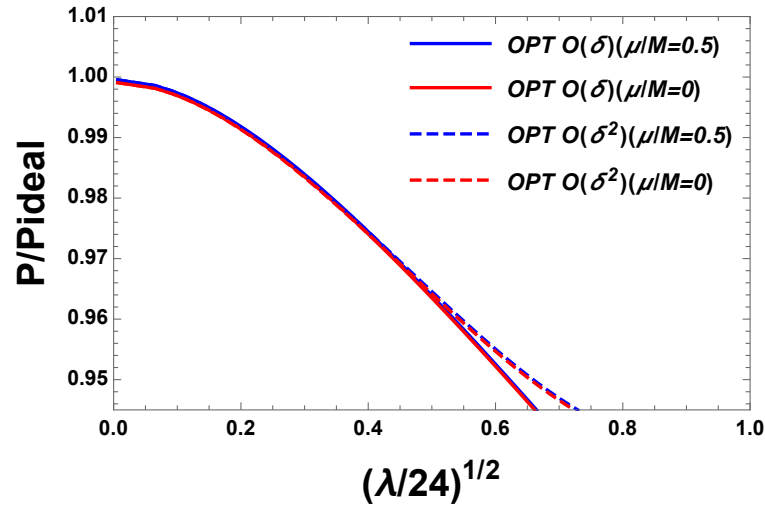
Figure 43. - Pressure against the coupling, via OPT and perturbation theory. We used $\mu/M = 0.5$, $m^2 = M^2$ and $M = T$



Source: The author, 2022.

Figure 43 shows how the optimized perturbation theory gets things fixed. An observable at equilibrium should display convergence, as we consider more and more high order corrections. So, the OPT fixes the perturbation computations, as far convergence at high orders is concerned. The resummation did seem to add the missing pieces of the Feynman diagrams, which a thermal field theory needed. So, the OPT seems to fix the perturbation computations. We can see how is the impact of the chemical potential for this analysis in Figure 44.

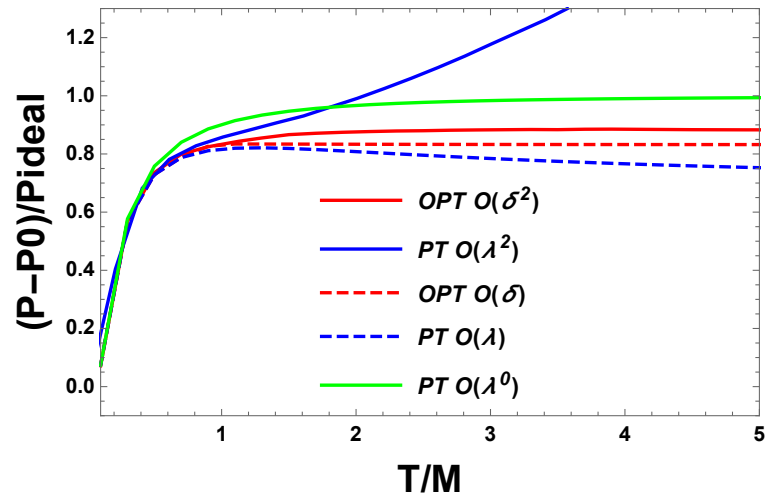
Figure 44. - Pressure against the coupling, via OPT. We used $m^2 = M^2$ and $M = T$



Source: The author, 2022.

Now, we can (without any concern) analyze the pressure, note that $\alpha = \lambda/(4\pi)^2$, so for $\alpha = 0.2$ (this was the value used in the perturbative analysis) we have $\lambda \approx 31$. Comparing all the orders, we have Figure 45.

Figure 45. - Pressure against Temperature for all orders, via OPT and perturbation theory. We used $\mu/M = 0.5$, $m^2 = M^2$, $\alpha = 0.2 \rightarrow \lambda \approx 31$ and $M = T$



Source: The author, 2022.

An important thing to notice is the proximity that the OPT curves have with the $O(\lambda^0)$, that is a good approximation for low orders of perturbation. The OPT result

can be conceived as a correction, since the result did not diverge, differently of those perturbative ones (the blue curves). In particular the perturbative $O(\lambda^2)$ result does not obey the Stefan-Boltzmann law at high temperatures as we would expected.

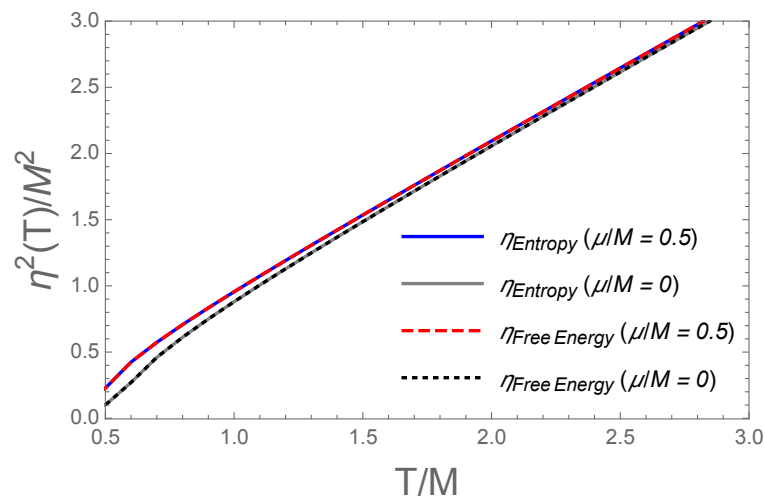
3.4 Changing the prescription for the OPT optimization

We will make use of the freedom on how to evaluate η . We could minimize the entropy, for example, but what we cannot do is to compute different η 's. If we do that, in the end, all the observables will have a different η and they will not be related to each other: a total mess!!! We need a consistent prescription for it.

3.4.1 PMS

The reader could ask if there is any difference in this choice. Of course, the parameter will be different if we choose to minimize S (entropy), or \mathcal{F} (free energy), but they behave in the same manner.

Figure 46. - Different variational parameters, with and without chemical potential. For all of them $\lambda = 31$ and $m^2 = M^2$



Source: The author, 2022.

In Figure 46, we see that it does not make any difference to choose the entropy or the free energy when obtaining the optimum value for η . The point is about what we can do. With the free energy, we can compute any thermodynamic observable. But it only makes sense if we choose always the same η . If the problem of the first-order phase

transition relies in the variational parameter, as we say previously, we should propose an improvement for the η computation. This is a problem we are currently working with and whose results will be referred elsewhere. This new prescription involves the use of the optimized renormalization group equations (FERNANDEZ; KNEUR, 2021; KNEUR; PINTO, 2015), but in a little different way.

CONCLUSIONS

We have calculated the free energy of a complex scalar field (ϕ^4 in $d = 4$ dimensions with $U(1)$ symmetry) taking into account the effects of finite temperature and chemical potential. The calculation was performed until second order in the coupling constant, which considers terms of two and three loops. Among these contributions, complicated diagrams as the setting sun (two-loops) and basketball diagrams (three-loops). The calculation of these terms is quite extensive and non-trivial, and we have performed in this dissertation the details of their derivation.

The setting sun diagram was done both in the off-shell and on-shell context. The off-shell contribution enters in the derivation of the thermodynamical potential, which here we have derived up to quadratic order in the coupling constant. And in the on-shell computation, which take into account explicitly the dependence on the external moment, enters as auxiliary part of the calculation of the basketball diagram at three-loop order. It also enters in the derivation of the effective thermal mass, with we have discussed at the end of this work.

It was analyzed the free energy and also the thermodynamical potential in the perturbative case up to second order in the coupling constant. We show that the perturbation theory ends up not being applicable in these studies, due to non-convergence of the same at high temperatures and with increasing the of magnitude of the coupling. To address this problem, we extended the calculation using a nonperturbative method. The nonperturbative method that we have considered in this work was the Optimized Perturbation Theory.

Although OPT with PMS leads to convergent results for the free energy, it predicts a first-order phase transition in the complex scalar field model studied here, which disagrees with what we expect for the phase transition for its class of model: it should be a second-order phase transition .

To address this issue, we are currently trying to implement this model in the context of the renormalization group procedure. More investigation are required to better understand this problem and we are conducting such studies, whose results will be report elsewhere.

REFERENCES

- ANDERSEN, O. J. et al. Massive basketball diagram for a thermal scalar field theory. **Phys. Rev. D**, [s. l.], v. 62, p. 045004, July 2000.
- ARNOLD, P. B.; ZHAI, C. The Three loop free energy for pure gauge QCD. **Phys. Rev. D**, [s. l.], v. 50, p. 7603–7623, 1994. DOI: 10.1103/PhysRevD.50.7603.
- BENDER, C. M. et al. A new perturbative approach to nonlinear problems. **J. Math. Phys.**, [s. l.], v. 30, p. 1447-1455, 1989.
- BENGHI, M. et al. QCD pressure: Renormalization group optimized perturbation theory confronts lattice. **Phys. Rev. D**, [s. l.], v. 104, 2021.
- BENSON, K. et al. Phase structure and the effective potential at fixed charge. **Phys. Rev. D**, [s. l.], v. 44, p. 2480–2497, Oct. 1991.
- BRAATEN, E.; PISARSKI, D. R. Soft amplitudes in hot gauge theories: A general analysis. **Nuclear Physics B**, [s. l.], v. 337, n. 3, p. 569-634, 1990. ISSN 0550-3213.
- BRANDT, F. T. et al. Thermal operator and cutting rules at finite temperature and chemical potential. **Phys. Rev. D**, [s. l.], v. 74, p. 085006, Oct.2006. DOI: 10.1103/PhysRevD.74.085006.
- CHIKU, S.; HATSUDA, T. Optimized perturbation theory at finite temperature. **Phys. Rev. D**, [s. l.], v. 58, Aug. 1998.
- DADIC, I. Two mechanisms for the elimination of pinch singularities in out of equilibrium thermal field theories. **Phys. Rev. D**, [s. l.], v. 59, p. 125012, 1999.
- DAS, A. **Finite Temperature Field Theory**. New York: World Scientific, 1997. ISBN 978-981-02-2856-9, 978-981-4498-23-4.
- DOLAN, L.; JACKIW, R. Symmetry behavior at finite temperature. **Phys. Rev. D**, [s. l.], v. 9, p. 12, 1974.
- DUARTE, D. C. et al. Optimized perturbation theory for charged scalar fields at finite temperature and in an external magnetic field. **Phys. Rev. D**, [s. l.], v. 84, Oct. 2011.
- DYSON, F. J. The Radiation Theories of Tomonaga, Schwinger, and Feynman. **Phys. Rev.**, [s. l.], v. 75, p. 486–502, Feb. 1949. DOI: 10.1103/PhysRev.75.486.
- FARIAS, R. L. et al. Reliability of the Optimized Perturbation Theory for scalar fields at finite temperature. **AIP Conf. Proc.**, [s. l.], v. 1520, n. 1, p. 330–332, 2013.

FARIAS, R. L. S.; RAMOS, R. O.; KREIN, G. Applicability of the Linear delta Expansion for the $\lambda\phi^4$ Field Theory at Finite Temperature in the Symmetric and Broken Phases. **Phys. Rev. D**, [s. l.], v. 78, p. 065046, 2008. DOI: 10.1103/PhysRevD.78.065046.

FERNANDEZ, L.; KNEUR, J. Renormalization group optimized $\lambda\phi^4$ pressure at next-to-next-to-leading order. **Phys. Rev. D**, [s. l.], v. 104, n. 9, p. 12, 2021.

FRENKEL, J.; SAA, A. V.; TAYLOR, J. C. The Pressure in thermal scalar field theory to three loop order. **Phys. Rev. D**, [s. l.], v. 46, p. 3670–3673, 1992. DOI: 10.1103/PhysRevD.46.3670.

GERGELY, M. et al. Bose-Einstein condensation and Silver Blaze property from the two-loop Φ -derivable approximation. **Phys. Rev. D**, [s. l.], v. 90, Dec. 2014.

GLEISER, M.; RAMOS, R. O. Microphysical approach to nonequilibrium dynamics of quantum fields. **Phys. Rev. D**, [s. l.], v. 50, p. 2441, 1994.

GUTH, A. H. The Inflationary Universe: A Possible Solution to the Horizon and Flatness Problems. **Phys. Rev. D**, [s. l.], v. 23, 1981a.

GUTH, A. H.; WEINBERG, E. J. Cosmological Consequences of a First Order Phase Transition in the SU(5) Grand Unified Model. **Phys. Rev. D**, [s. l.], v. 23, p. 876, 1981b. DOI: 10.1103/PhysRevD.23.876.

HABER, H. E.; WELDON, H. A. On the relativistic Bose–Einstein integrals. **J. Math. Phys.**, [s. l.], v. 23, p. 15, 1982.

JONES, H. F.; PARKIN, P. The renormalized thermal mass and critical temperature of a complex scalar field theory with non-zero charge density. **Nuclear Physics B**, [s. l.], v. 594, n. 1, p. 518–532, 2001. ISSN 0550-3213. DOI: [https://doi.org/10.1016/S0550-3213\(00\)00662-3](https://doi.org/10.1016/S0550-3213(00)00662-3).

KAPUSTA, J. I. Bose-Einstein condensation, spontaneous symmetry breaking, and gauge theories. **Phys. Rev. D**, [s. l.], v. 24, July 1981.

_____. **Finite-Temperature Field Theory**. [S.l.]: Cambridge University Press, 2006.

KLEINERT, H. **Path Integrals in Quantum Mechanics, Statistics, and Polymer Physics**. [S.l.]: Singapore: World Scientific, 1990.

_____. **Quantum Field Theory and Particle Physics**. [S.l.]: World Scientific, 1996.

KLEINERT, H.; SCHULTE-FROHLINDE'S, V. **Critical Properties of Φ^4 -Theories**. [S.l.]: World Scientific, 2001.

KNEUR, J.; PINTO, M. B. Renormalization group optimized perturbation theory at finite temperatures. **Phys. Rev. D**, [s. l.], v. 92, p. 116008, Dec. 2015.
DOI: 10.1103/PhysRevD.92.116008.

KNEUR, J. et al. Convergent Resummed Linear δ Expansion in the Critical $O(N)$ (ϕ^2)_{23d} Model. **Phys. Rev. Lett.**, [s. l.], v. 89, Nov. 2002.

LE BELLAC, Michel. **Thermal Field Theory**. [S.l.]: Cambridge University Press, 1996.

LEHMANN, H. et al. Zur Formulierung quantisierter Feldtheorien. **Il Nuovo Cimento** (1955-1965), [s. l.], p. 205–225, 1955.

LINDE, A. D. Inflationary Cosmology. **Lect. Notes Phys.**, [s. l.], v. 738, p. 1–54, 2008.
DOI: 10.1007/978-3-540-74353-8_1. arXiv: 0705.0164 [hep-th].

MARKO, G. et al. Broken phase effective potential in the two-loop Φ -derivable ' approximation and nature of the phase transition in a scalar theory. **Phys. Rev. D**, [s. l.], v. 86, Oct. 2012.

MILTON, K. M. et al. Logarithmic approximations to polynomial Lagrangians. **Phys. Rev. Lett.**, [s. l.], v. 58, June 1987.

PARWANI, R. R. Resummation in a hot scalar field theory. **Phys. Rev. D**, [s. l.], v. 45, p. 4695–4705, 1992. DOI: 10.1103/PhysRevD.45.4695.

PESKIN, M. E.; SCHROEDER, D. V. **An Introduction to quantum field theory**. Reading, USA: Addison-Wesley, 1995. ISBN 978-0-201-50397-5.

PICH, A. The Standard model of electroweak interactions. In: 2006 European School of High-Energy Physics. [**Proceedings...**]. [S.l.: s.n.], 2007. eprint: 0705.4264.

PIGUET, O.; SORELLA, S. P. **Algebraic renormalization**: perturbative renormalization, symmetries and anomalies. [S.l.: s.n.], 1995. V. 28. DOI: 10.1007/978-3-540-49192-7.

PINTO, M. B. Evaluating critical exponents in the optimized perturbation theory. **Physica A: Statistical Mechanics and its Applications**, [s. l.], v. 342, 2004.

POLITZER, D. H. Stevenson's optimized perturbation theory applied to factorization and mass scheme dependence. **Nuclear Physics B**, [s. l.], v. 194, n. 3, p. 493–512, 1982. ISSN 0550-3213.

RYDER, L. H. **Quantum field theory**. [S.l.]: Cambridge University Press, 1996.

SALAM, A. Weak and Electromagnetic Interactions. **Conf. Proc. C**, [s. l.], v. 680519, 1968.

SEZNEC, R.; ZINN-JUSTIN, J. Summation of divergent series by order dependent mappings: Application to the anharmonic oscillator and critical exponents in field theory. **Journal of Mathematical Physics**, [s. l.], v. 20, n. 7, 1979.

STEINHARDT, P. J. The Weinberg-Salam model and early cosmology. **Nuclear Physics B**, [s. l.], v. 179, n. 3, 1981. ISSN 0550-3213.

STEVENSON, P. M. Optimized perturbation theory. **Phys. Rev. D**, [s. l.], v. 23, p. 2916–2944, June 1981.

T'HOOFT, G.; VELTMAN, M. Regularization and renormalization of gauge fields. **Nuclear Physics B**, [s. l.], v. 44, n. 1, p. 189–213, 1972. ISSN 0550-3213.

WEINBERG, S. A Model of Leptons. **Phys. Rev. Lett.**, [s. l.], v. 21, 1967.

_____. Gauge and Global Symmetries at High Temperature. **Phys. Rev. D**, [s. l.], v. 9, p. 3357–3378, 1974.

WEINBERG, S. **The quantum theory of fields**, v. 2: modern applications. [S.l.]: Cambridge University Press, Aug. 2013. ISBN 978-1-139-63247-8, 978-0-521-67054-8, 978-0-521-55002-4.

YUKALOV, V. I. Basics of Bose-Einstein Condensation. **Phys. Part. Nucl.**, [s. l.], v. 42, p. 460–513, 2011.

YUKALOV, V. I.; YUKALOVA, E. P. Bose-Einstein condensation in self-consistent mean-field theory. **Journal of Physics B: Atomic, Molecular and Optical Physics**, [s. l.], v. 47, n. 9, Apr. 2014.

APPENDIX A - REGULARIZATION FORMULAS

All the integrals, except for the setting sun and the basketball diagram, can be calculated recursively. Let us define some quantities for that. The one-loop vacuum energy term (the bubble diagram shown in Figure 10) is given by,

$$I_0 = \int_p \log [p^2 + m^2] . \quad (304)$$

The momentum integral: The tadpole diagram and similars are given in terms of the momentum integral,

$$I_1 = \int_p \frac{1}{p^2 + m^2} \quad (305)$$

but,

$$\frac{\partial}{\partial m^2} I_0 = I_1 . \quad (306)$$

Generalizing this relation, we have

$$\frac{\partial}{\partial m^2} I_n = -n I_{n+1} , \quad (307)$$

where,

$$I_n = \int_p \frac{1}{(p^2 + m^2)^n} , \quad n \geq 1 . \quad (308)$$

For the thermal contributions, we have the following relations, that can be derived from Haber and Weldon (HABER; WELDON, 1982),

$$\frac{\partial h_{n+1}^e}{\partial m^2} = -\frac{1}{T^2} \frac{h_{n-1}^e}{2n} , \quad (309)$$

where the thermal functions h_n^e are explicitly defined in Appendix B. With these relations, the regularization of the 1st, 2nd and 3rd diagrams of Figure 10, the 1st and 2nd from Figure 15 and the vertex diagram, becomes easy. Since we chose to work in the \overline{MS}

scheme, the regularization for the I'_n s are,

$$I_0 = \frac{m^4}{(4\pi)^2} \left(\frac{\mathcal{M}}{m} \right)^{2\epsilon} e^{\gamma_E \cdot \epsilon} \frac{\Gamma[\epsilon - 1]}{(2 - \epsilon)} - \frac{8T^4}{\pi^2} h_5^\epsilon(y, r) , \quad (310)$$

$$I_1 = \frac{m^2}{(4\pi)^2} \left(\frac{\mathcal{M}}{m} \right)^{2\epsilon} e^{\gamma_E \cdot \epsilon} \Gamma[-1 + \epsilon] + \frac{T^2}{\pi^2} h_3^\epsilon(y, r) , \quad (311)$$

$$I_2 = \frac{1}{(4\pi)^2} \left(\frac{\mathcal{M}}{m} \right)^{2\epsilon} e^{\gamma_E \cdot \epsilon} \Gamma\epsilon - 1 + \frac{h_1^\epsilon(y, r)}{4\pi^2} ,$$

where the vacuum terms (first term) in the above integrals are obtained from the relation,

$$\int d^d k \frac{(k^2)^\alpha}{(k^2 + m^2)^\beta} = \pi^{d/2} (m^2)^{\frac{d}{2} + \alpha - \beta} \times \frac{\Gamma(\alpha + \frac{d}{2}) \Gamma(\beta - \alpha - \frac{d}{2})}{\Gamma(\frac{d}{2}) \Gamma(\beta)} . \quad (312)$$

Feynman Parameters:

$$\frac{1}{A_1 A_2 \cdots A_n} = \int_0^1 dx_1 \cdots dx_n \delta(\sum x_i - 1) \frac{(n-1)!}{[x_1 A_1 + x_2 A_2 + \dots + x_n A_n]^n} \quad (313)$$

$$\frac{1}{A^\alpha B^\beta} = \frac{\Gamma(\alpha + \beta)}{\Gamma(\alpha) \Gamma(\beta)} \int_0^1 dy \frac{y^{\alpha-1} (1-y)^{\beta-1}}{(yA + (1-y)B)^{\alpha+\beta}} . \quad (314)$$

APPENDIX B - THERMAL FUNCTIONS

The thermal functions are defined as follow,

$$h_1^e(y, r) = \frac{1}{2} \int_0^\infty \frac{dx}{(x^2 + y^2)^{1/2}} \left[\frac{1}{e^{(x^2+y^2)^{1/2}-ry} - 1} + \frac{1}{e^{(x^2+y^2)^{1/2}+ry} - 1} \right], \quad (315)$$

$$h_3^e(y, r) = \frac{1}{4} \int_0^\infty \frac{x^2 dx}{(x^2 + y^2)^{1/2}} \left[\frac{1}{e^{(x^2+y^2)^{1/2}-ry} - 1} + \frac{1}{e^{(x^2+y^2)^{1/2}+ry} - 1} \right], \quad (316)$$

and

$$h_5^e(y, r) = -\frac{1}{16} \int_0^\infty x^2 dx \{ \log [1 - e^{-(x^2+y^2)^{1/2}+ry}] + (r \rightarrow -r) \}, \quad (317)$$

where $y = m/T$ and $r = \mu/m$. All these functions are generalized and evaluated in different limits of T in the work of Haber and Weldon (HABER; WELDON, 1982). Where, in the approximation $y \ll 1$, we have for instance that (HABER; WELDON, 1982),

$$\begin{aligned} h_{2l+1}^e &= \frac{\pi y^{2l-1}}{2\Gamma(2l+1)} (-1)^l (1-r^2)^{l-\frac{1}{2}} + \frac{(-1)^l 2^{-2l} y^{2l}}{(2(\Gamma(l+1)))^2} \\ &\times \left\{ \left[lr^2 {}_3F_2(1, 1, 1-l; \frac{3}{2}, 2; r^2) + \frac{1}{2}(\gamma - \psi^{(0)}(l+1)) + \ln\left(\frac{y}{4\pi}\right) \right] \right\} \\ &+ \frac{1}{2\Gamma(1+l)} \sum_{k=0}^{l-1} \left[\frac{(-1)^k 2^{-2k} y^{2k} \zeta(2l-2k) \Gamma(l-k) {}_2F_1(-k, l-k; \frac{1}{2}; r^2)}{\Gamma(k+1)} \right] \\ &+ \frac{(-1)^l}{2\Gamma(l+1)} \left(\frac{y}{2}\right)^{2l} \sum_{k=1}^{\infty} (-1)^k \left(\frac{y}{4\pi}\right)^{2k} \frac{\zeta(2k+1) \Gamma(2k+1) {}_2F_1(-k, -k-l; \frac{1}{2}; r^2)}{\Gamma(k+1) \Gamma(k+l+1)} \end{aligned} \quad (318)$$

where $2l+1 = n$, which means that this formula (318) is valid for odd n 's.

APPENDIX C - COUNTERTERMS AND CORRECTIONS

Free energy counter-terms:

Figure 47. - Mass counterterms that cancel all the divergences associated to the two point function of a U(1) $\lambda\phi^4$ theory up to two-loop

$$\Delta m^2 = \left[\text{Diagram 1} + \text{Diagram 2} + \text{Diagram 3} \right] \Big|_{div} = \text{Diagram 4}$$

Source: The author, 2022.

Here we show all the counter-terms that are needed to renormalize the free energy for a U(1) scalar field theory with quartic interaction, until second-order in perturbation theory. The mass counter-terms (Figure 47) are,

$$\Delta m^2 = \frac{2}{3\epsilon} \frac{\lambda}{(4\pi)^2} m^2 + \frac{\lambda^2 m^2}{(4\pi)^4} \left(\frac{7}{9\epsilon^2} - \frac{5}{18\epsilon} \right). \quad (319)$$

Figure 48. - Vertex counterterm

$$\Delta_1 \lambda = \left[\text{Diagram 1} \right] \Big|_{div} = \text{Diagram 2}$$

Legend: Correction that cancel the divergence associate to a $2 \rightarrow 2$ scattering for a U(1) $\lambda\phi^4$ theory.

Source: The author, 2022.

The vertex counter-term (Figure 48) is,

$$\Delta_1 \lambda = \frac{5}{3} \frac{\lambda^2}{(4\pi)^2 \epsilon}. \quad (320)$$

Corrections to the vacuum of the theory:

Figure 49. - Zero point energy corrections, the vacuum counterterms of a U(1) $\lambda\phi^4$ theory

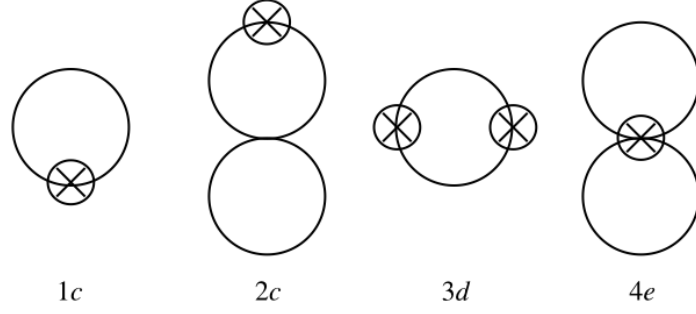
$$\Delta \mathcal{E}_0 = \left[\text{circle} + \text{two circles} + \text{three circles} + \text{four circles} \right] \Big|_{div}$$

Source: The author, 2022.

The zero point corrections (Figure 49), or the vacuum counter-terms are,

$$\Delta \mathcal{E}_0 = \frac{m^4}{(4\pi)^2 2\epsilon} + \frac{\lambda m^4}{(4\pi)^4 3\epsilon^2} + \frac{\lambda^2 m^4}{(4\pi)^6} \left(\frac{1}{3\epsilon^3} - \frac{5}{27\epsilon^2} + \frac{1}{36\epsilon} \right). \quad (321)$$

Figure 50. - Bubble corrections



Legend: The first can be understood as a mass counterterm, the second a mass counter-term for a two-loop diagram, the third a second order mass counterterm and the last also a vertex counterterm for a two-loop diagram.

Source: The author, 2022.

The bubble corrections (Figure 50) are given, as follow,

$$1c \equiv \frac{\partial \mathcal{F}_{1a}}{\partial m^2} \Delta_1 m^2 = \Delta_2 m^2 I_1 , \quad (322)$$

$$2c \equiv \frac{\partial \mathcal{F}_{2a}}{\partial m^2} \Delta_1 m^2 = -\frac{2}{3} \Delta_1 m^2 \lambda I_1 I_2 , \quad (323)$$

$$3d \equiv \frac{1}{2} \frac{\partial^2 \mathcal{F}_{1a}}{(\partial m^2)^2} (\Delta_1 m^2)^2 = -\frac{1}{2} (\Delta_1 m^2)^2 I_2 , \quad (324)$$

$$4e \equiv \frac{\mathcal{F}_{2a}}{\lambda} \Delta_1 \lambda = \frac{1}{3} \Delta_1 \lambda I_1^2 , \quad (325)$$

which can be written as,

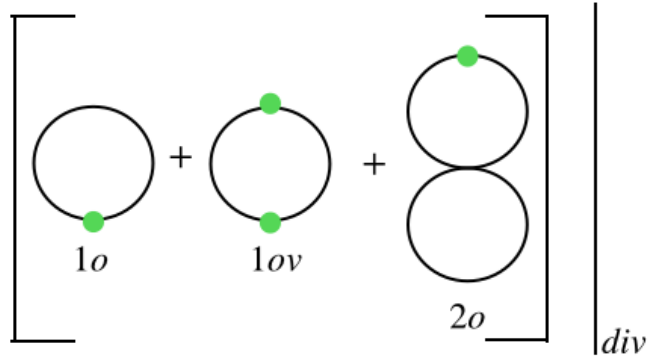
$$\Delta_2 m^2 I_1 = \frac{\lambda^2 m^2}{(4\pi)^4} \left(\frac{7}{9\epsilon^2} - \frac{5}{18\epsilon} \right) \left[\frac{m^2}{(4\pi)^2} \left(\frac{\mathcal{M}}{m} \right)^{2\epsilon} e^{\gamma_E \epsilon} \Gamma[-1 + \epsilon] + \frac{T^2}{\pi^2} h_3^e(y, r) \right] ,$$

and

$$\begin{aligned} \frac{1}{3}\Delta\lambda(I_1)^2 &= \frac{1}{3}\frac{5}{3}\frac{\lambda^2}{(4\pi)^2\epsilon}\left[\frac{m^2}{(4\pi)^2}\left(\frac{\mathcal{M}}{m}\right)^{2\epsilon}e^{\gamma_E\cdot\epsilon}\Gamma[-1+\epsilon]+\frac{T^2}{\pi^2}h_3^e(y,r)\right]^2, \\ -\frac{1}{2}(\Delta_1m^2)^2I_2 &= -\frac{1}{2}\left(\frac{2}{3\epsilon}\frac{\lambda}{(4\pi)^2}m^2\right)^2\left[\frac{1}{(4\pi)^2}\left(\frac{\mathcal{M}}{m}\right)^{2\epsilon}e^{\gamma_E\cdot\epsilon}\Gamma\epsilon-1+\frac{h_1^e(y,r)}{4\pi^2}\right], \\ -\frac{2}{3}\Delta m^2\lambda I_1I_2 &= -\frac{2\lambda}{3}\left(\frac{2}{3\epsilon}\frac{\lambda}{(4\pi)^2}m^2\right)\left[\frac{m^2}{(4\pi)^2}\left(\frac{\mathcal{M}}{m}\right)^{2\epsilon}e^{\gamma_E\cdot\epsilon}\Gamma[-1+\epsilon]+\frac{T^2}{\pi^2}h_3^e(y,r)\right] \\ &\times\left[\frac{1}{(4\pi)^2}\left(\frac{\mathcal{M}}{m}\right)^{2\epsilon}e^{\gamma_E\cdot\epsilon}\Gamma\epsilon-1+\frac{h_1^e(y,r)}{4\pi^2}\right], \end{aligned}$$

where we have expand the expressions in ϵ .

Figure 51. - OPT Bubble corrections, the OPT mass counterterms



Source: The author, 2022.

The OPT bubble corrections (Figure 51) are given, as follow,

$$\Delta 1o = -\frac{\delta\eta^2\Omega^2}{16\pi^2\epsilon}, \quad (326)$$

$$\Delta 1ov = \frac{\delta^2\eta^4}{2(16\pi^2)\epsilon}, \quad (327)$$

where for the two-loop diagram, we have three corrections, one with a mass insertion,

other with a OPT mass insertion and a vacuum OPT correction,

$$\Delta 2o \Big|_{\eta^2} = - \left(\frac{\delta^2 \eta^2 \lambda}{24\pi^2 \epsilon} \right) I_1, \quad (328)$$

$$\Delta 2o \Big|_{\Omega^2} = \left(\frac{\delta \Omega^2 \lambda}{24\pi^2 \epsilon} \right) \delta \eta^2 I_2, \quad (329)$$

$$\Delta 2o = - \frac{\delta^2 \eta^2 \lambda \Omega^2}{384\pi^4 \epsilon^2}. \quad (330)$$

Mass Counter-terms:

The self-energy corrections are given by,

$$\frac{\partial \Sigma_{1a}}{\partial m^2} \Delta_1 m^2 = - \frac{2\lambda}{3} \frac{\phi^2}{2} I_2 \Delta_1 m^2, \quad (331)$$

$$\frac{\Sigma_{1a}}{\lambda} \Delta_1 \lambda = \frac{2}{3} \frac{\phi^2}{2} I_1 \delta_1 \lambda, \quad (332)$$

where Σ_{1a} is the $1a$ diagram of Figure 15. Equation (331) is explicitly given by,

$$- \frac{2\lambda}{3} \frac{\phi^2}{2} I_2 \Delta_1 m^2 = - \frac{2\lambda}{3} \frac{\phi^2}{2} \left[\frac{1}{(4\pi)^2} \left(\frac{\mathcal{M}}{m} \right)^{2\epsilon} e^{\gamma_E \cdot \epsilon} \Gamma[\epsilon - 1] (\epsilon - 1) + \frac{h_1^e(y, r)}{4\pi^2} \right] \frac{2\lambda m^2}{3(4\pi)^2 \epsilon},$$

and Eq. (332) is

$$\frac{\Sigma_{1a}}{\lambda} \Delta_1 \lambda = \frac{2}{3} \frac{\phi^2}{2} \left[\frac{m^2}{(4\pi)^2} \left(\frac{\mathcal{M}}{m} \right)^{2\epsilon} e^{\gamma_E \cdot \epsilon} \Gamma(-1 + \epsilon) + \frac{T^2}{\pi^2} h_3^e(y, r) \right] \frac{5\lambda^2}{3(4\pi)^2 \epsilon}.$$

Proceeding, as we have already explained, we remove all the divergences from the self-energy and free energy (effective potential) by appropriately adding these counterterms to the tree-level potential.